UCGE Reports
Number 20096

Development of a Real-Time Attitude System Using a Quaternion Parameterization and Non-Dedicated GPS Receivers

Department of Geomatics Engineering

By

John B. Schleppe

July 1996

Calgary, Alberta, Canada

THE UNIVERSITY OF CALGARY

Development of a Real-Time Attitude System Using a Quaternion Parameterization and Non-Dedicated GPS Receivers

by

John B. Schleppe

A THESIS

SUBMITTED TO THE FACULTY OF GRADUATE STUDIES

IN PARTIAL FULFILLMENT OF THE REQUIREMENTS FOR THE

DEGREE OF MASTER OF ENGINEERING

DEPARTMENT OF GEOMATICS ENGINEERING

CALGARY, ALBERTA

JULY, 1996

ABSTRACT

A GPS attitude system was developed for use in real-time applications. Mathematical models were developed to allow for the direct estimation of the quaternion attitude representation from double difference interferometric phase and pseudorange observations. Robust on-the-fly carrier phase ambiguity resolution techniques were incorporated. A test system was designed and consisted of an antenna array, four OEM GPS receivers and a laptop computer. Real-time software was developed to process input from NovAtel, Leica and Motorola GPS receivers as well as display and log the results. A series of static and dynamic tests were conducted to verify the performance of the quaternion based algorithms and math models. Results of 3.9 mrads RMS in heading, 25 mrads RMS in pitch, and 15 mrads RMS in roll were achieved during the static test while using a 40 cm antenna array and NovAtel 2151™ GPS receivers.

ACKNOWLEDGMENTS

I would like to express my gratitude to my supervisor, Professor Gerard Lachapelle, for his support and encouragement throughout my graduate studies. His patience and understanding was appreciated while I fully explored my thesis topic.

Special thanks are extended to Professor M. Elizabeth Cannon for her input during the early stages of this project. Our collaberation during the DRES contract and the subsequent successes encouraged me to pursue attitude determination as my thesis topic. I am also grateful to Professor Edward Krakiwsky for his advice and encouragement. Our discussions on estimation techniques and the reference materials he has supplied have opened up many new and exciting areas for exploration.

Pulsearch Navigation Systems Inc. is acknowledged for funding my graduate studies and for providing the equipment and software libraries used in this research. The team at Pulsearch, especially Mr. Jim McLellan are thanked for their support. The people in the software group headed by Mr. Mike Forkheim are commended for their excellent contributions and maintainance of our software libraries. Dr. Yang Gao and Dr. Mohamed Abousalem are also recognized for their many contributions to the improvement of Pulsearch's GPS, estimation and statistical libraries. Appreciation is also extended to Mr. Jonathan Auld for his critique of this thesis.

Finally my deepest thanks go to my wife Vicki and three children, Michael, Caitlyn and Adam whose support, encouragement, understanding and gentle humour have helped me complete my studies.

TABLE OF CONTENTS

APPROVAL PAGE ii

ABSTRACT iii

ACKNOWLEDGMENTS iv

TABLE OF CONTENTS v

LIST OF TABLES viii

LIST OF FIGURES ix

NOTATION xii

CHAPTER

1.0 INTRODUCTION 1

1.1 Background And Objective 1

1.2 Project Background 5

1.3 Thesis Outline 6

2.0 COORDINATE FRAMES 8

2.1 Mathematical Background 8

2.1.1 Direction Cosine Matrix 9

2.1.2 Euler Angles 10

2.1.3 Quaternions 11

2.2 Earth-fixed Frame 16

2.3 Local-level Frame 18

2.3.1 Relationship Between Local-level and Earth-fixed Frames 19

2.3.2 Wander Frame 20

2.4 Body Frame 20

2.4.1 Relationship Between Body and Local-level Frames 22

2.4.2 Relationship Between Quaternions and Euler Angles 26
2.4.3 Relationship Between Body and Earth-fixed Frames 28

3.0 GLOBAL POSITIONING SYSTEM 30
3.1 System Description 30
3.2 GPS Receivers 31
3.3 Observation Equations and Error Sources 34
3.3.1 Pseudorange Observations 35
3.3.2 Phase Observations 38
3.4 Differenced Observations 40
3.4.1 Single Difference Observations 40
3.4.2 Interferometric Observation 44
3.4.3 Double Difference Observations 47
3.4.4 Double Difference Interferometry 50

4.0 ATTITUDE DETERMINATION 52
4.1 Kinematic Modelling and Attitude Dynamics 53
4.2 Kalman Filtering 56
4.3 Kalman Filtering for Quaternion Based Attitude Estimation 58
4.4 Quaternion Dilution of Precision Computation 66
4.5 Quality Control 67
4.6 Covariance Propagation from Quaternions to Euler Angles 69

5.0 GPS AMBIGUITY RESOLUTION 72
5.1 Ambiguity Search Techniques 73
5.2 Defining Search Volumes 77
5.3 Forming Ambiguity Combinations 79
5.4 Testing Ambiguity Combinations 81

6.0 ATTITUDE SYSTEM DESIGN AND IMPLEMENTATION 85
6.1 Hardware Overview 86

6.1.1 Antenna Array 86
6.1.2 GPS Receivers 90
6.1.3 Computer 92
6.2 Software Design and Implementation 92
6.3 Test Vehicle and System Installation 96
7.0 TEST DESCRIPTION AND RESULTS 97
7.1 Static Trials 98
7.1.1 Test Description 98
7.1.2 Comparison of Results From NovAtel, Leica and Motorola Receivers 100
7.2 Vehicle Trials Over a Level Course 110
7.2.1 Test Description 110
7.2.2 Comparison of Results From NovAtel, Leica and Motorola Receivers 113
7.3 Land Vehicle Trials over Hilly Terrain 123
7.3.1 Test Description 124
7.3.2 Data Analysis 125
8.0 CONCLUSIONS AND RECOMMENDATIONS 130
REFERENCES 134

LIST OF TABLES

Table 3.1 - Summary of Dedicated Attitude GPS Receivers 32
Table 3.2 - Summary of Non-Dedicated GPS Receivers For Attitude Systems 34
Table 3.3 - Interferometric Approximation Error..... 46
Table 3.4 - Magnitude of Residual Double Difference GPS Errors..... 50
Table 6.1 - GPS Antenna Specifications..... 88
Table 6.2 - GPS Receiver Specifications 91
Table 7.1 - Static Observation Times..... 99
Table 7.2 - Attitude Values Computed Using SEMIKIN™ 99
Table 7.3 - Input Parameters for CARDINAL™ Real-time System..... 100
Table 7.4 - Comparison of Static Attitude Results..... 105
Table 7.5 - NovAtel Static Ambiguity Resolution..... 108
Table 7.6 - Leica Static Ambiguity Resolution..... 109
Table 7.7 - Motorola Static Ambiguity Resolution..... 109
Table 7.8 - Dynamic Test Observation Times..... 113
Table 7.9 - NovAtel Dynamic Ambiguity Resolution..... 123
Table 7.10 - Leica Dynamic Ambiguity Resolution..... 123
Table 7.11 - Motorola Dynamic Ambiguity Resolution 123

LIST OF FIGURES

Figure 2.1 - Relationship Between Two Coordinate Frames 8
Figure 2.2 - Earth-fixed Coordinate Frame 16
Figure 2.3 - Local-level Coordinate Frame 18
Figure 2.4 - Body Coordinate Frame 21
Figure 2.5 - System's Antenna Array 22
Figure 3.1 - Pseudorange Model 36
Figure 3.2 - Between Receivers Single Difference 41
Figure 3.3 - Between Satellites Single Difference 43
Figure 3.4 - GPS Interferometry 45
Figure 3.5 - Double Difference 48
Figure 3.6 - Double Difference Interferometry 50
Figure 5.1 - Carrier Phase Ambiguity Resolution Flowchart 76
Figure 5.2 - Cubic Search Volume 77
Figure 5.3 - Spherical Surface Search Volume 78
Figure 6.1 - CARDINAL™ Hardware Design 86
Figure 6.2 - Antenna Array Design 87
Figure 6.3 - Antenna Gain Pattern 89
Figure 6.4 - CARDINAL™ Software Flowchart 94
Figure 6.5 - Attitude System Installation in Test Vehicle 96
Figure 7.1 - Static Test Area - Calgary, Alberta 98
Figure 7.2 - Estimated Heading Using NovAtel 2151™ 101
Figure 7.3 - Estimated Pitch Using NovAtel 2151™ 101
Figure 7.4 - Estimated Roll Using NovAtel 2151™ 101
Figure 7.5 - Estimated Heading Using Leica GPS Engine™ 102
Figure 7.6 - Estimated Pitch Using Leica GPS Engine™ 102
Figure 7.7 - Estimated Roll Using Leica GPS Engine™ 102

Figure 7.8 - Estimated Heading Using Motorola Oncore™ 103
Figure 7.9 - Estimated Pitch Using Motorola Oncore™..... 103
Figure 7.10 - Estimated Roll Using Motorola Oncore™..... 103
Figure 7.11 - Number of Observations - Static 106
Figure 7.12 - NovAtel RMS Double Difference Residuals..... 107
Figure 7.13 - Leica RMS Double Difference Residuals..... 107
Figure 7.14 - Motorola RMS Double Difference Residuals 107
Figure 7.15 - Dynamic Test Area - Calgary, Alberta 110
Figure 7.16 - Vehicle Trajectory For NovAtel 2151™ Trial 111
Figure 7.17 - Vehicle Trajectory For Leica GPS Engine™ Trial..... 112
Figure 7.18 - Vehicle Trajectory For Motorola Oncore™ Trial 112
Figure 7.19 - Estimated Dynamic Heading Using NovAtel 2151™..... 114
Figure 7.20 - Heading Covariance Using NovAtel 2151™ 114
Figure 7.21 - Estimated Dynamic Pitch Using NovAtel 2151™ 115
Figure 7.22 - Estimated Dynamic Roll Using NovAtel 2151™ 115
Figure 7.23 - NovAtel RMS Double Difference Phase Residuals Compared to Heading..... 116
Figure 7.24 - Vehicle Speed During NovAtel 2151™ Test 116
Figure 7.25 - Estimated Dynamic Heading Using Leica GPS Engine™ 117
Figure 7.26 - Heading Covariance Using Leica GPS Engine™..... 117
Figure 7.27 - Estimated Dynamic Pitch Using Leica GPS Engine™ 118
Figure 7.28 - Estimated Dynamic Roll Using Leica GPS Engine™..... 118
Figure 7.29 - Leica RMS Double Difference Phase Residuals Compared to Heading ... 119
Figure 7.30 - Vehicle Speed During Leica GPS Engine™ Test 119
Figure 7.31 - Estimated Dynamic Heading Using Motorola Oncore™..... 120
Figure 7.32 - Heading Covariance Using Motorola Oncore™ 120
Figure 7.33 - Estimated Dynamic Pitch Using Motorola Oncore™ 121

Figure 7.34 - Estimated Dynamic Roll Using Motorola Oncore™ 121
Figure 7.35 - Motorola RMS Double Difference Phase Residuals Compared to Heading 122
Figure 7.36 - Vehicle Speed During Motorola Oncore™ Test 122
Figure 7.37 - Hill Testing Course - Calgary, Alberta 124
Figure 7.38 - Vehicle Heading During Hill Trials 125
Figure 7.39 - Heading Covariance During Hill Trials 125
Figure 7.40 - Vehicle Pitch During Hill Trials 126
Figure 7.41 - Pitch Covariance During Hill Trials 126
Figure 7.42 - Vehicle Pitch Compared to Terrain Profile 127
Figure 7.43 - Vehicle Roll During Hill Trials 127
Figure 7.44 - Roll Covariance During Hill Trials 128
Figure 7.45 - Vehicle Speed During Hill Trials 128

NOTATION

i) Conventions

a) Matrices are represented by upper case bold letters.

b) Vectors are represented by lower case bold letters.

c) Rotation matrices between coordinate frames are defined by a subscript and a superscript denoting the two frames. For example $\mathbf{R}_b^l$ indicates the rotation matrix from the body frame (b) to the local-level frame (l).

d) The elements of a matrix are contained within brackets following the matrix and consist of the row and column number. For example **R**(2,3) indicates the element at the intersection of row 2 and column 3.

e) The operators used are defined as:

$\mathbf{x}^{(-)}$	the superscript (-) denotes Kalman prediction
$\mathbf{x}^{(+)}$	the superscript (+) Kalman update
$\dot{\mathbf{x}}$	derivative with respect to time
$\mathbf{A}^{\mathrm{T}}$	matrix transpose
$\mathbf{N}^{-1}$	matrix inverse
Δ	single difference between receivers
∇	single difference between satellites
$\nabla\Delta$	double difference between receivers and satellites
$\hat{\mathbf{x}}$	estimated value
$\tilde{\mathbf{x}}$	measured value
$\mathbf{x_0}$	initial value
$f(\mathrm{x})$	f is a function of x
$\frac{\partial \mathrm{R}}{\partial \psi}$	partial derivative of R with respect to ψ
$\otimes$	quaternion composition

ii) Symbols

a	semi-major axis of the ellipsoid
A	design matrix
b	semi-minor axis of the ellipsoid
c	speed of light
$\mathbf{C}_{\boldsymbol{l}}$	Kalman measurement noise covariance matrix
$\mathbf{C}_{w}$	Kalman filter process noise covariance matrix
$\mathbf{C}_{x}$	Kalman state vector covariance matrix
$\boldsymbol{\delta}$	Least squares correction vector
dT	receiver clock error
dt	satellite clock error
e	eccentricity of the ellipsoid
e	unit vector
F	dynamic matrix
H	orthometric height
h	ellipsoid height
I	identity matrix
l	vector of observations
λ	geodetic longitude
λ	GPS carrier wavelength
n	number of observations
N	geoid height
N	least squares normal matrix
N	carrier phase ambiguity
θ	pitch
p	pseudorange
ρ	geometrical distance between receiver and satellite
ϕ	geodetic latitude
Φ	carrier phase

Φ	Kalman filter transition matrix
$\mathbf{Q}$	Kalman spectral density matrix
$\mathbf{q}$	quaternion vector
$\mathbf{r}$	position vector
$\boldsymbol{r}$	residual vector
$\mathbf{R}_1$	right handed rotation matrix about the x axis
$\mathbf{R}_2$	right handed rotation matrix about the y axis
$\mathbf{R}_3$	right handed rotation matrix about the z axis
φ	roll
σ_0^2	apriori variance factor
$\hat{\sigma}_0^2$	aposteriori variance factor
$\boldsymbol{u}$	least squares u-vector
u	number of unknowns
$\mathbf{v}$	innovations vector
$\boldsymbol{w}$	least squares misclosure vector
$\mathbf{w}$	Kalman process noise vector
$\boldsymbol{\omega}$	angular rate vector
$\boldsymbol{x}$	vector of unknown parameters
$\mathbf{x}$	Kalman state vector
x,y,z	Cartesian coordinates
ψ	yaw

iii) Acronyms

A	amperes
AHRS	Attitude Heading Reference System
C/A Code	Clear / Acquisition Code
COG	Course Over Ground
DC	Direct Current
DoD	Department of Defense
DOP	Dilution of Precision
GPS	Global Positioning System
IF	Intermediate Frequency
INS	Inertial Navigation System
NRC	National Research Council
OEM	Original Equipment Manufacturer
OTF	On-The-Fly
P-Code	Precise Code
PRN	Pseudorandom Noise Code
QDOP	Quaternion Dilution of Precision
RF	Radio Frequency
RMS	Root Mean Square
RTCM	Radio Technical Commission For Maritime Services
SA	Selective Availability
SNR	Signal to Noise Ratio
SV	Space Vehicle
VDC	Direct Current Volts
VAC	Alternating Current Volts
WGS-84	World Geodetic System 1984

CHAPTER 1

INTRODUCTION

1.1 Background And Objective

Applications of the Global Positioning System (GPS) have blossomed in recent years and amongst the many innovative uses of GPS is attitude determination. Well rooted in mathematics and one of the primary applications of gyroscopes, attitude determination results in the measurement of vehicle orientation with respect to a reference frame. It is essential for a wide variety of navigation, guidance and control tasks. Most manned and unmanned aircraft, marine vessels and space vehicles have at least one type of attitude system onboard. The magnetic compass is probably the single most popular attitude determining (heading) device employed today. However as McMillan (1987) observes, there are geographical areas where the compass can not be used. These areas can be either natural or man made. In addition, with the increasing use of electrical motors and electronics on vehicles, fluctuating electro-magnetic fields can disturb the magnetic compass.

Other systems have been developed that do not have the shortcomings of the magnetic compass. Foremost amongst these is the north seeking gyrocompass. The gyrocompass can supply heading typically up to latitudes of 80°. Beyond that, the accuracy of the

gyrocompass declines as the distance to the rotation axis of the Earth decreases. The gyrocompass is extensively used onboard commercial marine vessels and prices start from $35,000. In addition to geographical limitations and high capital costs as disadvantages, most commercial gyrocompasses are electro-mechanical devices subject to mechanical failure and they are typically dampened to decrease short term noise. The main advantage of the gyrocompass is that it is self-contained and does not rely on external signals which may be denied.

Inertial Navigation Systems (INS) and inertial based Attitude Heading Reference Systems (AHRS) are used extensively on commercial airliners, military aircraft, military vessels, missiles, smart munitions and spacecraft. An INS for a naval vessel is typically very expensive (costing more than $200K), heavy, power intensive, requires long settling times and the accuracy of the system is degraded at higher latitudes (McMillan, 1994). Aircraft INS systems have prices exceeding $100,000, while tactical grade inertial AHRS sensor packages for missiles and munitions range in price from $15,000 to $40,000. Advantages of inertial systems include: high data rates, determination of values regardless of vehicle attitude, and self-contained and autonomous operation.

While GPS based attitude systems cannot compete with INS systems in high dynamic applications requiring high data rates and autonomous operation, there are a number of applications where the GPS system can enhance or replace existing heading and attitude systems. The ability of GPS attitude systems to not only provide attitude, but also absolute positioning is a major advantage. Cost effectiveness is the secondary advantage of GPS attitude systems. With the recent and rapid development of low-cost OEM GPS receiver cards capable of accurate phase measurement, coupled with the availability of low-cost processors, the cost of GPS attitude hardware has fallen dramatically. While several manufactures offer dedicated GPS attitude receivers, a greater number of manufactures offer OEM GPS receivers suitable for use as building blocks within a non-dedicated GPS receiver based attitude system.

The advantages offered by GPS attitude systems have led to a wide range of tests in a number of vehicles including: spacecraft and satellite attitude determination (Axelrad and Ward, 1994); naval vessel attitude determination (Kruczynski et al., 1989) (McMillan, 1994); hydrographic launch attitude determination (Lu et al., 1993); aircraft attitude determination (Van Graas and Braasch, 1991); artillery pointing (Jurgens et al., 1991); armoured vehicle pointing (Brown and Evans, 1990); commercial airlines (Kruczynski et al., 1995); geophysical ships (Nesbo, 1988); and unmanned vehicle heading determination (Cannon et al., 1992). As the reliability of GPS attitude techniques improve and costs decrease, attitude systems will likely be employed more often and in a wider range of applications.

A variety of techniques and equipment are being used for GPS attitude determination. One technique borrows most of its algorithms from kinematic positioning. Here, independent baselines are estimated using one antenna as the reference and the others treated as remotes. Since the carrier phase is used, this often involves ambiguity resolution on-the-fly (OTF). Following the determination of the baselines, the attitude parameters are either determined directly from the estimated antenna coordinates or in the case where redundant baselines exist, the attitude parameters are estimated using a least squares process (Lu, 1995). The known baseline lengths or body frame coordinates of the antennas are used to verify the attitude estimation process and in some cases used as a test in the ambiguity resolution. Systems that use this *baseline* technique include Ashtech's 3DF (Kuhl et al., 1994), Trimble's TANS Vector (Wilson and Tonnemacher, 1992), and MULTINAV (Lu, 1995).

A second approach is to *directly* estimate the attitude parameters from the GPS observations. Axelrad and Ward (1994) present a technique employing carrier phase single difference observations to directly estimate quaternion parameters. The *a priori* knowledge of the antenna body frame coordinates is incorporated into the measurement models. All measurements are used to estimate the three attitude parameters (four when

using quaternions). Theoretically, utilizing the *direct* approach to attitude estimation, the attitude can be determined using three antennas and only three single or double differences, one of which must be observed on a second, noncollinear remote antenna. Contrast this to the *baseline* approach where at least six single or double difference measurements must be used to determine three dimensional attitude.

Euler and Hill (1995) discuss how exploiting redundant GPS information and the *a priori* knowledge of the baseline components can aid ambiguity resolution. Increased redundancy improves ambiguity resolution, reliability and robustness. Since the *baseline* approach resolves the ambiguities one baseline at a time, the degrees of freedom during the resolution are less than those during resolution using the *direct* approach. For example, consider the case where one reference and two remote antennas observe 6 satellites each. Five double differences for each of the two baselines can be formed and during ambiguity resolution the *baseline* approach has 2 degrees of freedom (i.e., 5 observations - 3 coordinate unknowns) during its two searches. The *direct* approach has 7 degrees of freedom during its one search (i.e., 10 observations - 3 attitude unknowns).

The primary disadvantage of the *direct* approach is that it relies on the rigidity of the antenna array. Errors can result if the antennas are not rigidly mounted (i.e. the antenna array changes shape or size). Also, as we will see later, the Kalman filter transition matrix, process noise matrix and design matrix are more complex than similar matrices for the *baseline* approach.

A disadvantage of using non-dedicated GPS receivers in the design is that at least three (if height is known) or four GPS satellites must be tracked by each GPS receiver if simultaneous carrier phase and pseudorange measurement amongst the three or four receivers is desired. However, low elevation satellites (<15°) can be included in the position and timing computations within the receiver, while higher elevation satellites (>15°) are only used in the separate attitude computations.

The objective of this research is to develop a real-time attitude determination system that directly estimates the attitude parameters using phase and pseudorange observations from non-dedicated OEM GPS receivers. The goal is to design and build a system suitable for a wide range of applications using off-the-shelf GPS components. Design criteria include: portability (with a small antenna array), easy adaptability to new GPS receivers, utilizing low-cost components, running on a Pentium computer under DOS or Windows, robust ambiguity resolution, and the ability to detect cycle slips and correct ambiguities on-the-fly.

1.2 Project Background

The system developed during the thesis research has roots going back to 1991. In 1991, the Defence Research Establishment Suffield (DRES) of the Canadian Department of National Defence initiated an investigation into the use of low-cost GPS technology for real-time heading determination of an unmanned land vehicle. The investigation was conducted by Pulsearch Navigation Systems, with the author as the primary technical project engineer. The investigation lead to the design and testing of an integrated heading system comprised of two Leica GPS Engines with a 2 metre antenna spacing, a magnetic compass, a rate gyro and an odometer (Cannon et al., 1992). Investigated were the dynamic and static accuracies achievable using the system in an off-road enviroment. The accuracy requirements for the heading determined while underway were 10 mrad and 4 mrad following a ten second stop. Following the completion of the project in 1993, Pulsearch was asked to submit a proposal to design and build a three-dimensional attitude system based on low-cost GPS receivers and sensors. However, before the contract could be awarded, funding was withdrawn for the project. Nevertheless, the author had decided to pursue three dimensional attitude determination as a thesis topic and proceeded with research and development on his own. During 1994, an Euler angle based system was developed by the author, but subsequent testing revealed instabilities typical of the Euler angle parameterization. The author adopted a quaternion parameterization in late 1994

following Axelrad and Ward (1994) and development continued into 1995. The final system met all of the design criteria and results exceeded the original DRES specification for heading while using a baseline one fifth of that employed in the original research.

1.3 Thesis Outline

In Chapter 2, coordinate transformations and attitude parameterizations are discussed. The Euler angle, direction cosine and quaternion representations of three axis attitude are discussed along with transformations between the three representations. The Earth-fixed, local-level and body frames are defined and rotation matrices between the frames are derived. The coordinate frames, the transformations and attitude representations are fundamental to developments in subsequent chapters.

In Chapter 3, the Global Positioning System (GPS) and its application to attitude determination is discussed. A description of GPS is given followed by a summary of GPS receivers. A discussion of GPS pseudorange and carrier phase models and their error sources is given with emphasis on their role in attitude determination. Single and double difference models are examined along with the interferometric models.

In Chapter 4, attitude determination using GPS is covered. The Kalman filter equations are reviewed. The kinematic equations for attitude are presented and Kalman filter elements for quaternion based attitude estimation are given. A quality control method is examined. The double difference interferometric pseudorange and carrier phase models are linearized. The propagation of the quaternion covariance matrix to the Euler angle covariance matrix is derived.

In Chapter 5, GPS carrier phase ambiguity resolution is investigated. A technique based on the Least Squares Ambiguity Search Technique (LSAST) is presented. Methods for defining the ambiguity search area and determining potential search solutions are given. Techniques for testing potential solutions are described.

In Chapter 6, the attitude system design and implementation is presented. The hardware integration and software design are discussed. A description of the test vehicle and system installation is given.

In Chapter 7, the field tests are described, the results presented and analyses given. The real-time results from three different tests are presented and in the first two tests compared against post-mission results determined using SEMIKIN™. The first test was a one hour static test conducted with NovAtel, Leica and Motorola receivers. The second test was a dynamic test over level ground again conducted with the same three sets of receivers. The final test was a dynamic test conducted over hilly terrain using the NovAtel receivers.

Chapter 8, contains the conclusions and recommendations for further development of the real-time attitude system.

CHAPTER 2

COORDINATE FRAMES

2.1 Mathematical Background

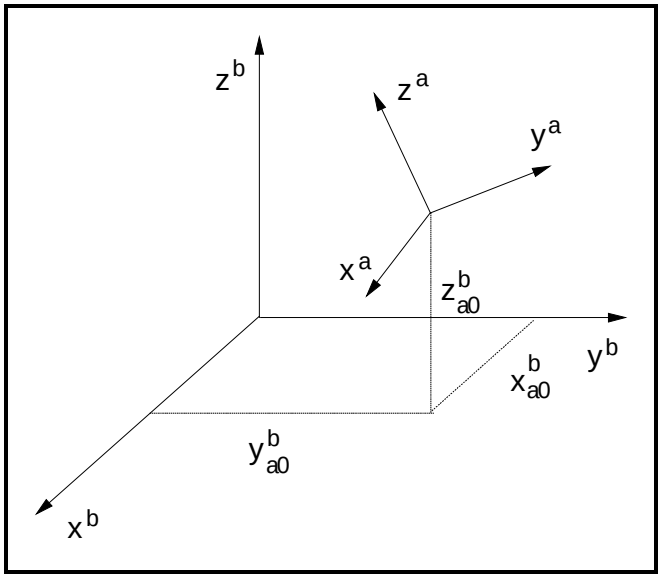

Figure 2.1 - Relationship Between Two Coordinate Frames

Coordinate transformations between three-dimensional Cartesian coordinate frames have three components: rotations, translations, and scale. The relationship of coordinate frame “a” and a second coordinate frame “b” as shown in Figure 2.1 is described by the Helmert relationship given in equation 2.1 (Hofmann-Wellenhof et al., 1992).

$$\mathbf{r}_b = s\mathbf{R}_a^b \mathbf{r}_a + \mathbf{r}_{a0}^b \quad (2.1)$$

where s …is the scale factor,

$\mathbf{R}_a^b$ …is the rotation matrix from coordinate frame a to coordinate frame b,

and $\mathbf{r}_{a0}^b$ …is the translation vector described as the position vector of the origin of the coordinate system "a" as expressed in the coordinate frame of "b".

Provided that both coordinate frames "a" and "b" are orthogonal, the rotation matrix has the property of orthogonality such that

$$(\mathbf{R}_a^b)^{-1} = (\mathbf{R}_a^b)^T \quad (2.2)$$

and, consequently,

$$\mathbf{R}_a^b \, (\mathbf{R}_a^b)^T = \mathbf{I} \quad (2.3)$$

Wertz (1978) mentions five representations of three axis attitude including: direction cosine matrix, Euler axis/angle, Gibbs Vector, Euler angles, and quaternions. Of particular interest within this research are the direction cosine matrix, Euler angle, and quaternion representations.

2.1.1 Direction Cosine Matrix

The rotation matrix $\mathbf{R}_a^b$ is a 3 x 3 matrix, consisting of nine unique parameters. Each of these parameters is the cosine of the angle between an axis of coordinate frame "a" and an axis of frame "b". For example, element (1,1) of $\mathbf{R}_a^b$ is the cosine of the angle between x_a and x_b. For attitude determination, the rotation matrix $\mathbf{R}_a^b$ is often referred to as the direction cosine matrix and is considered the fundamental quantity specifying the orientation of a rigid body (ibid.). Direction cosine matrices completely describe the

orientation of one coordinate frame with respect to another without singularities unlike the Euler angle parameterization. The direction cosine matrix by itself does not contain trigonometric functions making direction cosine matrices attractive over other parameterizations for use in computer applications because of potential improvements in computational speed and accuracy. The main disadvantage of the direction cosine parameterization of attitude is that it contains nine parameters, whereas the Euler angle parameterization has three parameters and the quaternion parameterization has four.

2.1.2 Euler Angles

Leonhard Euler (1707-1783), a Swiss mathematician, showed that a maximum of three successive rotations along the coordinate axes were necessary to rotate one coordinate frame into second coordinate frame. The rotation angles are referred to as the Euler angles. The rotation about the x, y and z axes by an angle α can be represented as a direction cosine matrix. Equations 2.4, 2.5 and 2.6 give the explicit form of the primitive direction cosine matrices for right handed rotations about the x, y and z axes, respectively.

$$\mathbf{R}_1(\alpha) = \begin{bmatrix} 1 & 0 & 0 \\ 0 & \cos\alpha & -\sin\alpha \\ 0 & \sin\alpha & \cos\alpha \end{bmatrix} \tag{2.4}$$

$$\mathbf{R}_2(\beta) = \begin{bmatrix} \cos\beta & 0 & \sin\beta \\ 0 & 1 & 0 \\ -\sin\beta & 0 & \cos\beta \end{bmatrix} \tag{2.5}$$

$$\mathbf{R}_3(\gamma) = \begin{bmatrix} \cos\gamma & -\sin\gamma & 0 \\ \sin\gamma & \cos\gamma & 0 \\ 0 & 0 & 1 \end{bmatrix} \tag{2.6}$$

The product of direction cosine matrices is an orthogonal direction cosine matrix. Using the primitive direction cosines, the Euler angles can be represented by a single direction cosine matrix through a series of three matrix multiplications. Depending on the order of

the rotations from one coordinate system to another, there are twelve possible sets of Euler angles, and hence twelve direction cosine matrices possible from these Euler angles. Euler angles are useful for describing the attitude of one coordinate frame with respect to another because of the clear physical interpretation of the angles. They are used for system input and output, but are a poor choice for computer computations because of the need for trigonometric functions when forming the direction cosine matrix in terms of the Euler angles. In addition, depending on how the sequence of rotations from one frame to the other are performed, Euler angles will have a singularity at particular orientations (Giardina et al., 1981). An example of this is for the 3-1-2 rotation sequence for yaw, pitch, and roll described later in Section 2.4.1. This particular sequence exhibits a singularity when the body has a 90 degree pitch angle (i.e. the yaw and roll angles are undefined). This is a serious disadvantage in software development, since additional logic is necessary to guard against the conditions that cause the singularity. In addition, an attitude system based on the 3-1-2 rotation sequence would not be suitable for missile, fighter aircraft, or spacecraft. This is the main reason why the direction cosine or the quaternion parameterizations are preferred for system computations and the Euler angles are reserved for system input and output.

2.1.3 Quaternions

Quaternions, also referred to as Euler symmetric parameters, are based on Euler's theorem that given two coordinate systems, there is one invariant axis, along which measurements are the same in both coordinate systems and that it is possible to move from one coordinate system to the other through one rotation β about that invariant axis (Crenshaw, 1994). The invariant axis is referred to as the Euler axis. Given a unit vector **e** along the Euler axis, the quaternion is defined to be

$$\mathbf{q} = \begin{bmatrix} \mathbf{e}\sin\frac{\beta}{2} \\ \cos\frac{\beta}{2} \end{bmatrix}. \qquad 2.7$$

Expanding the vector **e** gives

$$\mathbf{q} = \begin{bmatrix} q_1 \\ q_2 \\ q_3 \\ q_4 \end{bmatrix} = \begin{bmatrix} e_x \sin\frac{\beta}{2} \\ e_y \sin\frac{\beta}{2} \\ e_z \sin\frac{\beta}{2} \\ \cos\frac{\beta}{2} \end{bmatrix}. \tag{2.8}$$

The primitive quaternions representing rotations about the x, y, and z axis of vector **e** are given in equations 2.9, 2.10 and 2.11 respectively

$$\mathbf{q}_1(\alpha) = \begin{bmatrix} \sin\frac{\alpha}{2} \\ 0 \\ 0 \\ \cos\frac{\alpha}{2} \end{bmatrix}, \tag{2.9}$$

$$\mathbf{q}_2(\beta) = \begin{bmatrix} 0 \\ \sin\frac{\beta}{2} \\ 0 \\ \cos\frac{\beta}{2} \end{bmatrix}, \tag{2.10}$$

$$\mathbf{q}_3(\gamma) = \begin{bmatrix} 0 \\ 0 \\ \sin\frac{\gamma}{2} \\ \cos\frac{\gamma}{2} \end{bmatrix}. \tag{2.11}$$

When the two coordinate systems are parallel, β becomes zero, reducing the quaternion to

$$\mathbf{q} = \begin{bmatrix} 0 \\ 0 \\ 0 \\ 1 \end{bmatrix}. \tag{2.12}$$

As we increase the angle of rotation β of one coordinate system relative to the other and β reaches 180°, the quaternion becomes

$$\mathbf{q} = \begin{bmatrix} e_x \\ e_y \\ e_z \\ 0 \end{bmatrix}. \tag{2.13}$$

As the rotation of one coordinate system relative to the second exceeds 180° the sign of q_4 becomes negative. The four parameters of the quaternion are not independent. In all cases they satisfy the following equation

$$q_1^2 + q_2^2 + q_3^2 + q_4^2 = 1\ . \tag{2.14}$$

The attitude defined by **q** and by **-q** are identical, namely:

$$\mathbf{q} = (-\mathbf{q})\,. \tag{2.15}$$

The inverse of a quaternion **q** corresponds to a rotation in an opposite direction

$$\mathbf{q}^{-1} = \begin{bmatrix} -q_1 \\ -q_2 \\ -q_3 \\ q_4 \end{bmatrix}. \tag{2.16}$$

The direction cosine matrix expressed in terms of the quaternion parameters is

$$\mathbf{R} = \begin{bmatrix} q_1^2 - q_2^2 - q_3^2 + q_4^2 & 2(q_1q_2 + q_3q_4) & 2(q_1q_3 - q_2q_4) \\ 2(q_1q_2 - q_3q_4) & -q_1^2 + q_2^2 - q_3^2 + q_4^2 & 2(q_2q_3 + q_1q_4) \\ 2(q_1q_3 + q_2q_4) & 2(q_2q_3 - q_1q_4) & -q_1^2 - q_2^2 + q_3^2 + q_4^2 \end{bmatrix}. \quad 2.17$$

The quaternion parameters expressed in terms of the direction cosine matrix parameters are (Wertz, 1978)

$$\begin{bmatrix} q_1 \\ q_2 \\ q_3 \\ q_4 \end{bmatrix} = \begin{bmatrix} \frac{1}{4q_4}(R(2,3) - R(3,2)) \\ \frac{1}{4q_4}(R(3,1) - R(1,3)) \\ \frac{1}{4q_4}(R(1,2) - R(2,1)) \\ \frac{1}{2}(1 + R(1,1) + R(2,2) + R(3,3))^{\frac{1}{2}} \end{bmatrix}. \quad 2.18$$

If denominator (q_4) of the equations for q_1, q_2, or q_3 is close to zero, the quaternion parameters can be computed using either equations 2.19, 2.20, or 2.21. A denominator close to zero can result in numerical ill conditioning and loss of accuracy. The alternate equations for expression of the quaternion parameters in terms of the direction cosine matrix parameters are

$$\begin{bmatrix} q_1 \\ q_2 \\ q_3 \\ q_4 \end{bmatrix} = \begin{bmatrix} \frac{1}{2}(1 + R(1,1) - R(2,2) - R(3,3))^{\frac{1}{2}} \\ \frac{1}{4q_1}(R(1,2) + R(2,1)) \\ \frac{1}{4q_1}(R(3,1) + R(1,3)) \\ \frac{1}{4q_1}(R(3,2) - R(2,3)) \end{bmatrix}, \quad 2.19$$

$$\begin{bmatrix} q_1 \\ q_2 \\ q_3 \\ q_4 \end{bmatrix} = \begin{bmatrix} \frac{1}{4q_2}(R(1,2)+R(2,1)) \\ \frac{1}{2}(1+R(2,2)-R(1,1)-R(3,3))^{\frac{1}{2}} \\ \frac{1}{4q_2}(R(2,3)+R(3,2)) \\ \frac{1}{4q_2}(R(1,3)-R(3,1)) \end{bmatrix}, \tag{2.20}$$

$$\begin{bmatrix} q_1 \\ q_2 \\ q_3 \\ q_4 \end{bmatrix} = \begin{bmatrix} \frac{1}{4q_3}(R(1,3)+R(3,1)) \\ \frac{1}{4q_3}(R(2,3)+R(3,2)) \\ \frac{1}{2}(1+R(3,3)-R(1,1)-R(2,2))^{\frac{1}{2}} \\ \frac{1}{4q_3}(R(2,1)-R(1,2)) \end{bmatrix}. \tag{2.21}$$

Two individual rotations can be combined using quaternion notation with an operation referred to as quaternion composition by Axelrad and Ward (1994). Given the direction cosine operation

$$\mathbf{R}_a^c = \mathbf{R}_b^c \mathbf{R}_a^b, \tag{2.22}$$

a similar operation for quaternions can be accomplished by

$$\mathbf{q}_a^c = \mathbf{q}_b^c \otimes \mathbf{q}_a^b, \tag{2.23}$$

and expanding yields

$$\mathbf{q}_a^c = \begin{bmatrix} q_1 \\ q_2 \\ q_3 \\ q_4 \end{bmatrix}_a^c = \begin{bmatrix} q_4 & q_3 & -q_2 & q_1 \\ -q_3 & q_4 & q_1 & q_2 \\ q_2 & -q_1 & q_4 & q_3 \\ -q_1 & -q_2 & -q_3 & q_4 \end{bmatrix}_b^c \begin{bmatrix} q_1 \\ q_2 \\ q_3 \\ q_4 \end{bmatrix}_a^b. \tag{2.24}$$

Quaternions are useful for attitude parameterization because they lack the singularities exhibited by the Euler angle parameterization. Also the direction cosine matrix expressed

in terms of quaternions does not contain trigonometric functions, providing potential speed and accuracy improvements when used in software. However, quaternions lack a clear, easily visualized physical meaning, which is the main reason the Euler angles are usually relied upon for system input and output. Quaternions for attitude parameterization are a useful compromise, combining the stability of the direction cosine parameterization while only having four parameters versus the nine of the direction cosine and three for the Euler angle parameterization.

2.2 Earth-fixed Frame

The Earth-fixed frame is non-inertial, it is fixed to the Earth and rotates with it. The origin of the Earth-fixed coordinate system is at centre of mass of the Earth, with the z-axis coincident with the mean spin axis of Earth, positive towards the north celestial pole. The x-axis is in the equatorial plane pointing towards the mean meridian of Greenwich, and the y-axis completes the right handed Cartesian coordinate system. Figure 2.2 illustrates the Earth-fixed frame.

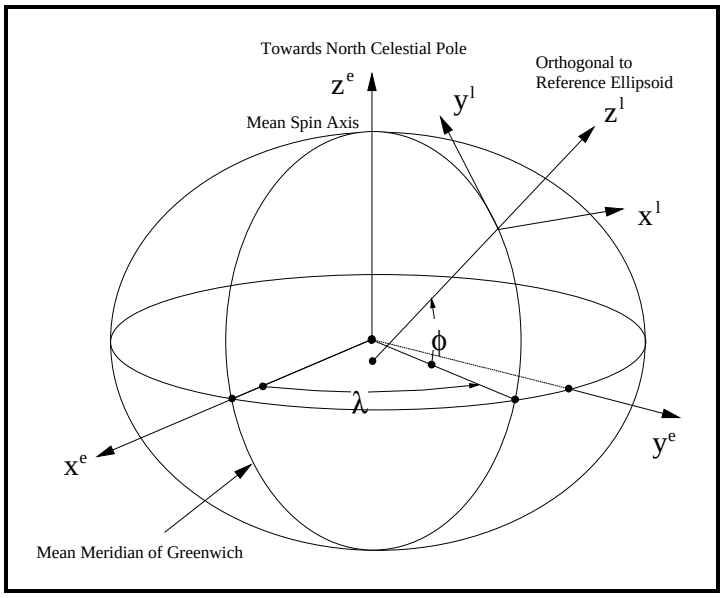

Figure 2.2 - Earth-fixed Coordinate Frame

The Earth-fixed frame rotates with the Earth at a rate of $7.2921151467 \times 10^{-5}$ radians per second. The Earth-fixed coordinate frame is the same as the Earth Centred Earth Fixed

(ECEF) Cartesian coordinate system also referred to as the Conventional Terrestrial (CT) system (Wells et al., 1986) used for GPS position computations. The current realization of the Earth-fixed coordinate frame for this research is defined by the WGS84 datum.

The WGS84 datum has an ellipsoid associated with it. The semi-major axis and semi-minor axis of the ellipsoid are (DMA, 1987)

$$a = 6378137.0m, \tag{2.25}$$

$$b = 6356752.3142m. \tag{2.26}$$

An arbitrary position on the ellipsoid of the WGS-84 datum can be represented by a set of curvilinear coordinates referred to as the geodetic coordinates. The geodetic latitude (ϕ) is the right handed angle between the plane perpendicular to the z axis of the Earth-fixed system and the ellipsoid normal measured along a meridian. The geodetic longitude (λ) is the right handed angle from the Greenwich (zero) meridian to the meridian passing through point P, measured in the plane perpendicular to the z axis of the Earth-fixed system. The height (h) of point P is measured along the ellipsoid normal, and is the distance from the ellipsoid to the point. The relationship between the Cartesian and geodetic coordinates of the Earth-fixed system are (Vanicek and Krakiwsky, 1986)

$$\begin{bmatrix} x \\ y \\ z \end{bmatrix}^e = \begin{bmatrix} (N+h)\cos\phi\cos\lambda \\ (N+h)\cos\phi\sin\lambda \\ \left(\frac{Nb^2}{a^2}+h\right)\sin\phi \end{bmatrix}, \tag{2.27}$$

where N is the prime vertical radius of curvature at P and is computed from

$$N = \frac{a}{\left(1-e^2\sin^2\phi\right)^{\frac{1}{2}}}, \tag{2.28}$$

and where e is the eccentricity of the ellipsoid and is computed from

$$e^2 = \frac{a^2 - b^2}{a^2}. \qquad 2.29$$

2.3 Local-level Frame

The local-level frame is useful when modelling the direction and attitude of a vehicle. Its origin coincides with the phase centre of GPS antenna number 1 of the attitude array, with the z-axis normal to the reference ellipsoid, pointing upwards and the y-axis pointing towards geodetic north. The x-axis completes the right handed Cartesian coordinate system by pointing east. Figure 2.3 illustrates the local-level frame and its relationship relative to the Earth-fixed frame.

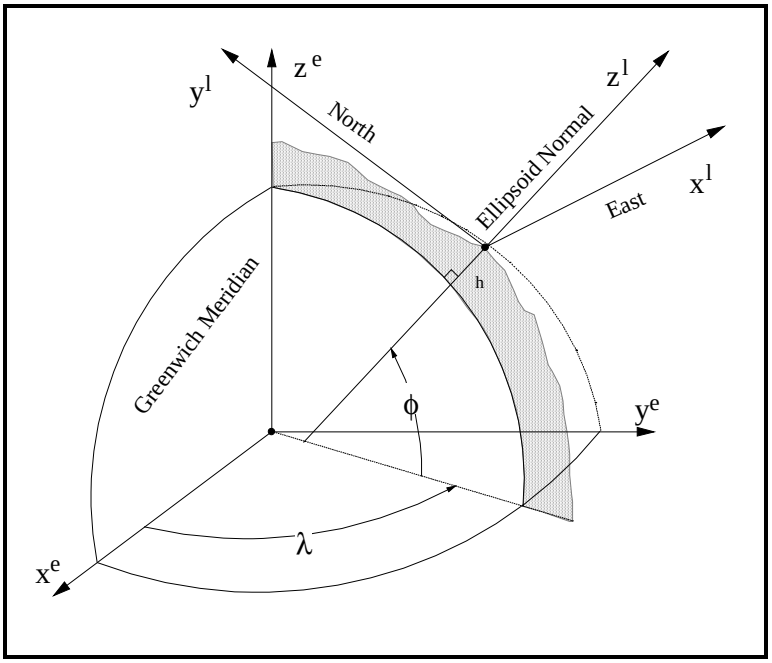

Figure 2.3 - Local-level Coordinate Frame

2.3.1 Relationship Between Local-level and Earth-fixed Frames

The transformation of a vector **r** from the local-level frame to the Earth-fixed frame is accomplished using

$$\mathbf{r}_e = \mathbf{R}_l^e \mathbf{r}_l + \mathbf{r}_{e_0}, \tag{2.30}$$

where $\mathbf{r}_{e_0}$ represents the Earth-fixed frame coordinates of the local-level frames origin and the rotation matrix $\mathbf{R}_l^e$ is given by (Wong, 1988)

$$\mathbf{R}_l^e = \mathbf{R}_3\left(-\lambda - \frac{\pi}{2}\right)\mathbf{R}_1\left(\phi - \frac{\pi}{2}\right). \tag{2.31}$$

Expanding equation 2.31 yields

$$\mathbf{R}_l^e = \begin{bmatrix} -\sin(\lambda) & -\cos(\lambda)\sin(\phi) & \cos(\lambda)\cos(\phi) \\ \cos(\lambda) & -\sin(\lambda)\sin(\phi) & \sin(\lambda)\cos(\phi) \\ 0 & \cos(\phi) & \sin(\phi) \end{bmatrix}. \tag{2.32}$$

The rotation matrix for transforming a vector r from the Earth-fixed to the local-level frame can be formed by transposing $\mathbf{R}_l^e$:

$$\mathbf{R}_e^l = (\mathbf{R}_l^e)^T. \tag{2.33}$$

Expanding equations 2.32 and 2.33,

$$\mathrm{R}_e^l = \begin{bmatrix} -\sin(\lambda) & \cos(\lambda) & 0 \\ -\cos(\lambda)\sin(\phi) & -\sin(\lambda)\sin(\phi) & \cos(\phi) \\ \cos(\lambda)\cos(\phi) & \sin(\lambda)\cos(\phi) & \sin(\phi) \end{bmatrix}. \tag{2.34}$$

2.3.2 Wander Frame

The local-level y axis is always pointing towards geodetic north. At very high latitudes, a large rotation about the z axis is necessary to maintain the orientation of the local-level frame whenever the longitude of the origin changes (Wong, 1988). The wander frame is used in this case, since the y axis is not slaved to geodetic north. Instead it wanders off north at a predefined rate. The wander angle (α) is defined as the angle between the y

axis of the wander frame and geodetic north and is equal to the meridian convergence from the startup location:

$$\dot{\alpha} = -\dot{\lambda}\sin\phi\,. \tag{2.35}$$

Within this research, the wander angle mechanization is not used for attitude determination. However, it should be considered for any potential polar application.

2.4 Body Frame

The body frame is an idealized orthogonal frame related to the sensors of the navigation system. It is considered idealized because it is free of manufacturing inaccuracies associated with sensor arrays. Its orientation and origin are arbitrary and normally defined by the designer of the navigation system. For this report the body frame has its origin at the phase centre of GPS antenna 1 which also corresponds to the origin of the local-level frame. The x and y axis lie on an imaginary plane approximately level with the antenna arrays mounting plate. The y axis points in the forward direction of the plate, while the z axis points upwards, normal to the imaginary plane passing through antenna 1. The x-axis completes the right handed system by pointing to the right of the plate. Figure 2.4 illustrates the relationship between the body frame and the local-level frame.

Two methods can be used to measure the body frame coordinates of the GPS antennas. The first is often called a self-survey, with GPS measurements used to calculate the relationship between the antennas and then conventional means are used to establish the relationship between the antenna array and the vehicle. The second technique involves using conventional measurements to establish both the relationship between the antennas and between the antenna array and the vehicle. Here the body frame coordinates of the GPS antennas are measured relative to representations of the body frame x and y axis scribed onto the antenna array plate or in the absence of a plate, relative to baselines established on the vehicle or the ground in proximity of the vehicle (i.e. dock relative to a ship).

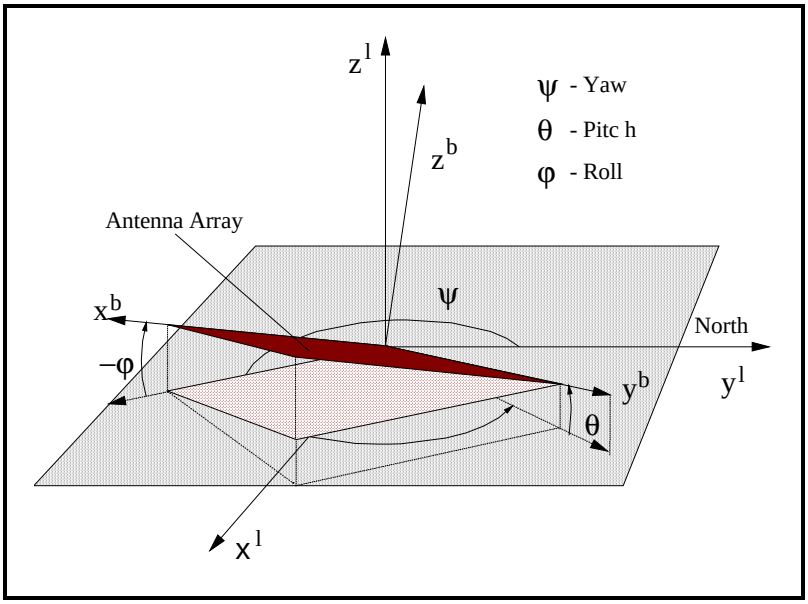

Figure 2.4 - Body Coordinate Frame

Using either technique, body frame measurement errors cause misalignment errors between the actual and theoretical body frame axes, resulting in a non-orthogonal frame. The measurement errors of the body frame coordinates should be minimized and the measurement techniques should be designed with the ultimate use of the attitude system in mind. The relationship between the GPS antenna array and the body frame are illustrated in Figure 2.5.

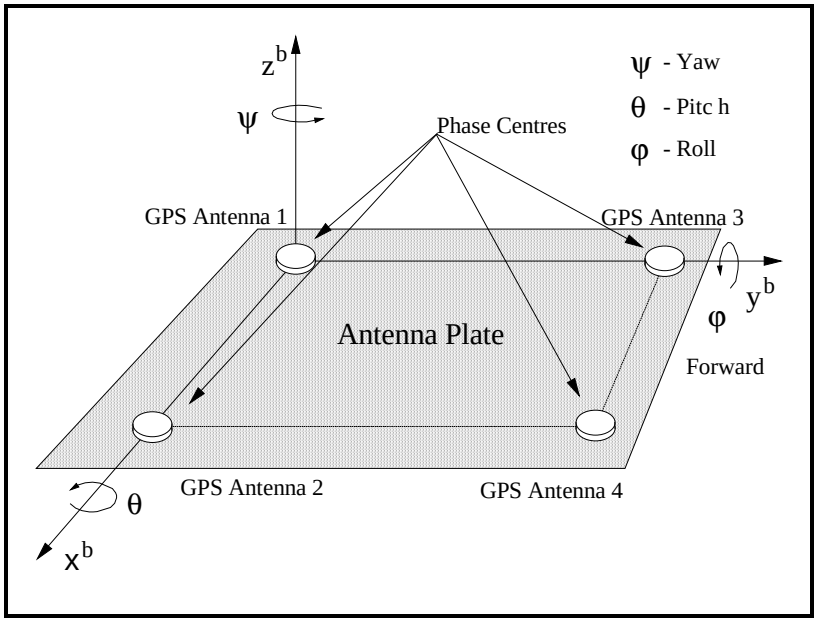

Figure 2.5 - System's Antenna Array

2.4.1 Relationship Between Body and Local-level Frames

By describing the relationship between the body and local-level frames, we are describing the parameterization of the vehicle attitude. A vector **r** is transformed from the local-level coordinate frame to the body frame using the relationship described in equation 2.1. Since the body and local-level frame theoretically share the same origin and scale, the relationship becomes

$$\mathbf{r}_b = \mathbf{R}_l^b \mathbf{r}_l, \tag{2.36}$$

where the direction cosine matrix $\mathbf{R}_l^b$ can be described in terms of quaternions as given in equation 2.17, or in terms of the Euler angles yaw, pitch, and roll. Using primitive direction cosine matrices, the relationship between the Euler angles and the direction cosine matrix can be described twelve ways as mentioned in section 2.1.2. Within this research the transformation from the local-level frame to the body frame is accomplished first by a rotation about the z axis by the yaw angle, then about the x axis by the pitch angle and finally about the y axis by the roll angle, yielding the equation

$$\mathbf{R}_l^b = \mathbf{R}_2(\varphi)\,\mathbf{R}_1(\theta)\,\mathbf{R}_3(\psi). \tag{2.37}$$

This 3-1-2 (i.e. multiply position vector **r** by $\mathbf{R}_3$, then $\mathbf{R}_1$, and then $\mathbf{R}_2$) sequence of rotations is adopted because it is commonly used in geomatics engineering applications. Also, the yaw angle is in the same plane as the heading angle, allowing for a simple conversion between the two angles

$$\text{heading} = 2\pi - \psi. \tag{2.38}$$

The yaw-pitch-roll sequence of rotations is conceptually similar to that found in Van Graas and Braasch (1991) and in VanBronkhorst (1978). They arrive at a different direction cosine matrix representation than the one presented here because their definitions of the body frame and local-level frames are different, resulting in the pitch rotation being about the y axis and the roll rotation about the x axis. Expanding equation 2.37 yields

$$\mathbf{R}_l^b = \begin{bmatrix} \cos\psi\cos\varphi - \sin\psi\sin\theta\sin\varphi & \sin\psi\cos\varphi + \cos\psi\sin\theta\sin\varphi & -\cos\theta\sin\varphi \\ -\sin\psi\cos\theta & \cos\psi\cos\theta & \sin\theta \\ \cos\psi\sin\varphi + \sin\psi\sin\theta\cos\varphi & \sin\psi\sin\varphi - \cos\psi\sin\theta\cos\varphi & \cos\theta\cos\varphi \end{bmatrix}. \tag{2.39}$$

The rotation matrix for transforming a vector **r** from the body to the local-level frame can be formed by transposing $\mathbf{R}_l^b$.

$$\mathbf{R}_b^l = \left(\mathbf{R}_l^b\right)^T. \tag{2.40}$$

Equations 2.39 and 2.40 yield

$$\mathbf{R}_b^l = \begin{bmatrix} \cos\psi\cos\varphi - \sin\psi\sin\theta\sin\varphi & -\sin\psi\cos\theta & \cos\psi\sin\varphi + \sin\psi\sin\theta\cos\varphi \\ \sin\psi\cos\varphi + \cos\psi\sin\theta\sin\varphi & \cos\psi\cos\theta & \sin\psi\sin\varphi - \cos\psi\sin\theta\cos\varphi \\ -\cos\theta\sin\varphi & \sin\theta & \cos\theta\cos\varphi \end{bmatrix}. \tag{2.41}$$

The Euler angles can be determined from the direction cosine matrix presented in equation 2.39 by

$$\theta = \sin^{-1}\left(R_l^b(2,3)\right) \quad , \tag{2.42}$$

$$\psi = \tan^{-1}\left(\frac{-R_l^b(2,1)}{R_l^b(2,2)}\right), \tag{2.43}$$

$$\varphi = \tan^{-1}\left(\frac{-R_l^b(1,3)}{R_l^b(3,3)}\right). \tag{2.44}$$

By examining equations 2.43 and 2.44, it is observed that when the pitch angle is 90°, the denominator of the equations is 0 and the yaw and roll angles cannot be defined, demonstrating that the Euler angle representation is not robust. A more robust conversion from the direction cosine matrix to the Euler angles is established herein using a technique developed in Crenshaw (1994a). For the case where the pitch is 90°, we can write the following

$$R_l^b(1,1) = -R_l^b(3,2) = \cos(\psi + \varphi), \tag{2.45}$$

$$R_l^b(1,2) = R_l^b(3,1) = \sin(\psi + \varphi). \tag{2.46}$$

Combining equations 2.45, and 2.46 yields

$$\psi + \varphi = \tan^{-1}\left(\frac{R_l^b(1,2)}{R_l^b(1,1)}\right). \tag{2.47}$$

Let

$$\alpha = \psi + \varphi, \tag{2.48}$$

$$\beta = \psi - \varphi. \tag{2.49}$$

Therefore

$$\psi = \frac{(\alpha + \beta)}{2}, \tag{2.50}$$

$$\varphi = \frac{(\alpha - \beta)}{2}. \tag{2.51}$$

Trigonometric identities allow us to write

$$\sin\psi\cos\varphi = \frac{1}{2}(\sin\alpha + \sin\beta), \tag{2.52}$$

$$\cos\psi\sin\varphi = \frac{1}{2}(\sin\alpha - \sin\beta), \tag{2.53}$$

$$\cos\psi\cos\varphi = \frac{1}{2}(\cos\alpha + \cos\beta), \tag{2.54}$$

$$\sin\psi\sin\varphi = \frac{1}{2}(-\cos\alpha + \cos\beta). \tag{2.55}$$

Rewriting key members of the direction cosine matrix in equation 2.39 gives

$$R_l^b(1,1) = \frac{1}{2}(1+\sin\theta)\cos\alpha + \frac{1}{2}(1-\sin\theta)\cos\beta, \tag{2.56}$$

$$R_l^b(3,2) = -\frac{1}{2}(1+\sin\theta)\cos\alpha + \frac{1}{2}(1-\sin\theta)\cos\beta, \tag{2.57}$$

$$R_l^b(1,2) = \frac{1}{2}(1+\sin\theta)\sin\alpha + \frac{1}{2}(1-\sin\theta)\sin\beta, \tag{2.58}$$

$$R_l^b(3,1) = \frac{1}{2}(1+\sin\theta)\sin\alpha - \frac{1}{2}(1-\sin\theta)\sin\beta. \tag{2.59}$$

We can now write

$$R_l^b(1,1) + R_l^b(3,2) = (1-\sin\theta)\cos\beta, \tag{2.60}$$

$$R_l^b(1,1) - R_l^b(3,2) = (1+\sin\theta)\cos\alpha, \tag{2.61}$$

$$R_l^b(1,2) + R_l^b(3,1) = (1+\sin\theta)\sin\alpha, \tag{2.62}$$

$$R_l^b(1,2) - R_l^b(3,1) = (1 - \sin\theta)\sin\beta. \tag{2.63}$$

Rearranging the terms yields

$$\tan\alpha = \frac{R_l^b(1,2) + R_l^b(3,1)}{R_l^b(1,1) - R_l^b(3,2)}, \tag{2.64}$$

$$\tan\beta = \frac{R_l^b(1,2) - R_l^b(3,1)}{R_l^b(1,1) + R_l^b(3,2)}. \tag{2.65}$$

Substituting equations 2.64 and 2.65 into equations 2.50 and 2.51 yields

$$\psi = \frac{1}{2}\tan^{-1}\left(\frac{R_l^b(1,2) + R_l^b(3,1)}{R_l^b(1,1) - R_l^b(3,2)}\right) + \frac{1}{2}\tan^{-1}\left(\frac{R_l^b(1,2) - R_l^b(3,1)}{R_l^b(1,1) + R_l^b(3,2)}\right), \tag{2.66}$$

$$\varphi = \frac{1}{2}\tan^{-1}\left(\frac{R_l^b(1,2) + R_l^b(3,1)}{R_l^b(1,1) - R_l^b(3,2)}\right) - \frac{1}{2}\tan^{-1}\left(\frac{R_l^b(1,2) - R_l^b(3,1)}{R_l^b(1,1) + R_l^b(3,2)}\right). \tag{2.67}$$

2.4.2 Relationship Between Quaternions and Euler Angles

Better suited to real-time applications are quaternions (Van Graas et al., 1991). The relationship between the Euler angles and the quaternions is established herein by performing the individual rotations given in equation 2.37 with primitive quaternions instead of primitive direction cosine matrices. Quaternion composition shown in equation 2.23 and 2.24 is used to combine the primitive quaternions:

$$\mathbf{q}_l^b = \mathbf{q}_2(\varphi) \otimes \mathbf{q}_1(\theta) \otimes \mathbf{q}_3(\psi). \tag{2.68}$$

Expanding equation 2.68 yields

$$\mathbf{q}_l^b = \begin{bmatrix} q_1 \\ q_2 \\ q_3 \\ q_4 \end{bmatrix}_l^b = \begin{bmatrix} \cos\left(\frac{\psi}{2}\right)\cos\left(\frac{\varphi}{2}\right)\sin\left(\frac{\theta}{2}\right) - \sin\left(\frac{\psi}{2}\right)\sin\left(\frac{\varphi}{2}\right)\cos\left(\frac{\theta}{2}\right) \\ \sin\left(\frac{\psi}{2}\right)\cos\left(\frac{\varphi}{2}\right)\sin\left(\frac{\theta}{2}\right) + \cos\left(\frac{\psi}{2}\right)\sin\left(\frac{\varphi}{2}\right)\cos\left(\frac{\theta}{2}\right) \\ \sin\left(\frac{\psi}{2}\right)\cos\left(\frac{\varphi}{2}\right)\cos\left(\frac{\theta}{2}\right) + \cos\left(\frac{\psi}{2}\right)\sin\left(\frac{\varphi}{2}\right)\sin\left(\frac{\theta}{2}\right) \\ \cos\left(\frac{\psi}{2}\right)\cos\left(\frac{\varphi}{2}\right)\cos\left(\frac{\theta}{2}\right) - \sin\left(\frac{\psi}{2}\right)\sin\left(\frac{\varphi}{2}\right)\sin\left(\frac{\theta}{2}\right) \end{bmatrix}_l^b . \tag{2.69}$$

A proof of the validity of Euler angle to quaternion conversion can be performed by substitution of the Euler angle representations for the quaternions given in equation 2.69 into quaternion representation of the direction cosine matrix given in equation 2.17. The result of the substitution yields the direction cosine matrix in terms of the Euler angles as given in equation 2.39.

Substitution of the elements of the quaternion representation of the direction cosine matrix given in equation 2.17 into the direction cosine matrix to Euler angle conversions given in equations 2.39 yields the conversion from quaternions to the pitch angle:

$$\theta = \sin^{-1}\left(2\left(q_2 q_3 + q_1 q_4\right)\right). \tag{2.70}$$

A robust equation for the yaw and roll angles can be formed using techniques in Crenshaw (1994b). Rearranging the terms in equation 2.69 and using the definition of α and β given in equations 2.48 and 2.49, respectively, yields

$$q_3 + q_2 = \left(\cos\left(\frac{\theta}{2}\right) + \sin\left(\frac{\theta}{2}\right)\right)\sin\left(\frac{\alpha}{2}\right), \tag{2.71}$$

$$q_3 - q_2 = \left(\cos\left(\frac{\theta}{2}\right) - \sin\left(\frac{\theta}{2}\right)\right)\sin\left(\frac{\beta}{2}\right), \tag{2.72}$$

$$q_4 + q_1 = \left(\cos\left(\frac{\theta}{2}\right) + \sin\left(\frac{\theta}{2}\right)\right)\cos\left(\frac{\alpha}{2}\right), \tag{2.73}$$

$$q_4 - q_1 = \left(\cos\left(\frac{\theta}{2}\right) - \sin\left(\frac{\theta}{2}\right)\right)\cos\left(\frac{\beta}{2}\right), \tag{2.74}$$

where

$$\alpha = 2\tan^{-1}\left(\frac{q_3 + q_2}{q_4 + q_1}\right), \tag{2.75}$$

$$\beta = 2\tan^{-1}\left(\frac{q_3 - q_2}{q_4 - q_1}\right). \tag{2.76}$$

Substituting equations 2.74 and 2.75 into equations 2.49 and 2.50 yields

$$\psi = \tan^{-1}\left(\frac{q_3 + q_2}{q_4 + q_1}\right) + \tan^{-1}\left(\frac{q_3 - q_2}{q_4 - q_1}\right), \tag{2.77}$$

$$\varphi = \tan^{-1}\left(\frac{q_3 + q_2}{q_4 + q_1}\right) - \tan^{-1}\left(\frac{q_3 - q_2}{q_4 - q_1}\right). \tag{2.78}$$

The attitude system developed in this research uses the Euler angles for system input and output, while all internal computations are performed using quaternions. In this section we have developed the direction cosine matrix representation in terms of Euler angles, along with the conversions between Euler angles and quaternions. These are only valid for the 3-1-2 sequence of rotations when rotating from the local-level frame to the body frame and would have to be derived again if a different sequence is used.

2.4.3 Relationship Between Body and Earth-fixed Frames

A vector **r** in the body coordinate frame is transformed to the Earth-fixed frame using the relationship described in equation 2.1. Since the body and Earth-fixed frames share the same scale, the relationship becomes

$$\mathbf{r}_e = \mathbf{R}_b^e \mathbf{r}_b + \mathbf{r}_{e0}, \tag{2.79}$$

where $\mathbf{r}_{e_0}$ represents the body frames origin in the Earth-fixed coordinate system. The direction cosine matrix $\mathbf{R}_b^e$ can be formed by multiplying the $\mathbf{R}_b^l$ and $\mathbf{R}_l^e$ matrices

$$\mathbf{R}_b^e = \mathbf{R}_l^e \mathbf{R}_b^l . \tag{2.80}$$

CHAPTER 3

GLOBAL POSITIONING SYSTEM

The Global Positioning System (GPS) is fully operational and capable of providing accurate positioning, velocity and timing information to an unlimited number of users. In addition to its mainstream functions, GPS is used in applications made possible through the novel use of the basic GPS measurements of pseudorange, carrier phase and phase rate. One such application is attitude determination which relies on the accurate measurement of the GPS carrier phase measurement. The GPS system is described in this chapter along with a summary of the receivers suitable for use in attitude determination systems. The GPS observation equations applicable to attitude determination and their error sources are described and linear combinations of the observation equations are derived.

3.1 System Description

GPS is a satellite based radio navigation system designed for all weather use, 24 hours a day. Designed for the US military, its primary function is to provide position, velocity and timing information to troops. Civilian users have had access to the system since the late 1970s and the number of users and applications have grown steadily, so that currently the number of civilian users far exceed the military users (NRC, 1995). Nevertheless, the system remains primarily a military system operated and controlled by the US Department of Defense (DoD).

GPS currently consists of 24 operational Block II satellites orbiting approximately 20,051 km above the Earth. The orbit planes are inclined 55° with respect to the equator and each satellite has a period of one half of a sidereal day. Each satellite continuously transmits radio navigation data on two carrier frequencies, the L1 carrier at 1575.42 MHz and the L2 carrier at 1227.60 MHz. The carrier frequencies are derived from onboard frequency standards which generate the fundamental L band frequency of 10.23 MHz. The broadcast by the satellite is a spread spectrum signal and each satellite modulates the carriers with two unique pseudorandom noise (PRN) codes. The L1 carrier is modulated with the clear/acquisition code (C/A-code), the precise code (P-code), and data message, while the L2 carrier is only modulated with the P-code and data message. Civilians have full access to the P-code, however when antispoofing (AS) is activated, the P-code is replaced by the military-only Y-code. In addition to the PRN codes, the L1 and L2 carriers are also modulated with the data message which contains the satellite ephemeris, ionospheric modelling parameters, status, system time, and satellite clock information (Hofman-Wellenhof et al., 1994). The GPS system provides users with a variety of observations, including pseudoranges derived from the C/A-code and P-code, and carrier phase observations of the L1 and L2 carriers. However, we are primarily interested in the measurements made by low-cost OEM boards, which at the present time only provide single frequency, L1 derived measurements.

3.2 GPS Receivers

A wide variety of GPS receivers are currently available, from inexpensive handheld units to expensive dual frequency geodetic receivers. Receivers suitable for use within GPS attitude systems can be divided into two classes. The first class contains those dedicated receivers designed specifically for attitude systems which typically feature a single oscillator and either dedicated satellite tracking channels, as is the case with the Ashtech 3DF system (Ferguson et al., 1991), or fast multiplexing channels as is the case of the Trimble TANS Vector (Krucyznski et al., 1995). The use of a common local oscillator within the dedicated receivers results in the ability to theoretically make use of single

difference observations (the biases associated with the common receiver clock cancel out), which have a lower noise than double difference observations. However residual receiver clock biases (line biases) still exist between antenna banks, necessitating special treatment or calibration to remove the line biases. The biases can be caused by different antenna cable lengths and different RF section delays related to each antenna (Lu., 1995). In some cases double differencing is used to remove the line biases, thereby cancelling the advantage of a common oscillator.

A summary of the specification and costs for currently available dedicated receivers is given in Table 3.1.

Table 3.1 - Summary of Dedicated Attitude GPS Receivers

Specification	Ashtech 3DF	Trimble TANS Vector
Channels	24 (6 channels per antenna)	Effective 24
Tracking	Parallel, L1 C/A-Code	Multiplex, L1 C/A-Code
Number of Satellites Tracked	6	6
Physical	195 x 215 x99 mm, 2.5 kg	127x207x56 mm, 1.4 kg
I/O	RS-232, 2 Hz	RS-422, 10 Hz
Power	10 - 36 VDC, 18 Watts	10-40 VDC, 7.5 Watts
Environment	-20° to +55° C	-40° to +50° C
Antenna Type	Microstrip	Microstrip
Accuracy (RMS) **Hdg: Pitch: Roll**	0.13°: 0.23°: 0.23° 1 metre baseline	0.30°: 0.30°: 0.30° 1 metre baseline
Cost in US Dollars	$39,000	$20,000 - $25,000

The second class of receivers used within attitude systems are “off-the-shelf” OEM receivers capable of carrier phase and pseudorange measurement output. The non-dedicated OEM receivers typically integrated within the attitude systems feature 6 or more channels with dedicated tracking of a single satellite on each channel. These receivers are designed to be the building blocks of a variety of positioning, attitude, and timing systems and as such are versatile and can be deployed for applications other than attitude determination. However, the price to be paid for such versatility is that each receiver has a separate clock bias which must either be estimated or removed through differencing. As we will see later, the disadvantage of differencing is the reduction in the number of observation equations and an increase in observation noise. Either way, there are fewer degrees of freedom in the attitude estimation when non-dedicated receivers are used in the attitude system unless the non-dedicated receivers can track more available satellites. Nevertheless, their price, availability and versatility is appealing, and for these reasons the non-dedicated design was chosen for the system developed here. The specifications and cost for available, non-dedicated GPS receivers suitable for integration into attitude systems is given in Table 3.2. The selection of receivers was limited to single frequency, L1, C/A-code parallel channel single board receivers capable of providing pseudorange and phase data at rates of 1 Hz or faster. The single frequency L1 GPS receiver is adequate for attitude determination, whereas for high-accuracy positioning applications, dual frequency receivers with their higher unit cost are becoming more common. The ability to directly determine ionospheric refraction while using dual frequency receivers is not necessary with attitude determination given the relatively short baselines. In addition the short baselines, which are usually of known length, allow the L1 double difference phase ambiguities to be resolved without resorting to a second frequency and wide-laning.

The output rates of many of the non-dedicated receivers rival those of the dedicated receivers and most non-dedicated receivers can track more satellites. In addition, many of

the non-dedicated receivers are capable of tracking more available satellites than the dedicated receivers.

Table 3.2 - Summary of Non-Dedicated GPS Receivers For Attitude Systems

Specification	Ashtech G12	Leica GPS Engine	Motorola VP Oncore	NovAtel 3151	Trimble DSM
Channels	12	6	8	12	8 or 12
Physical Dimensions (mm)	167x100 EuroCard	126x161	100x70	167x100 EuroCard	167x100 EuroCard
I/O	RS-232 20 Hz	TTL 1 Hz	RS-232 1 Hz	RS-232/422 20 Hz	RS-232 2,5,10 Hz
Power	±5 VDC 1.4 Watts	±7 VDC 1.7 Watts	±5 VDC 1.0 Watts	5 VDC, ±12VDC 5.0 Watts	5 VDC 2.5 Watts
Environment	-40° / 70° C	-20° / 70° C	-30° / 85° C	0° / 70° C	-40° / 70° C
Acceleration	20g	> 3g	4g	4g	N/A
Cost in US Dollars	$2,495	$1,500	$1,200	$3,495	$2,000-$3,000

In this research, the 10 channel NovAtel 2151R was used because of its availability. NovAtel has replaced the 2151R with the 12 channel NovAtel 3151R receiver.

3.3 Observation Equations and Error Sources

The GPS receivers used in this research to construction the real-time GPS attitude system provide two primary types of observations. The Motorola Oncore™ (Motorola, 1994), the Leica GPS Engine™ (Magnavox, 1991), and the NovAtel 2151™ (Fenton et al., 1991) are capable of providing L1 C/A-code pseudorange observations and L1 carrier phase

observations. All three employ a Phase Lock Loop or as it is sometimes referred to, a Costas Loop (Van Dierendonck, 1994), to provide carrier phase measurements. Both the GPS Engine™ and Oncore™ provide pseudorange and phase measurements at a rate of 1Hz, while the 2151™ is capable of providing the raw measurements at 10 Hz. In addition, each of these three receivers is capable of internally computing position and velocity from the raw observations. Since each of the receivers used in the GPS attitude system are fully capable of computing position and velocity, the position solutions from the reference receiver of the attitude system were used within the attitude software rather than performing the position computations on the PC. A brief discussion of the GPS pseudorange and carrier phase models and their error sources is given in the following two sections. The emphasis will be on their role within a GPS attitude system for attitude determination rather than position or velocity determination.

3.3.1 Pseudorange Observations

The pseudorange model for one of the attitude receivers and a satellite j at epoch t_k is illustrated in Figure 3.1. Letting α represent a receiver, the pseudorange model can be written as (Lachapelle, 1992):

$$p_\alpha^j = \rho_\alpha^j + d\rho_n + d\rho_{sa} + c\left(dt^j - dT_\alpha\right) + d_{ion}^j + d_{trop}^j + \varepsilon\left(p_{rx}\right) + \varepsilon\left(p_{mult}\right), \qquad 3.1$$

where
- p_α^j …is the pseudorange measurement made from receiver α to satellite j at t_k (m),
- ρ_α^j …is geometric range from antenna α to satellite j at t_k (m),
- $d\rho_n$ …is nominal broadcast orbital error (m),
- $d\rho_{sa}$ …is the error due to selective availability (SA) (m),
- dt^j …is the satellite clock error (m),
- dT_α …is the receiver clock error (m),
- d_{ion}^j …is the ionospheric delay (m),

d^{j}_{trop} …is the tropospheric delay (m),

$\varepsilon(p_{rx})$ …is the error in the pseudorange measurement due to receiver noise (m),

and $\varepsilon(p_{mult})$ …is the error in the pseudorange measurement due to multipath (m).

The geometric range equation expressed in terms of Earth-fixed coordinates is:

$$\rho^{j}_{\alpha} = \left|\mathbf{r}^{j} - \mathbf{r}_{\alpha}\right| = \left[\left(x^{j} - x_{\alpha}\right)^{2} + \left(y^{j} - y_{\alpha}\right)^{2} + \left(z^{j} - z_{\alpha}\right)^{2}\right]^{\frac{1}{2}} \quad , \tag{3.2}$$

where $\mathbf{r}^{j}$ …is satellite position vector referenced to the Earth-fixed frame computed using the broadcast ephemeris at epoch t_k (m),

and $\mathbf{r}_{\alpha}$ …is the position vector for antenna α referenced to the Earth-fixed frame at epoch t_k (m).

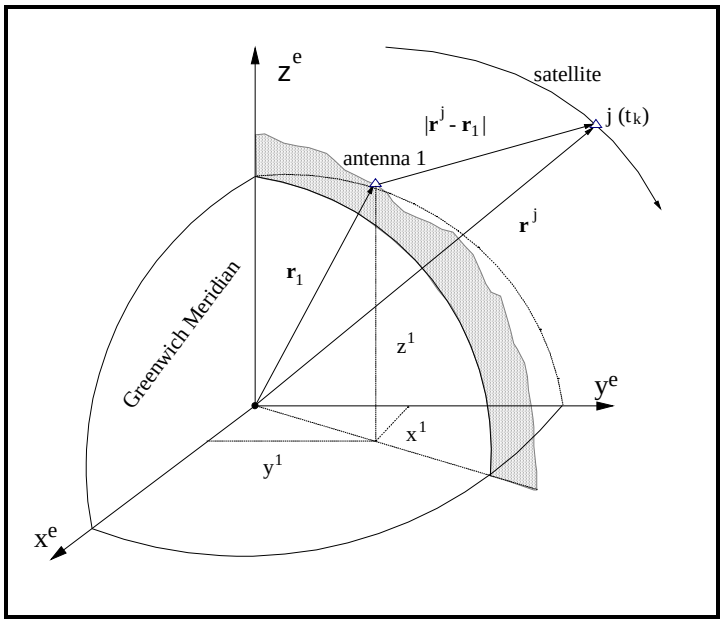

Figure 3.1 - Pseudorange Model

Error terms potentially affecting satellite position determination include those due to nominal or unintentional errors in broadcast ephemeris and those errors intentionally introduced by DoD through the possible addition of SA epsilon in the broadcast ephemeris. Satellite clock and receiver clock error terms represent the offset of the respective clocks from GPS time. A portion of the satellite clock offset is due to the systematic drift in the atomic clocks and can be removed using clock corrections contained in the satellite ephemeris. A significant portion of the satellite clock error is due to intentional varying of the satellite clocks through the SA dither (National Research Council, 1995). Other errors contained in the pseudorange model include atmospheric errors due to ionospheric and tropospheric delays of the GPS signal. All of the above errors to a certain extent can be considered as biases (Wells et al., 1986). If measurements at the attitude system are made in conjunction with those made at a known station, differential techniques are available to minimize the systematic pseudorange errors. If differential corrections are not available, models can help reduce the atmospheric error, but not errors due to the satellite clock or position due SA dither or epsilon (not currently implemented). All three of the GPS receivers used in the attitude system are capable of using RTCM 104 differential corrections to correct its pseudorange observations for position and velocity computations. Differencing techniques introduced in section 3.4 also help reduce systematic errors. With single frequency L1 receivers such as those used with the attitude system, correction terms can be used to remove approximately 50% of the ionospheric delay and most of the tropospheric delay leaving approximately 7 m of ionospheric error and 0.7 m of tropospheric error in the pseudorange (National Research Council, 1995). SA errors in a non-differential corrected pseudorange are approximately 24 m, while non-SA induced satellite clock and ephemeris errors are approximately 3.6 m (ibid.). The receiver clock offset along with the position of antenna 1 can be estimated provided that at least four pseudorange observations are available.

Random effects due to the orbital, clock, and atmospheric errors along with errors due to receiver measurement noise and systematic effects which are not common such as multipath can not be removed through differential corrections or models. Lachapelle et al. (1992) places receiver measurement errors at 1 to 3 m for C/A code receivers while the National Research Council (1995) gives a figure of 0.6 m. Fenton et al. (1991) gives a value of 6 cm for the receiver measurement error from a narrow correlator receiver such as the NovAtel 2151™. Pseudorange multipath can reach 10 m (Lachapelle et al., 1992), with an average figure of 1.2 m given by the National Research Council (1995).

3.3.2 Phase Observations

The carrier phase model for a receiver α and a satellite j at epoch t_k can be written as (Lachapelle et al., 1992):

$$\Phi_\alpha^j = \rho_\alpha^j + d\rho_n + d\rho_{sa} + c\left(dt^j - dT_\alpha\right) + \lambda N_\alpha^j - d_{ion}^j + d_{trop}^j + \varepsilon\left(\Phi_{rx}\right) + \varepsilon\left(\Phi_{mult}\right), \qquad 3.3$$

where Φ_α^j …is the carrier phase measurement made from receiver α to satellite j at tk,

N_α^j …is the carrier phase ambiguity,

$\varepsilon\left(\Phi_{rx}\right)$ …is the error in the carrier phase measurement due to receiver noise,

and $\varepsilon\left(\Phi_{mult}\right)$ …is the error in the carrier phase measurement due to multipath.

Carrier phase measurement errors due to receiver noise vary from less than 1mm to 10 mm, while errors due to multipath are less than 5 cm (ibid.). In contrast to the pseudorange measurement and multipath errors, those for the carrier phase are significantly smaller making it advantageous to use the carrier phase as the primary observation in the attitude system. Loss of lock on the carrier phase by the receiver due to high multipath and/or signal blockage can result in the need to periodically recalulate

the ambiguity term. Incorrect computation of the ambiguity can lead to erroneous attitude determination and significant research throughout the GPS community has been performed to solve this problem. Chapter 5 will expand on one method used for ambiguity resolution.

Critical for accurate attitude determination is the antenna phase stability. The phase model assumes that the antenna act as a single point source, whereas in reality there are deviations from the ideal due to a nonspherical phase response of the antenna element and case mounting point offsets (Tranquilla and Colpitts, 1989). Essentially the measured phase from the same signal coming in at a different elevation or azimuth will be different. A 1mm deviation in antenna receiving phase characteristics can result in a potential deviation of 2.5 mrads in attitude over a 40cm baseline. To minimize the effect of phase centre instability, the same antennas for the array should be used and they should be oriented in the same direction. In addition, the baseline between antennas should be kept as long as feasible. Tranquilla and Colpitts (1989) recommend mapping the phase characteristics of each GPS antenna through a grid of azimuth and elevation angles. The resulting grid could then be used as a lookup table to correct the phase measurements based on azimuth and elevation to the satellite.

The use of large ground planes, such as was used in this research, can also affect phase centre stability. Ground planes are used to limit the antenna response to reflected signals from below the antenna horizon. Tranquilla and Colpitts (1989) point out that this trait is always achieved through phase interference of the edge-diffracted waves from the edges of the ground plane. This effectively forms a large distributed antenna. However, the phase interference that produces the desired amplitude pattern null at the horizon will also cause phase interference throughout the remainder of the observation region of the antenna. Large phase variations can result from the phase interference.

3.4 Differenced Observations

Linear combinations of GPS observations can be advantageous for relative positioning applications such as GPS attitude systems. Differencing is one effective technique for combining observations between receivers and between satellites to take advantage of the correlation of satellite clock, receiver clock, satellite orbit, and atmospheric propagation errors to improve relative positioning accuracy (Wells et al., 1986). For this attitude determining application the pseudorange and carrier phase double difference between receiver and satellites is used. The primary observation is based on the carrier phase double difference because of its significantly better observation accuracy than the pseudorange double difference. The pseudorange double difference is used primarily to provide stability to the attitude filter during start-up when the carrier phase double difference ambiguity has not yet been resolved. This can be particularly effective when using a narrow correlator receiver such as the NovAtel 2151™ with its 10 cm pseudorange measurement error.

3.4.1 Single Difference Observations

There are two types of single differences that help reduce pseudorange and carrier phase observation errors: the single difference between two receivers observing the same satellite, and the single difference between two satellites, observed by the same receiver. Figure 3.2 illustrates the carrier phase single difference between two of the four receivers of the attitude system. The single difference between receivers is of most interest here. In the next section the single differences between receivers will be differenced again for different satellites to form the double differences. The differencing concepts are the same for pseudoranges as they are for carrier phase observations.

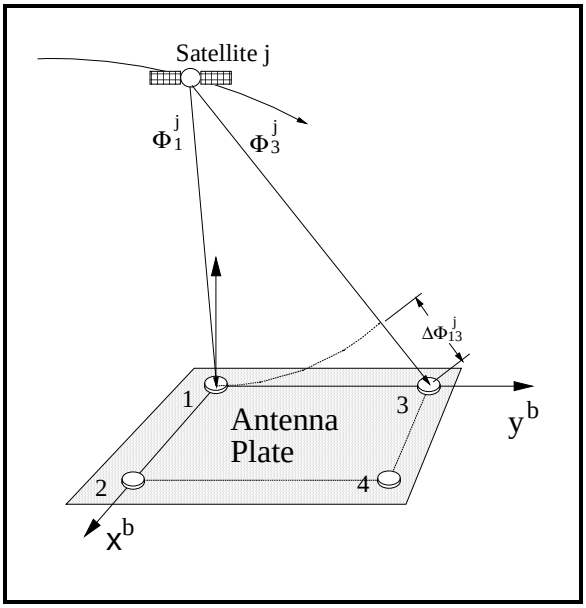

Figure 3.2 - Between Receivers Single Difference

The single differences for pseudoranges between two receivers, 1 and 3 to a GPS satellite j are formed by subtracting the pseudorange observation from receiver 1 (reference receiver) to satellite j from the pseudorange observation from receiver 3 (remote receiver) to satellite j (equation 3.1). Letting α represent the reference receiver and β represent the remote receiver, the between receiver pseudorange single difference takes the form

$$\begin{aligned}\Delta p_{\alpha\beta}^{j} &= \left(p_{\beta}^{j} - p_{\alpha}^{j}\right) \\ &= \left[\rho_{\beta}^{j} + d\rho_{\beta}^{j} + c\left(dt^{j} - dT_{\beta}\right) + d_{ion_{\beta}}^{j} + d_{trop\beta}^{j} + \varepsilon(p)\right] \\ &\quad -\left[\rho_{\alpha}^{j} + d\rho_{\alpha}^{j} + c\left(dt^{j} - dT_{\alpha}\right) + d_{ion\alpha}^{j} + d_{trop\alpha}^{j} + \varepsilon(p)\right],\end{aligned} \tag{3.4}$$

with the Δ denoting a single difference between receivers. Equation 3.4 can be rewritten as

$$\begin{aligned}\Delta p_{\alpha\beta}^{j} &= \left(\rho_{\beta}^{j} - \rho_{\alpha}^{j}\right) + \left(d\rho_{\beta}^{j} - d\rho_{\alpha}^{j}\right) - c\left(dT_{\beta} - dT_{\alpha}\right) \\ &\quad +\left(d_{ion\beta}^{j} - d_{ion\alpha}^{j}\right) + \left(d_{trop\beta}^{j} - d_{trop\alpha}^{j}\right) + \varepsilon(\Delta p),\end{aligned} \tag{3.5}$$

or expressed as a difference

$$\Delta p^{j}_{\alpha\beta} = \Delta\rho^{j}_{\alpha\beta} + \Delta d\rho^{j}_{\alpha\beta} - c\Delta dT_{\alpha\beta} + \Delta d^{j}_{ion_{\alpha\beta}} + \Delta d^{j}_{trop_{\alpha\beta}} + \varepsilon(\Delta p), \qquad 3.6$$

where $\Delta d\rho^{j}_{\alpha\beta}$ …is the orbital error remaining after differencing which is approximately 1 ppm of the distance between antenna 1 and 3.

The single difference for carrier phase observations between two receivers, 1 and 3 to a GPS satellite j are formed by subtracting the carrier phase observation from receiver 3 to satellite j from the carrier phase observation from receiver 1 (reference antenna) to satellite j (equation 3.3). Letting α represent the reference receiver and β represent the remote receiver, the between receiver carrier phase single difference takes the form

$$\begin{aligned}\Delta\Phi^{j}_{\alpha\beta} &= \left(\Phi^{j}_{\beta} - \Phi^{j}_{\alpha}\right) \qquad 3.7\\ &= \left[\rho^{j}_{\beta} + d\rho^{j}_{\beta} + c\left(dt^{j} - dT_{\beta}\right) - d^{j}_{ion_{\beta}} + d^{j}_{trop\beta} + \varepsilon(\Phi)\right]\\ &\quad -\left[\rho^{j}_{\alpha} + d\rho^{j}_{\alpha} + c\left(dt^{j} - dT_{\alpha}\right) - d^{j}_{ion\alpha} + d^{j}_{trop\alpha} + \varepsilon(\Phi)\right],\end{aligned}$$

which can be rewritten as

$$\begin{aligned}\Delta\Phi^{j}_{\alpha\beta} &= \left(\rho^{j}_{\beta} - \rho^{j}_{\alpha}\right) + \left(d\rho^{j}_{\beta} - d\rho^{j}_{\alpha}\right) - c\left(dT_{\beta} - dT_{\alpha}\right) + \lambda\left(N^{j}_{\beta} - N^{j}_{\alpha}\right) \qquad 3.8\\ &\quad -\left(d^{j}_{ion_{\beta}} - d^{j}_{ion\alpha}\right) + \left(d^{j}_{trop\beta} - d^{j}_{trop\alpha}\right) + \varepsilon(\Delta\Phi),\end{aligned}$$

or expressed as a difference

$$\Delta\Phi^{j}_{\alpha\beta} = \Delta\rho^{j}_{\alpha\beta} + \Delta d\rho^{j}_{\alpha\beta} - c\Delta dT_{\alpha\beta} + \lambda\Delta N^{j}_{\alpha\beta} - \Delta d^{j}_{ion_{\alpha\beta}} + \Delta d^{j}_{trop_{\alpha\beta}} + \varepsilon(\Delta\Phi) \quad . \qquad 3.9$$

Examining equation 3.9 reveals that by single differencing between receivers, the satellite clock offset term can be eliminated. In addition, given the short baselines typical of an attitude system, the residual ionospheric and tropospheric refraction effects are negligible.

The single difference between receivers assumes that measurements are made simultaneously amongst the system GPS receivers. However, with non-dedicated GPS receivers the measurements are not simultaneous. Most OEM GPS receiver allow the

user to specify that the receivers clock be steered to GPS time. However, the accuracy of the receiver clock steering are affected by the stability of the receiver clock and the accuracy of the last time estimation. As a result the measurements between receivers can be as far apart as 1 msec (Motorola Oncore™). To mitigate the error that can result, measurement transmit times and thus satellite coordinates are calculated independently for each receiver. Care must be exercised when estimating attitude to insure that the correct set of receiver dependent satellite coordinates are used.

The single difference between different satellites for the same receiver is illustrated in Figure 3.3.

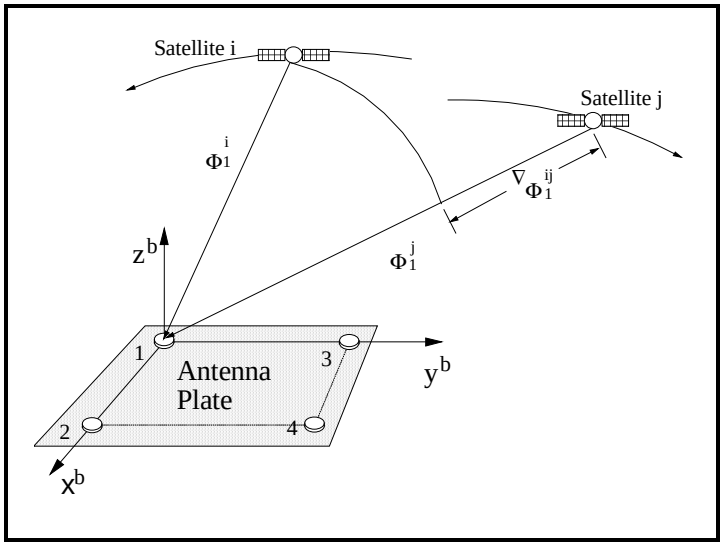

Figure 3.3 - Between Satellites Single Difference

The single difference for carrier phase observations between two satellites i and j to a GPS receiver 1 are formed by subtracting the carrier phase observation from receiver 1 to satellite i (reference satellite) from the carrier phase observation from receiver 1 to satellite j (equation 3.1). Letting α represent the receiver, the between satellite carrier phase single difference model takes the form

$$\begin{aligned}\nabla\Phi_{\alpha}^{ij} &= \left(\Phi_{\alpha}^{j} - \Phi_{\alpha}^{i}\right) \\ &= \left[\rho_{\alpha}^{j} + d\rho_{\alpha}^{j} + c\left(dt^{j} - dT_{\alpha}\right) + \lambda N_{\alpha}^{j} - d_{ion_{\alpha}}^{j} + d_{trop_{\alpha}}^{j} + \varepsilon(\Phi)\right] \\ &\quad -\left[\rho_{\alpha}^{i} + d\rho_{\alpha}^{i} + c\left(dt^{i} - dT_{\alpha}\right) + \lambda N_{\alpha}^{i} - d_{ion\alpha}^{i} + d_{trop\alpha}^{i} + \varepsilon(\Phi)\right],\end{aligned} \tag{3.10}$$

where ∇ denotes a single difference between satellites. Equation 3.10 can be rewritten as

$$\begin{aligned}\nabla\Phi_{\alpha}^{ij} &= \left(\rho_{\alpha}^{j} - \rho_{\alpha}^{i}\right) + \left(d\rho_{\alpha}^{j} - d\rho_{\alpha}^{i}\right) + c\left(dt^{j} - dt^{i}\right) + \lambda\left(N_{\alpha}^{j} - N_{\alpha}^{i}\right) \\ &\quad -\left(d_{ion_{\alpha}}^{j} - d_{ion\alpha}^{i}\right) + \left(d_{trop_{\alpha}}^{j} - d_{trop\alpha}^{i}\right) + \varepsilon(\nabla\Phi),\end{aligned} \tag{3.11}$$

or expressed as a difference

$$\nabla\Phi_{\alpha}^{ij} = \nabla\rho_{\alpha}^{ij} + \nabla d\rho_{\alpha}^{ij} + c\nabla dt^{ij} + \lambda\nabla N_{\alpha}^{ij} - \nabla d_{ion_{\alpha}}^{ij} + \nabla d_{trop_{\alpha}}^{ij} + \varepsilon(\nabla\Phi) \quad . \tag{3.12}$$

Examining equation 3.12 shows that by single differencing between satellite, the receiver clock offset terms are eliminated. By combining the concept of single differencing between receivers with the concept of single differencing between satellites we obtain double differencing.

3.4.2 Interferometric Observation

An alternate means of expressing the between receiver single difference is to use the interferometric model. While similar to the single difference model, certain assumptions can compromise accuracy over longer baseline lengths. However, the interferometry model will prove useful later, when we wish to express the differenced models in terms of the quaternions. GPS interferometry uses the GPS carrier as the radio signal and assumes that its wave front is a flat rather than spherical surface. This assumption is valid only if the distance between the antenna array and GPS satellite is far greater than the distance between the array antennas. Figure 3.4 illustrates the concept of interferometry.

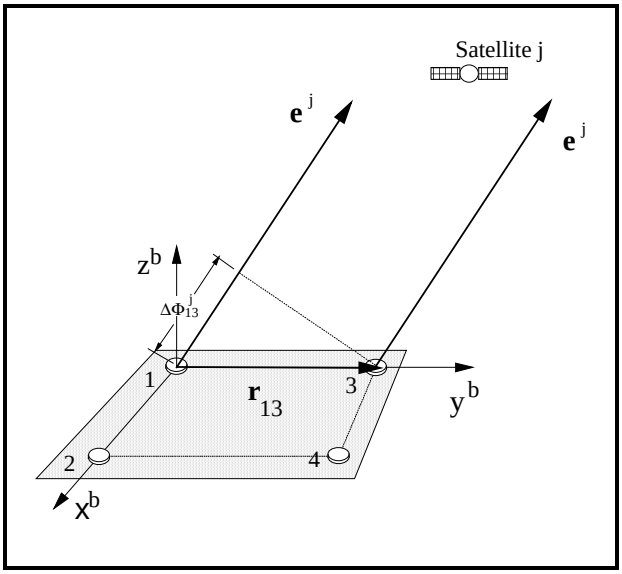

Figure 3.4 - GPS Interferometry

By assuming that the GPS carrier signal has a flat wave front, it follows that a vector from the reference antenna to the satellite is parallel to a vector from the remote antenna to the satellite. Given the geometry illustrated in Figure 3.4, the difference in range between a measurement arriving at the reference antenna and one arriving at the remote antenna is approximated by taking the vector dot product of the vector $\mathbf{r}_{\alpha\beta}$ from the reference antenna (α) to the remote antenna (β) and the unit vector $\mathbf{e}_{\beta}^{j}$ from the remote antenna (β) to the satellite (j) to represent the range difference (Brown et al., 1982)

$$\rho_{\beta}^{j} - \rho_{\alpha}^{j} = \Delta\rho_{\alpha\beta}^{j} \approx -\mathbf{r}_{\alpha\beta} \bullet \mathbf{e}_{\beta}^{j}. \qquad 3.13$$

Simulations were performed using different baseline lengths to test the accuracy of the approximation in equation 3.13. Table 3.3 shows the results of the simulations. The interferometric approximation appears to give satisfactory results for baseline lengths up to 100 m, which is more than adequate for most attitude determination applications. Clearly beyond 100 metres, the interferometric approach introduces significant errors to the single difference model, and the range differencing approach is preferred.

Table 3.3 - Interferometric Approximation Error

Baseline Length	Interferometric Error
2 m	1.0×10^{-7} m
100 m	0.000247 m
1,000 m	0.0247 m
10,000 m	2.476 m
50,000 m	273 m
100,000 m	19737 m

The unit vector $\mathbf{e}_{\beta}^{j}$ for satellite j can be written in terms of Earth-fixed coordinates for the satellite (j) and the remote antenna (β)

$$\mathbf{e}_{\beta}^{j} = \begin{bmatrix} \dfrac{\left(x^{j} - x_{\beta}\right)}{\rho_{\beta}^{j}} \\ \dfrac{\left(y^{j} - y_{\beta}\right)}{\rho_{\beta}^{j}} \\ \dfrac{\left(z^{j} - z_{\beta}\right)}{\rho_{\beta}^{j}} \end{bmatrix}. \qquad 3.14$$

In equation 3.13, the antenna baseline vector is expressed in Earth-fixed coordinates. However, $\mathbf{r}_{\alpha\beta}$ can be written in terms of the antenna array body frame coordinates, utilizing the direction cosine matrix from the body frame to the local-level frame and the rotation matrix from the local-level frame to the Earth-fixed frame

$$\mathbf{r}_{\alpha\beta}^{e} = \mathbf{R}_{l}^{e}\mathbf{R}_{b}^{l}\begin{bmatrix} x_{\beta} - x_{\alpha} \\ y_{\beta} - y_{\alpha} \\ z_{\beta} - z_{\alpha} \end{bmatrix}_{b}. \qquad 3.15$$

Substituting equations 3.14, and 3.15, into equation 3.13 and then replacing the range difference in equation 3.6 yields the GPS interferometry model for the pseudorange

$$\Delta p^{j}_{\alpha\beta} = \begin{bmatrix} \frac{-\left(x^{j} - x_{\alpha}\right)}{\rho^{j}_{\alpha}} \\ \frac{-\left(y^{j} - y_{\alpha}\right)}{\rho^{j}_{\alpha}} \\ \frac{-\left(z^{j} - z_{\alpha}\right)}{\rho^{j}_{\alpha}} \end{bmatrix}^{T} \mathbf{R}^{e}_{l}\mathbf{R}^{l}_{b} \begin{bmatrix} x_{\beta} - x_{\alpha} \\ y_{\beta} - y_{\alpha} \\ z_{\beta} - z_{\alpha} \end{bmatrix}_{b} + \Delta d\rho^{j}_{\alpha\beta} - c\Delta dT_{\alpha\beta} + \Delta d^{j}_{ion_{\alpha\beta}} + \Delta d^{j}_{trop_{\alpha\beta}} + \varepsilon(\Delta p) \quad . \tag{3.16}$$

Replacing the range difference in equation 3.9 yields the GPS interferometry model for the carrier phase

$$\Delta\Phi^{j}_{\alpha\beta} = \begin{bmatrix} \frac{-\left(x^{j} - x_{\alpha}\right)}{\rho^{j}_{\alpha}} \\ \frac{-\left(y^{j} - y_{\alpha}\right)}{\rho^{j}_{\alpha}} \\ \frac{-\left(z^{j} - z_{\alpha}\right)}{\rho^{j}_{\alpha}} \end{bmatrix}^{T} \mathbf{R}^{e}_{l}\mathbf{R}^{l}_{b} \begin{bmatrix} x_{\beta} - x_{\alpha} \\ y_{\beta} - y_{\alpha} \\ z_{\beta} - z_{\alpha} \end{bmatrix}_{b} + \Delta d\rho^{j}_{\alpha\beta} - c\Delta dT_{\alpha\beta} + \lambda\Delta N^{j}_{\alpha\beta} - \Delta d^{j}_{ion_{\alpha\beta}} + \Delta d^{j}_{trop_{\alpha\beta}} + \varepsilon(\Delta\Phi) \quad . \tag{3.17}$$

3.4.3 Double Difference Observations

The double difference between receivers and then satellites is illustrated in Figure 3.5. The reference satellite is “i”, while the reference antenna is “1”. The remote satellite is “j”, while the remote antenna in Figure 3.5 is “3”.

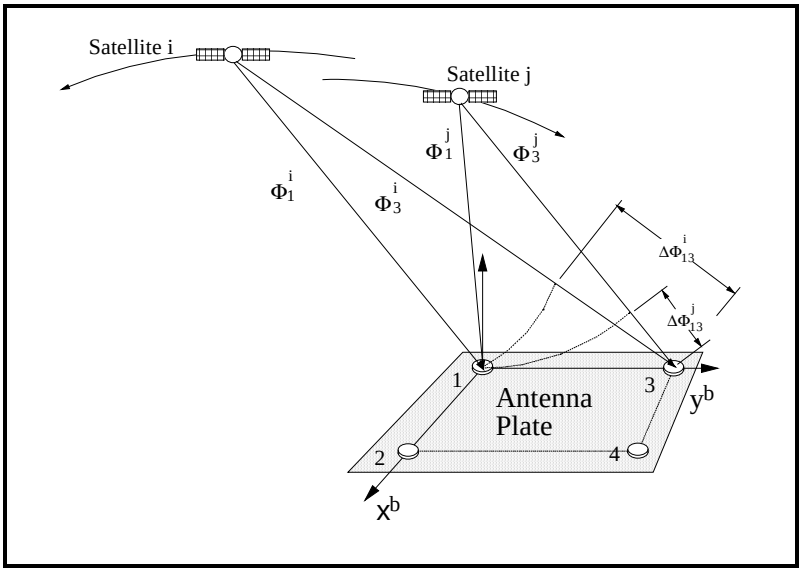

Figure 3.5 - Double Difference

The double difference equation is formed by differencing the 'between receiver' single difference for satellite "i" (equation 3.6) from the 'between receiver' single difference for satellite "j". Letting α represent the reference receiver, and β represent the remote receiver, the pseudorange model takes the form

$$\begin{aligned}\nabla\Delta p_{\alpha\beta}^{ij} &= \Delta p_{\alpha\beta}^{j} - \Delta p_{\alpha\beta}^{i} \\ &= \left[\Delta\rho_{\alpha\beta}^{j} + \Delta d\rho_{\alpha\beta}^{j} - c\Delta dT_{\alpha\beta} + \Delta d_{ion\alpha\beta}^{j} + \Delta d_{trop\alpha\beta}^{j} + \varepsilon(\Delta p)\right] \\ &\quad -\left[\Delta\rho_{\alpha\beta}^{i} + \Delta d\rho_{\alpha\beta}^{i} - c\Delta dT_{\alpha\beta} + \Delta d_{ion_{\alpha\beta}}^{i} + \Delta d_{trop_{\alpha\beta}}^{i} + \varepsilon(\Delta p)\right],\end{aligned} \tag{3.18}$$

which can be rewritten as

$$\begin{aligned}\nabla\Delta p_{\alpha\beta}^{ij} &= \left(\Delta\rho_{\alpha\beta}^{j} - \Delta\rho_{\alpha\beta}^{i}\right) + \left(\Delta d\rho_{\alpha\beta}^{j} - \Delta d\rho_{\alpha\beta}^{i}\right) + \left(\Delta d_{ion_{\alpha\beta}}^{j} - \Delta d_{ion_{\alpha\beta}}^{i}\right) \\ &\quad +\left(\Delta d_{trop\alpha\beta}^{j} - \Delta d_{trop_{\alpha\beta}}^{i}\right) + \varepsilon(\nabla\Delta p),\end{aligned} \tag{3.19}$$

or expressed as a double difference

$$\nabla\Delta p_{\alpha\beta}^{ij} = \nabla\Delta\rho_{\alpha\beta}^{ij} + \nabla\Delta d\rho_{\alpha\beta}^{ij} + \nabla\Delta d_{ion\alpha\beta}^{ij} + \nabla\Delta d_{trop\alpha\beta}^{ij} + \varepsilon(\nabla\Delta p). \tag{3.20}$$

The phase double difference is

$$\begin{aligned}\nabla\Delta\Phi_{\alpha\beta}^{ij} &= \Delta\Phi_{\alpha\beta}^{j} - \Delta\Phi_{\alpha\beta}^{i} \\ &= \left[\Delta\rho_{\alpha\beta}^{j} + \Delta d\rho_{\alpha\beta}^{j} - c\Delta dT_{\alpha\beta} + \lambda N_{\alpha\beta}^{j} - \Delta d_{ion_{\alpha\beta}}^{j} + \Delta d_{trop_{\alpha\beta}}^{j} + \varepsilon(\Delta\Phi)\right] \\ &\quad -\left[\Delta\rho_{\alpha\beta}^{j} + \Delta d\rho_{\alpha\beta}^{i} - c\Delta dT_{\alpha\beta} + \lambda N_{\alpha\beta}^{i} - \Delta d_{ion\alpha\beta}^{i} + \Delta d_{trop_{\alpha\beta}}^{i} + \varepsilon(\Delta\Phi)\right],\end{aligned} \tag{3.21}$$

which can be rewritten as

$$\begin{aligned}\nabla\Delta\Phi_{\alpha\beta}^{ij} &= \left(\Delta\rho_{\alpha\beta}^{j} - \Delta\rho_{\alpha\beta}^{i}\right) + \left(\Delta d\rho_{\alpha\beta}^{j} - \Delta d\rho_{\alpha\beta}^{i}\right) + \lambda\left(N_{\alpha\beta}^{j} - N_{\alpha\beta}^{i}\right) \\ &\quad -\left(\Delta d_{ion_{\alpha\beta}}^{j} - \Delta d_{ion\alpha\beta}^{i}\right) + \left(\Delta d_{trop\alpha\beta}^{j} - \Delta d_{trop_{\alpha\beta}}^{i}\right) + \varepsilon(\nabla\Delta\Phi),\end{aligned} \tag{3.22}$$

or expressed as a double difference

$$\nabla\Delta\Phi_{\alpha\beta}^{ij} = \nabla\Delta\rho_{\alpha\beta}^{ij} + \nabla\Delta d\rho_{\alpha\beta}^{ij} + \lambda\nabla\Delta N_{\alpha\beta}^{ij} - \nabla\Delta d_{ion\alpha\beta}^{ij} + \nabla\Delta d_{trop\alpha\beta}^{ij} + \varepsilon(\nabla\Delta\Phi) \quad . \tag{3.23}$$

In both the pseudorange and phase double difference, the dT receiver clock term has cancelled out. The $\nabla\Delta d\rho$, $\nabla\Delta d_{ion}$, and $\nabla\Delta d_{trop}$ terms are negligible for short reference - remote receiver distances (Lachapelle et al., 1992). The receiver noise term for a double difference observation is twice that for an observation that has not been differenced. Using the values given in sections 3.3.1 and 3.3.2 for the pseudorange and phase observables respectively, the receiver noise term for the double difference pseudorange measured by a L1 C/A code receiver such as the GPS Engine™ or Oncore™ can vary from 2 to 6 m, while it will be approximately 20 cm for a narrow correlator receiver such as the NovAtel 2151™. The receiver noise term for the double difference phase can range from 6 mm to 20 mm for the aforementioned receivers. Multipath errors are also amplified by a factor of 2 for double difference observations if we assume that they are random and affect each antenna differently. Table 3.4 summarizes the residual GPS errors (Cannon, 1992) and their magnitude over a 1 m baseline. Clearly, the magnitude of the residual GPS errors are insignificant compared to receiver measurement errors and multipath errors. This allows us to drop these terms from the double difference equations when applying them to attitude determination. The non-simultaneity of reception times at

receivers can be another source of error if not treated properly. However, by computing transmit times and thus satellite coordinates independently for each receiver and by the careful insertion of these values in the equations the error due to the non-simultaneity of reception times can be reduced.

Table 3.4 - Magnitude of Residual Double Difference GPS Errors

GPS Error Source	Residual Error (ppm)	Residual Error over 1 m
Troposphere - $\nabla\Delta d^{ij}_{trop\alpha\beta}$	0.2 - 0.4	0.2 - 0.4 μm
Ionosphere - $\nabla\Delta d^{ij}_{ion\alpha\beta}$	0.25 - 2	0.25 - 2 μm
Orbit (broadcast) - $\nabla\Delta d\rho^{ij}_{\alpha\beta}$	0.5 - 2	0.5 - 2 μm
Orbit (SA) - $\nabla\Delta d\rho^{ij}_{\alpha\beta_{sa}}$ (not currently implemented)	3 - 5	3 - 5 μm

3.4.4 Double Difference Interferometry

Differencing two GPS interferometry models allows us to form the double difference interferometry model, which is illustrated in Figure 3.6.

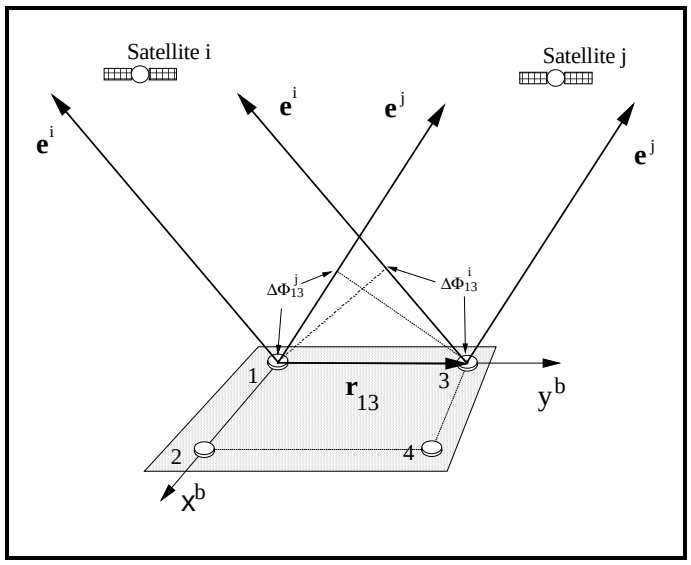

Figure 3.6 - Double Difference Interferometry

The double difference interferometric model for pseudoranges is formed by differencing a GPS interferometric model (equation 3.16) for satellite j from an interferometric model for satellite i and is

$$\nabla\Delta p_{\alpha\beta}^{ij} = -\mathbf{e}_{\beta}^{ij\,T}\mathbf{R}_{l}^{e}\mathbf{R}_{b}^{l}\begin{bmatrix} x_{\beta}-x_{\alpha} \\ y_{\beta}-y_{\alpha} \\ z_{\beta}-z_{\alpha} \end{bmatrix}_{b} + \nabla\Delta d\rho_{\alpha\beta}^{ij} + \nabla\Delta d_{ion\alpha\beta}^{ij} + \nabla\Delta d_{trop\alpha\beta}^{ij} + \varepsilon(\nabla\Delta p), \tag{3.24}$$

where

$$-\mathbf{e}_{\beta}^{ij} = \begin{bmatrix} \dfrac{-(x^{j}-x_{\beta})}{\rho_{\beta}^{j}} + \dfrac{(x^{i}-x_{\beta})}{\rho_{\beta}^{j}} \\ \dfrac{-(y^{j}-y_{\beta})}{\rho_{\beta}^{j}} + \dfrac{(y^{i}-y_{\beta})}{\rho_{\beta}^{j}} \\ \dfrac{-(z^{j}-z_{\beta})}{\rho_{\beta}^{j}} + \dfrac{(z^{i}-z_{\beta})}{\rho_{\beta}^{j}} \end{bmatrix}. \tag{3.25}$$

The local-level to Earth-fixed frame rotation matrix $\mathbf{R}_{l}^{e}$ is given in equation 2.32, and the body frame to local-level frame direction cosine matrix $\mathbf{R}_{b}^{l}$ is given in equations 2.40, and 2.17 in terms of the Euler angles and quaternions, respectively.

The double difference interferometric model for carrier phase observations is

$$\nabla\Delta\Phi_{\alpha\beta}^{ij} = -\mathbf{e}_{\beta}^{ij\,T}\mathbf{R}_{l}^{e}\mathbf{R}_{b}^{l}\begin{bmatrix} x_{\beta}-x_{\alpha} \\ y_{\beta}-y_{\alpha} \\ z_{\beta}-z_{\alpha} \end{bmatrix}_{b} + \nabla\Delta d\rho_{\alpha\beta}^{ij} + \lambda\nabla\Delta N_{\alpha\beta}^{ij} - \nabla\Delta d_{ion\alpha\beta}^{ij} + \nabla\Delta d_{trop\alpha\beta}^{ij} + \varepsilon(\nabla\Delta\Phi) \quad . \tag{3.26}$$

CHAPTER 4

ATTITUDE DETERMINATION

Attitude determination using non-dedicated GPS receivers relies on either the double difference carrier phase model, or the double difference interferometry model. The double difference carrier phase model familiar in static and kinematic positioning is typically used in baseline based attitude determination systems. These systems estimate the baselines in the Earth-fixed coordinate frame, and then the attitude parameters are either directly determined or in the case of redundant information, estimated using the baseline information. However, for the direct estimation of the attitude parameters from the double differences, the interferometry model provides us with a clearer approach. Advantages of either approach include: the greatest potential for accuracy, the absence of satellite and receiver clock states, the elimination of atmospheric terms for short baselines, unnecessary to model line biases, and being expressible in terms of the quaternions. Disadvantages include: the need to estimate ambiguity terms, the correlation amongst the observations, and the increased measurement noise associated with the linear combination of measurements.

A discrete Kalman filter is used to estimate the quaternions and rotation rates, along with their associated variances. There are a number of advantages to using a discrete Kalman filter over other estimators including the epoch-by-epoch least squares technique. The

Kalman filter provides for the estimation of rotation rates and provides a rigorous technique for the propagation of the states and their variances forward in time; an important feature for applications where real-time display of the vehicle attitude is necessary. In addition, the discrete Kalman filter provides a means for the integration of a variety of sensors including inertial sensors such as rate gyros. Also, quality control techniques such as innovations testing are available when using the discrete Kalman filter. Disadvantages include: increased complexity and computational burden, a potential for poor performance if the kinematic modelling is incorrect or incomplete, and difficulty in the initial tuning and the requirement to retune the filter for different dynamic applications.

In this chapter, the discrete Kalman filtering algorithm is outlined and kinematic models for the quaternion parameterization are developed. A Kalman filter transition matrix, process noise matrix and design matrix unique to this research will be developed. The linearized double difference interferometry model as it applies to attitude determination will also be developed. Quality control for real-time Kalman filtering will be discussed. The propagation of quaternion variance-covariance matrix to Euler angle variance-covariance matrix unique to this research is also developed.

4.1 Kinematic Modelling and Attitude Dynamics

The angular movement of the attitude system antenna array can be modelled using either our knowledge of the forces causing the movement or the measurement of the movement in a given three-dimensional coordinate system (Schwarz et al., 1989). The former modelling method is referred to as dynamic modelling and relies on Newton's second law of motion, while the later is referred to as kinematic modelling and is the study of motion regardless of the forces that bring about that motion (Wertz, 1978). With vehicle attitude determination using GPS, we are not measuring the forces which are acting on the antenna array, rather the measured quantities describe the attitude and change in attitude of the array. For this reason, kinematic modelling is relied upon to describe the rotation of the array over time with respect to the local-level coordinate frame.

Kinematic modelling relating the antenna array attitude at time epochs t_k and t_{k+1} can be described by a set of first-order differential equations specifying the time evolution of the quaternions. Wertz (1978) derives the general attitude motion equations for the quaternions assuming a constant rotation rate over an infinitesimal time Δt such that

$$\mathbf{q}_{k+1} = \mathbf{q}_k + \dot{\mathbf{q}}\,\Delta t\,, \tag{4.27}$$

where $\mathbf{q} = \left[q_1, q_2, q_3, q_4\right]^T$ and the quaternion differentiated with respect to time is approximated by

$$\dot{\mathbf{q}} = \frac{1}{2}\mathbf{\Omega}\,\mathbf{q}_k\,, \tag{4.28}$$

with the skew symmetric form of the body rotations about the reference frame as

$$\mathbf{\Omega} = \begin{bmatrix} 0 & \omega_z & -\omega_y & \omega_x \\ -\omega_z & 0 & \omega_x & \omega_y \\ \omega_y & -\omega_x & 0 & \omega_z \\ -\omega_x & -\omega_y & -\omega_z & 0 \end{bmatrix}, \tag{4.29}$$

and $\boldsymbol{\omega} = \left[\omega_x, \omega_y, \omega_z\right]^T$ is the angular velocity of body rotation.

The constant angular velocity form of the kinematic model is obviously an approximation, since in order to completely model the kinematics of the attitude array higher orders of time differentiation are also required. However, the constant angular velocity model will have sufficient accuracy for applications where the dynamics of the vehicle are low (ships, land vehicles, mapping aircraft) or the measurement interval is short.

This section provides a unique kinematic model adequate for low dynamic attitude determination applications using quaternions, while section 3.4.4 provided the measurement models relating GPS double difference phase observations and quaternions. A method of combining the kinematic attitude model and the discrete, noisy GPS

measurements is required such that we can rigorously relate time and attitude while also estimating the accuracy of the attitude. The state-space model is one such method that models the deviations of $\mathbf{q}$ and $\dot{\mathbf{q}}$ from a reference attitude $\mathbf{q}_0$, $\dot{\mathbf{q}}_0$ by the first order differential equation

$$\dot{\mathbf{x}} = \mathbf{F}\mathbf{x} + \mathbf{w}\,, \tag{4.30}$$

where $\mathbf{x}$ …is the state vector which models the attitude deviations,

$\dot{\mathbf{x}}$ …is the time derivative of the state vector,

$\mathbf{F}$ …describes the system dynamics,

and $\mathbf{w}$ …is the system noise caused by modeling imperfections.

Exploring the similarities between equations 4.30 and 4.28 leads us to note that for quaternions, the dynamics matrix can be approximated by

$$\mathbf{F} = \frac{1}{2}\mathbf{\Omega}\ . \tag{4.31}$$

The measurement model that allows us to relate the discrete epoch-by-epoch GPS measurements with the state vector is

$$\mathbf{l} = f(\mathbf{x})\,, \tag{4.32}$$

where $\boldsymbol{l}$ …is the vector of observations at time t_k,

and f …is the mathematical model relating the state vector $\mathbf{x}$ and the observation vector $\mathbf{l}$.

The double difference interferometric models for the carrier phase and pseudorange presented in Chapter 3 are non-linear and not explicit in terms of $\boldsymbol{x}$, the unknowns. In order to solve for the unknowns using either least squares, or Kalman filtering, the models must be linearized. In the case of the double difference interferometric models,

they are explicit in ***l***, the observations, making them parametric. Linearized, equation 4.32 takes the form

$$\mathbf{l}_k + \mathbf{r}_k = \mathbf{A}_k \mathbf{x}_k , \qquad 4.33$$

where $\mathbf{A}_k$ …provides the linear connection between the states and the observations,

and $\mathbf{r}_k$ …is the measurement noise with covariance $\mathbf{C}_l$.

Estimation of the state vector **x** utilizing the measurement model and the kinematic model can be accomplished using Kalman filtering. The design matrix **A** for the double difference interferometric models will be given following the Kalman filtering section.

4.2 Kalman Filtering

Kalman filtering has been used extensively for kinematic positioning in real-time and post-mission applications during the past three decades. It provides a recursive method for the determination of trajectory and attitude by permitting the integration of a wide variety of navigation sensors and the rigorous propagation of system covariances. Gelb (1974) along with Brown and Hwang (1992) both give the derivation of the discrete Kalman filtering equations and hence they will not be included here. Instead, within this section we will present a summary of the common discrete Kalman filtering principles and equations used for discrete time linearized kinematic systems.

The Kalman filter equations for predicting the states and their associated covariances from time t_k to t_{k+1} using the kinematic model are

$$\hat{\mathbf{x}}_{k+1}^{(-)} = \mathbf{\Phi}_k \hat{\mathbf{x}}_k^{(+)}, \qquad 4.34$$

$$\mathbf{C}_{x,k+1}^{(-)} = \mathbf{\Phi}_k \mathbf{C}_{x,k}^{(+)} \mathbf{\Phi}_k^{T} + \mathbf{C}_{w,k} , \qquad 4.35$$

where $\mathbf{\Phi}_k$ …is the transition matrix evaluated with information available at time t_k,

$\mathbf{C}_x$ …is the covariance matrix of the state vector,

and $\mathbf{C}_w$ …is the covariance matrix of the system noise.

The transition matrix can be approximated from the dynamics matrix **F** by (Gelb, 1974)

$$\mathbf{\Phi}_k = e^{\Delta t\, F}, \tag{4.36}$$

provided that **F** can be considered time invariant. Expanding equation 4.36 yields

$$\mathbf{\Phi}_k = \sum_{u=0}^{\infty} \frac{\Delta t^{u} \mathbf{F}^{u}}{u!}. \tag{4.37}$$

If Δt is sufficiently small, equation 4.37 can be approximated by

$$\mathbf{\Phi}_k = \mathbf{I} + \Delta t\, \mathbf{F}, \tag{4.38}$$

where **I** is an identity matrix of size u by u, with u being the number of states.

The Kalman filter update equations for updating the states and their associated covariances using the discrete measurement model at time $t_{k+1}$are

$$\hat{\mathbf{x}}_{k+1}^{(+)} = \hat{\mathbf{x}}_{k+1}^{(-)} + \mathbf{K}_{k+1}\left(\mathbf{l}_{k+1} - \mathbf{A}_{k+1}\hat{\mathbf{x}}_{k+1}^{(-)}\right) \quad , \tag{4.39}$$

$$\mathbf{C}_{x,k+1}^{(+)} = \left(\mathbf{I} - \mathbf{K}_{k+1}\mathbf{A}_{k+1}\right)\mathbf{C}_{x,k+1}^{(-)}, \tag{4.40}$$

$$\mathbf{K}_{k+1} = \mathbf{C}_{x,k+1}^{(-)}\mathbf{A}_{k+1}^{T}\left(\mathbf{A}_{k+1}\mathbf{C}_{x,k+1}^{(-)}\mathbf{A}_{k+1}^{T} + \mathbf{C}_{l,k+1}\right)^{-1}, \tag{4.41}$$

where $\mathbf{K}_{k+1}$ is the Kalman gain matrix.

4.3 Kalman Filtering for Quaternion Based Attitude Estimation

The state vector for a quaternion based attitude system contains corrections to the quaternions, corrections to the body angular velocities, and corrections to the double difference phase ambiguities. The state vector takes the form

$$\mathbf{x} = \begin{bmatrix} \delta q_1 \\ \delta q_2 \\ \delta q_3 \\ \delta q_4 \\ \delta \omega_x \\ \delta \omega_y \\ \delta \omega_z \\ \delta N_1 \\ . \\ . \\ \delta N_j \end{bmatrix}, \tag{4.42}$$

where δN is the correction to a double difference ambiguity, with one correction for each ambiguity 1 to j not yet resolved. When the double difference ambiguities are resolved, the corresponding ambiguity correction states will be removed from the state vector.

Expanding equation 4.31 and factoring with respect to the states yields the quaternion portion of the dynamics matrix **F**. A random-walk or Wiener process (Brown and Hwang, 1992) will be used to model the dynamics for the angular velocity and double difference ambiguity states

$$\mathbf{F} = \begin{bmatrix} 0 & 0 & 0 & 0 & \frac{1}{2}q_4 & -\frac{1}{2}q_3 & \frac{1}{2}q_2 & 0 & . & . & 0 \\ 0 & 0 & 0 & 0 & \frac{1}{2}q_3 & \frac{1}{2}q_4 & -\frac{1}{2}q_1 & 0 & . & . & 0 \\ 0 & 0 & 0 & 0 & -\frac{1}{2}q_2 & \frac{1}{2}q_1 & \frac{1}{2}q_4 & 0 & . & . & 0 \\ 0 & 0 & 0 & 0 & -\frac{1}{2}q_1 & -\frac{1}{2}q_2 & -\frac{1}{2}q_3 & 0 & . & . & 0 \\ 0 & 0 & 0 & 0 & 0 & 0 & 0 & 0 & . & . & 0 \\ 0 & 0 & 0 & 0 & 0 & 0 & 0 & 0 & . & . & 0 \\ 0 & 0 & 0 & 0 & 0 & 0 & 0 & 0 & . & . & 0 \\ 0 & 0 & 0 & 0 & 0 & 0 & 0 & 0 & . & . & 0 \\ . & . & . & . & . & . & . & . & . & . & . \\ . & . & . & . & . & . & . & . & . & . & . \\ 0 & 0 & 0 & 0 & 0 & 0 & 0 & 0 & . & . & 0 \end{bmatrix}, \qquad 4.43$$

where **F**, the dynamics matrix is a u by u matrix.

The corresponding transition matrix is approximated using equation 4.38. Following the substitution of equation 4.43, the u by u transition matrix is of the form

$$\mathbf{\Phi}_{k+1,k} = \begin{bmatrix} 1 & 0 & 0 & 0 & \frac{1}{2}q_4\Delta t & -\frac{1}{2}q_3\Delta t & \frac{1}{2}q_2\Delta t & 0 & . & . & 0 \\ 0 & 1 & 0 & 0 & \frac{1}{2}q_3\Delta t & \frac{1}{2}q_4\Delta t & -\frac{1}{2}q_1\Delta t & 0 & . & . & 0 \\ 0 & 0 & 1 & 0 & -\frac{1}{2}q_2\Delta t & \frac{1}{2}q_1\Delta t & \frac{1}{2}q_4\Delta t & 0 & . & . & 0 \\ 0 & 0 & 0 & 1 & -\frac{1}{2}q_1\Delta t & -\frac{1}{2}q_2\Delta t & -\frac{1}{2}q_3\Delta t & 0 & . & . & 0 \\ 0 & 0 & 0 & 0 & 1 & 0 & 0 & 0 & . & . & 0 \\ 0 & 0 & 0 & 0 & 0 & 1 & 0 & 0 & . & . & 0 \\ 0 & 0 & 0 & 0 & 0 & 0 & 1 & 0 & . & . & 0 \\ 0 & 0 & 0 & 0 & 0 & 0 & 0 & 1 & . & . & 0 \\ . & . & . & . & . & . & . & . & . & . & . \\ . & . & . & . & . & . & . & . & . & . & . \\ 0 & 0 & 0 & 0 & 0 & 0 & 0 & 0 & . & . & 1 \end{bmatrix}. \qquad 4.44$$

A constant angular rate model is used to model the kinematics of the attitude system. The system will be subject to periodic angular accelerations and the deficiency in the constant angular velocity modelling will have to be accounted for in the process noise matrix. Assuming a constant Δt, the process noise matrix $\mathbf{C}_w$ can be obtained by integrating the spectral density matrix of the system noise (Gelb, 1974) (Schwarz et al., 1989)

$$\mathbf{C}_w = \int_{\tau=0}^{\Delta t} \mathbf{\Phi}_{k+1,k}(\tau)\, \mathbf{Q}(\tau)\, \mathbf{\Phi}^T_{k+1,k}(\tau)\, d\tau, \qquad 4.45$$

where **Q** is the u by u spectral density matrix of the system noise.

The spectral density matrix is

$$\mathbf{Q} = \begin{bmatrix} 0 & 0 & 0 & 0 & 0 & 0 & 0 & 0 & . & . & 0 \\ 0 & 0 & 0 & 0 & 0 & 0 & 0 & 0 & . & . & 0 \\ 0 & 0 & 0 & 0 & 0 & 0 & 0 & 0 & . & . & 0 \\ 0 & 0 & 0 & 0 & 0 & 0 & 0 & 0 & . & . & 0 \\ 0 & 0 & 0 & 0 & S_\omega & 0 & 0 & 0 & . & . & 0 \\ 0 & 0 & 0 & 0 & 0 & S_\omega & 0 & 0 & . & . & 0 \\ 0 & 0 & 0 & 0 & 0 & 0 & S_\omega & 0 & . & . & 0 \\ 0 & 0 & 0 & 0 & 0 & 0 & 0 & S_N & . & . & 0 \\ . & . & . & . & . & . & . & . & . & . & . \\ . & . & . & . & . & . & . & . & . & . & . \\ 0 & 0 & 0 & 0 & 0 & 0 & 0 & 0 & . & . & S_N \end{bmatrix}, \qquad 4.46$$

where S_ω …is the spectral amplitude for the angular velocity random process,

and S_N …is the spectral amplitude for the double difference ambiguity random process.

The covariance matrix for the process noise $\mathbf{C}_w$ is formed by substitution of equations 4.44 and 4.46 into equation 4.45 and integrating. The resulting process noise matrix is

$$\mathbf{C}_w = \left[\begin{array}{c|c} \mathbf{C}_w(1,1) & \mathbf{C}_w(1,2) \\ \hline \mathbf{C}_w(2,1) & \mathbf{C}_w(2,2) \end{array}\right]. \qquad 4.47$$

The four portions of the process noise hypermatrix are

$$\mathbf{C}_w(1,1)=\begin{bmatrix} \frac{1}{12}S_\omega\left(q_4^2+q_3^2+q_2^2\right)\Delta t^3 & \frac{1}{12}S_\omega\left(-q_1q_2\right)\Delta t^3 & \frac{1}{12}S_\omega\left(-q_1q_3\right)\Delta t^3 & \frac{1}{12}S_\omega\left(-q_1q_4\right)\Delta t^3 \\ \frac{1}{12}S_\omega\left(-q_1q_2\right)\Delta t^3 & \frac{1}{12}S_\omega\left(q_4^2+q_3^2+q_1^2\right)\Delta t^3 & \frac{1}{12}S_\omega\left(-q_2q_3\right)\Delta t^3 & \frac{1}{12}S_\omega\left(-q_2q_4\right)\Delta t^3 \\ \frac{1}{12}S_\omega\left(-q_1q_3\right)\Delta t^3 & \frac{1}{12}S_\omega\left(-q_2q_3\right)\Delta t^3 & \frac{1}{12}S_\omega\left(q_4^2+q_2^2+q_1^2\right)\Delta t^3 & \frac{1}{12}S_\omega\left(-q_3q_4\right)\Delta t^3 \\ \frac{1}{12}S_\omega\left(-q_1q_4\right)\Delta t^3 & \frac{1}{12}S_\omega\left(-q_2q_4\right)\Delta t^3 & \frac{1}{12}S_\omega\left(-q_3q_4\right)\Delta t^3 & \frac{1}{12}S_\omega\left(q_1^2+q_2^2+q_3^2\right)\Delta t^3 \end{bmatrix}, \tag{4.48}$$

$$\mathbf{C}_w(2,1)=\begin{bmatrix} \frac{1}{4}S_\omega q_4\,\Delta t^2 & \frac{1}{4}S_\omega q_3\,\Delta t^2 & -\frac{1}{4}S_\omega q_2\,\Delta t^2 & -\frac{1}{4}S_\omega q_1\,\Delta t^2 \\ -\frac{1}{4}S_\omega q_3\,\Delta t^2 & \frac{1}{4}S_\omega q_4\,\Delta t^2 & \frac{1}{4}S_\omega q_1\,\Delta t^2 & -\frac{1}{4}S_\omega q_2\,\Delta t^2 \\ \frac{1}{4}S_\omega q_2\,\Delta t^2 & -\frac{1}{4}S_\omega q_1\,\Delta t^2 & \frac{1}{4}S_\omega q_4\,\Delta t^2 & -\frac{1}{4}S_\omega q_3\,\Delta t^2 \\ 0 & 0 & 0 & 0 \\ . & . & . & . \\ . & . & . & . \\ 0 & 0 & 0 & 0 \end{bmatrix}, \tag{4.49}$$

$$\mathbf{C}_w(1,2)=\begin{bmatrix} \frac{1}{4}S_\omega q_4\,\Delta t^2 & -\frac{1}{4}S_\omega q_3\,\Delta t^2 & \frac{1}{4}S_\omega q_2\,\Delta t^2 & 0 & . & . & 0 \\ \frac{1}{4}S_\omega q_3\,\Delta t^2 & \frac{1}{4}S_\omega q_4\,\Delta t^2 & -\frac{1}{4}S_\omega q_1\,\Delta t^2 & 0 & . & . & 0 \\ -\frac{1}{4}S_\omega q_2\,\Delta t^2 & \frac{1}{4}S_\omega q_1\,\Delta t^2 & \frac{1}{4}S_\omega q_4\,\Delta t^2 & 0 & . & . & 0 \\ -\frac{1}{4}S_\omega q_1\,\Delta t^2 & -\frac{1}{4}S_\omega q_2\,\Delta t^2 & -\frac{1}{4}S_\omega q_3\,\Delta t^2 & 0 & . & . & 0 \end{bmatrix}, \tag{4.50}$$

$$\mathbf{C}_w(2,2)=\begin{bmatrix} S_\omega\Delta t & 0 & 0 & 0 & . & . & 0 \\ 0 & S_\omega\Delta t & 0 & 0 & . & . & 0 \\ 0 & 0 & S_\omega\Delta t & 0 & . & . & 0 \\ 0 & 0 & 0 & S_N\Delta t & . & . & 0 \\ . & . & . & . & . & . & 0 \\ . & . & . & . & . & . & 0 \\ 0 & 0 & 0 & 0 & 0 & 0 & S_N\Delta t \end{bmatrix}. \tag{4.51}$$

The observation vector ***l*** for an filter update with double difference interferometric phase observations measured during one epoch is of the form

$$\boldsymbol{l} = \begin{bmatrix} \nabla\Delta\Phi^{ij}_{\alpha\beta}(\text{obs}) - \nabla\Delta\Phi^{ij}_{\alpha\beta}(\text{predicted}) \\ \nabla\Delta\Phi^{ik}_{\alpha\beta}(\text{obs}) - \nabla\Delta\Phi^{ik}_{\alpha\beta}(\text{predicted}) \\ . \\ . \\ . \\ \nabla\Delta\Phi^{it}_{\alpha\delta}(\text{obs}) - \nabla\Delta\Phi^{it}_{\alpha\delta}(\text{predicted}) \end{bmatrix}. \qquad 4.52$$

The elements of the observation vector ***l*** are the differences between the observed and predicted double difference interferometric phases. The predicted values are computed using equation 3.26, with the satellite coordinates calculated from the broadcast ephemeris. The coordinates for each of the four GPS antenna are computed using the predicted quaternion states. The quaternions are converted to a direction cosine matrix using equation 2.17, following which the Earth-fixed frame coordinates of the antenna are computed from the body frame coordinates using equation 2.78.

The design matrix **A** for an update using the double difference interferometric phase observations from one epoch is of the form

$$\mathbf{A} = \begin{bmatrix} \frac{\partial\nabla\Delta\Phi^{ij}_{\alpha\beta}}{\partial q_1} & \frac{\partial\nabla\Delta\Phi^{ij}_{\alpha\beta}}{\partial q_2} & \frac{\partial\nabla\Delta\Phi^{ij}_{\alpha\beta}}{\partial q_3} & \frac{\partial\nabla\Delta\Phi^{ij}_{\alpha\beta}}{\partial q_4} & 0 & 0 & 0 & \frac{\partial\nabla\Delta\Phi^{ij}_{\alpha\beta}}{\partial\lambda\nabla\Delta N^{ij}_{\alpha\beta}} & 0 & . . & 0 \\ \frac{\partial\nabla\Delta\Phi^{ik}_{\alpha\beta}}{\partial q_1} & \frac{\partial\nabla\Delta\Phi^{ik}_{\alpha\beta}}{\partial q_2} & \frac{\partial\nabla\Delta\Phi^{ik}_{\alpha\beta}}{\partial q_3} & \frac{\partial\nabla\Delta\Phi^{ik}_{\alpha\beta}}{\partial q_4} & 0 & 0 & 0 & 0 & \frac{\partial\nabla\Delta\Phi^{jk}_{\alpha\beta}}{\partial\lambda\nabla\Delta N^{ik}_{\alpha\beta}} & . . & 0 \\ . & . & . & . & . & . & . & . & . & . . & 0 \\ . & . & . & . & . & . & . & . & . & . . & 0 \\ . & . & . & . & . & . & . & . & . & . . & 0 \\ \frac{\partial\nabla\Delta\Phi^{jt}_{\alpha\delta}}{\partial q_1} & \frac{\partial\nabla\Delta\Phi^{jt}_{\alpha\delta}}{\partial q_2} & \frac{\partial\nabla\Delta\Phi^{jt}_{\alpha\delta}}{\partial q_3} & \frac{\partial\nabla\Delta\Phi^{jt}_{\alpha\delta}}{\partial q_4} & 0 & 0 & 0 & 0 & 0 & . . & \frac{\partial\nabla\Delta\Phi^{jt}_{\alpha\delta}}{\partial\lambda\nabla\Delta N^{jt}_{\alpha\delta}} \end{bmatrix}, \qquad 4.53$$

where the partial derivatives of double difference carrier phase $\nabla\Delta\Phi^{ij}_{\alpha\beta}$ with respect to the quaternions are

$$\frac{\partial \nabla \Delta \Phi_{\alpha\beta}^{ij}}{\partial q_1} = \begin{bmatrix} \frac{-\left(x^j - x_\beta\right)}{\rho_\beta^j} + \frac{\left(x^i - x_\beta\right)}{\rho_\beta^i} \\ \frac{-\left(y^j - y_\beta\right)}{\rho_\beta^j} + \frac{\left(y^i - y_\beta\right)}{\rho_\beta^i} \\ \frac{-\left(z^j - z_\beta\right)}{\rho_\beta^j} + \frac{\left(z^i - z_\beta\right)}{\rho_\beta^i} \end{bmatrix}^T \mathbf{R}_l^e \frac{\partial \mathbf{R}_b^l}{\partial q_1} \begin{bmatrix} x_\beta - x_\alpha \\ y_\beta - y_\alpha \\ z_\beta - z_\alpha \end{bmatrix}_b , \tag{4.54}$$

$$\frac{\partial \nabla \Delta \Phi_{\alpha\beta}^{ij}}{\partial q_2} = \begin{bmatrix} \frac{-\left(x^j - x_\beta\right)}{\rho_\beta^j} + \frac{\left(x^i - x_\beta\right)}{\rho_\beta^i} \\ \frac{-\left(y^j - y_\beta\right)}{\rho_\beta^j} + \frac{\left(y^i - y_\beta\right)}{\rho_\beta^i} \\ \frac{-\left(z^j - z_\beta\right)}{\rho_\beta^j} + \frac{\left(z^i - z_\beta\right)}{\rho_\beta^i} \end{bmatrix}^T \mathbf{R}_l^e \frac{\partial \mathbf{R}_b^l}{\partial q_2} \begin{bmatrix} x_\beta - x_\alpha \\ y_\beta - y_\alpha \\ z_\beta - z_\alpha \end{bmatrix}_b , \tag{4.55}$$

$$\frac{\partial \nabla \Delta \Phi_{\alpha\beta}^{ij}}{\partial q_3} = \begin{bmatrix} \frac{-\left(x^j - x_\beta\right)}{\rho_\beta^j} + \frac{\left(x^i - x_\beta\right)}{\rho_\beta^i} \\ \frac{-\left(y^j - y_\beta\right)}{\rho_\beta^j} + \frac{\left(y^i - y_\beta\right)}{\rho_\beta^i} \\ \frac{-\left(z^j - z_\beta\right)}{\rho_\beta^j} + \frac{\left(z^i - z_\beta\right)}{\rho_\beta^i} \end{bmatrix}^T \mathbf{R}_l^e \frac{\partial \mathbf{R}_b^l}{\partial q_3} \begin{bmatrix} x_\beta - x_\alpha \\ y_\beta - y_\alpha \\ z_\beta - z_\alpha \end{bmatrix}_b , \tag{4.56}$$

$$\frac{\partial \nabla \Delta \Phi_{\alpha\beta}^{ij}}{\partial q_4} = \begin{bmatrix} \frac{-\left(x^j - x_\beta\right)}{\rho_\beta^j} + \frac{\left(x^i - x_\beta\right)}{\rho_\beta^i} \\ \frac{-\left(y^j - y_\beta\right)}{\rho_\beta^j} + \frac{\left(y^i - y_\beta\right)}{\rho_\beta^i} \\ \frac{-\left(z^j - z_\beta\right)}{\rho_\beta^j} + \frac{\left(z^i - z_\beta\right)}{\rho_\beta^i} \end{bmatrix}^T \mathbf{R}_l^e \frac{\partial \mathbf{R}_b^l}{\partial q_4} \begin{bmatrix} x_\beta - x_\alpha \\ y_\beta - y_\alpha \\ z_\beta - z_\alpha \end{bmatrix}_b . \tag{4.57}$$

The partial derivative of $\mathbf{R}_b^l$ with respect to the quaternions is obtained by taking the partial derivatives of the transpose of equation 2.17

$$\frac{\partial \mathbf{R}_b^l}{\partial q_1} = \begin{bmatrix} 2q_1 & 2q_2 & 2q_3 \\ 2q_2 & -2q_1 & -2q_4 \\ 2q_3 & 2q_4 & -2q_1 \end{bmatrix}, \tag{4.58}$$

$$\frac{\partial \mathbf{R}_b^l}{\partial q_2} = \begin{bmatrix} -2q_2 & 2q_1 & 2q_4 \\ 2q_1 & 2q_2 & 2q_3 \\ -2q_4 & 2q_3 & -2q_2 \end{bmatrix}, \tag{4.59}$$

$$\frac{\partial \mathbf{R}_b^l}{\partial q_3} = \begin{bmatrix} -2q_3 & -2q_4 & 2q_1 \\ 2q_4 & -2q_3 & 2q_2 \\ 2q_1 & 2q_2 & 2q_3 \end{bmatrix}, \tag{4.60}$$

$$\frac{\partial \mathbf{R}_b^l}{\partial q_4} = \begin{bmatrix} 2q_4 & -2q_3 & 2q_2 \\ 2q_3 & 2q_4 & -2q_1 \\ -2q_2 & 2q_1 & 2q_4 \end{bmatrix}. \tag{4.61}$$

The partial derivatives of double difference carrier phase $\nabla\Delta\Phi_{\alpha\beta}^{ij}$ with respect to the double difference interferometry phase ambiguities are

$$\frac{\partial \nabla\Delta\Phi_{\alpha\beta}^{ij}}{\partial \lambda \nabla\Delta N_{\alpha\beta}^{ij}} = 1, \tag{4.62}$$

where the ambiguity term $\nabla\Delta N_{\alpha\beta}^{ij}$ has been converted to metres.

Since we consider the double difference observations from one epoch uncorrelated, it is possible to update the Kalman filter with one measurement at a time. By ignoring the correlation between the double difference observations, the covariance matrix for the observations is diagonal. However, ignoring the correlation amongst the double differences will increase the accuracy estimates. Processing one measurement at a time reduces the design matrix **A** to a single row, with u columns, where u is equal to the number of states. Processing observations one at a time improves the efficiency of the computations. The Kalman filter update equations require an inversion of a square matrix of size n, where n is the number of observations. If we process the observations one at a

time, we are only required to take the inverse of a scalar rather than the potential inversion of 16 x 16 matrix (i.e. observing 6 satellites on each of four receivers = 15 double differences and 1 quaternion constraint equation). Assuming that we are using the strategy of processing observations one at a time, the double difference phase observation vector ***l,*** design matrix **A** and the covariance of the observations $\mathbf{C}_l$ are of the form

$$\boldsymbol{l} = \left[\nabla\Delta\Phi^{ij}_{\alpha\beta}(\text{obs}) - \nabla\Delta\Phi^{ij}_{\alpha\beta}(\text{predicted})\right] \quad , \tag{4.63}$$

$$\mathbf{A} = \left[\frac{\partial\nabla\Delta\Phi^{ij}_{\alpha\beta}}{\partial q_1} \quad \frac{\partial\nabla\Delta\Phi^{ij}_{\alpha\beta}}{\partial q_2} \quad \frac{\partial\nabla\Delta\Phi^{ij}_{\alpha\beta}}{\partial q_3} \quad \frac{\partial\nabla\Delta\Phi^{ij}_{\alpha\beta}}{\partial q_4} \quad 0 \quad 0 \quad 0 \quad 1 \quad 0 \quad . \quad . \quad 0\right] \quad , \tag{4.64}$$

$$C_{\boldsymbol{l}} = \left[\sigma^2_{\nabla\Delta\Phi}\right] \quad . \tag{4.65}$$

The observation vector ***l***, design matrix **A** and covariance $\mathbf{C}_l$ for a filter update with double difference interferometric pseudorange observations are of the form

$$\boldsymbol{l} = \left[\nabla\Delta p^{ij}_{\alpha\beta}(obs) - \nabla\Delta p^{ij}_{\alpha\beta}(predicted)\right] \quad , \tag{4.66}$$

$$\mathbf{A} = \left[\frac{\partial\nabla\Delta p^{ij}_{\alpha\beta}}{\partial q_1} \quad \frac{\partial\nabla\Delta p^{ij}_{\alpha\beta}}{\partial q_2} \quad \frac{\partial\nabla\Delta p^{ij}_{\alpha\beta}}{\partial q_3} \quad \frac{\partial\nabla\Delta p^{ij}_{\alpha\beta}}{\partial q_4} \quad 0 \quad 0 \quad 0 \quad 0 \quad 0 \quad . \quad . \quad 0\right] \quad , \tag{4.67}$$

$$\mathbf{C}_{\boldsymbol{l}} = \left[\sigma^2_{\nabla\Delta p}\right] \quad . \tag{4.68}$$

where the partial derivatives of double difference interferometric pseudoranges $\nabla\Delta p^{ij}_{\alpha\beta}$ with respect to the quaternions are identical to those for the double difference interferometric phase in equations 4.54, 4.55, 4.56, and 4.57.

The double difference phase observations will provide the highest accuracy, but the double difference pseudorange observation provide some stability to the filter, since they do not have an ambiguity state.

From equation 2.14, it is obvious that the four quaternion states are not independent. To ensure that a singularity does not occur within the filter, a pseudo-observation is added at

each measurement epoch to account for the dependency. The observation vector ***l***, design matrix A and covariance C_l for a filter update with quaternion condition equation relationship are of the form

$$\boldsymbol{l} = \left[1 - \left(q_1^2 + q_2^2 + q_3^2 + q_4^2\right)\right] \quad , \tag{4.69}$$

$$\mathbf{A} = \begin{bmatrix} 2q_1 & 2q_2 & 2q_3 & 2q_4 & 0 & 0 & 0 & 0 & 0 & . & . & 0 \end{bmatrix} \quad , \tag{4.70}$$

$$C_{\boldsymbol{l}} = \left[\sigma_q^2\right] \quad , \tag{4.71}$$

where σ_q^2 is the variance for the quaternion condition equation, of sufficient magnitude to maintain filter stability.

4.4 Quaternion Dilution of Precision Computation

The Quaternion Dilution of Precision (QDOP) is an indicator of the quality of the attitude estimation. It is computed by first forming

$$\mathbf{C}_q = \left(\mathbf{A}_q^T \mathbf{A}_q\right)^{-1} \quad , \tag{4.72}$$

where $\mathbf{C}_q$ …is the 4 by 4 quaternion variance-covariance matrix without observation weighting,

and $\mathbf{A}_q$ …is the first four columns of the design matrix relating to the quaternions.

The QDOP is computed by

$$\text{QDOP} = \sqrt{\text{trace}\left(\mathbf{C}_q\right)} \quad . \tag{4.73}$$

Values determined in this research for a QDOP reflecting satisfactory attitude estimation quality range from 1 to 4 while utilizing 6 satellites tracked above a 15 degree elevation cutoff by four GPS receivers.

4.5 Quality Control

Outlined above are estimation techniques that can be used for real-time attitude determination. However, testing of the dynamics and measurement models are required if a reliable and robust system is desired. The Kalman filter produces optimal estimators of the state vector that are: unbiased, have minimum variance, and have a Gaussian distribution (Teunissen and Salzmann, 1989). However, if the assumptions underlying the model are compromised, the estimators are no longer optimal. Blunders in the measurements such as cycle slips or errors in the dynamic model can invalidate the results of the estimation.

Quality control techniques are comprised of three steps: fault detection, fault identification, and recovery (FDIR) (Abousalem, 1993). Within an attitude system, we are primarily concerned with carrier phase cycle slips. An undetected cycle slip could adversely affect the attitude estimates, yet the accuracy estimates would in some cases not reflect the effect of the slip. A reliable means of slip detection and identification of biased measurements is required. Once a slip is detected, the ambiguity resolution routines can be called on to redetermine the ambiguities for the measurements identified.

Testing of the predicted residuals or innovations is a useful tool for fault detection and identification and is well suited to real-time applications. The innovations are central to this technique and represent the difference between the actual system output and the predicted output based on the predicted states. The innovations are computed from

$$\mathbf{v}_{k+1} = \mathbf{l}_{k+1} - \mathbf{A}_{k+1}\hat{\mathbf{x}}_{k+1}^{(-)}, \tag{4.74}$$

and have a variance-covariance matrix given by

$$\mathbf{C}_{v,k+1} = \mathbf{A}_{k+1}\mathbf{C}_{x,k+1}^{(-)}\mathbf{A}_{k+1}^{T} + \mathbf{C}_{l,k+1}. \tag{4.75}$$

The innovations are considered to have a Gaussian distribution and deviations from this hypothesis can be used to detect and identify blunders. The null and alternate hypothesis are, respectively,

$$H_{0,k+1}: v_{k+1} \sim N\left(0, \mathbf{C}_{v,k+1}\right) = 0, \tag{4.76}$$

$$H_{a,k+1}: v_{k+1} \sim N\left(\nabla_{k+1}, \mathbf{C}_{v,k+1}\right) = 0, \tag{4.77}$$

where ∇_{k+1} is the failure vector under the alternate hypothesis H_a. The test statistic for testing H_0 against H_a is

$$T_{k+1} = \mathbf{v}_{k+1}^{T} \mathbf{C}_{v,k+1}^{-1} \mathbf{v}_{k+1} \sim \chi^2\left(m_{k+1}, 0\right), \tag{4.78}$$

where $m_{k+1}$is the degrees of freedom. This test statistic can be used to perform an overall model test for detecting model errors in the null hypothesis. If the test fails, the faulty innovation can be identified using

$$t_{k+1}^{i} = \frac{\left(\mathbf{e}_i^{T} \mathbf{C}_{v,k+1}^{-1} \mathbf{v}_{k+1}\right)^2}{\mathbf{e}_i^{T} \mathbf{C}_{v,k+1}^{-1} \mathbf{e}_i} \sim \chi^2\left(1,0\right), \tag{4.79}$$

where $\mathbf{e}_i$=[0,0,0...,1,...0,0]^{T}is used to pick the ith element from the innovations vector for testing (Gao, 1992). Failure of the local slippage test indicates a possible slippage in the observation, the predicted state or a combination of the two. In either case, the observation corresponding to the slippage is marked for immediate input into the ambiguity resolution routines. The innovations testing method proved reliable in detecting cycle slips of 1 cycle, primarily due to the redundancy available while using of the direct attitude estimation approach. However, innovations testing is usually not capable of detecting cycle slips on more than one satellite at a time and caution must be exercised. In the case of this research, ambiguity resolution was attempted on all observations whenever a cycle slip was detected.

4.6 Covariance Propagation from Quaternions to Euler Angles

While quaternions have a number of advantages for attitude computations, one of the main disadvantages of quaternions for attitude display is the inability of most human operators to relate them to their physical world. This is why many systems, including the one developed here, perform their computations using quaternions, but display the results in terms of Euler angles. The conversions from quaternions to Euler angles were given in section 2.4.2. In addition to the attitude parameters themselves, the variance-covariance information from the filter should also be propagated from the quaternion parameterization to the Euler angle parameterization. The propagation from quaternion covariance to Euler angle covariance is accomplished by employing the covariance law [Vanicek and Krakiwsky, 1986]

$$\mathbf{C}_{\psi\theta\varphi} = \mathbf{G}\mathbf{C}_q\mathbf{G}^T \quad , \tag{4.80}$$

where $\mathbf{C}_{\psi\theta\varphi}$ …is the covariance matrix (3x3) for the Euler angle parameters,

$\mathbf{G}$ …is the Jacobian matrix (3x4) containing the partial derivatives of the Euler angle equations with respect to the quaternions,

and $\mathbf{C}_q$ …is the estimated variance-covariance matrix (4x4) for the quaternions.

The Jacobian matrix **G** is formed by taking the partial derivatives of equations 2.69, 2.76, and 2.77 with respect to the four quaternion parameters. It is of the form

$$\mathbf{G} = \begin{bmatrix} \frac{\delta\psi}{\delta q_1} & \frac{\delta\psi}{\delta q_2} & \frac{\delta\psi}{\delta q_3} & \frac{\delta\psi}{\delta q_4} \\ \frac{\delta\theta}{\delta q_1} & \frac{\delta\theta}{\delta q_2} & \frac{\delta\theta}{\delta q_3} & \frac{\delta\theta}{\delta q_4} \\ \frac{\delta\varphi}{\delta q_1} & \frac{\delta\varphi}{\delta q_2} & \frac{\delta\varphi}{\delta q_3} & \frac{\delta\varphi}{\delta q_4} \end{bmatrix}. \tag{4.81}$$

The partial derivatives of the Euler angles taken with respect to the quaternions are

$$\frac{\delta\psi}{\delta q_1} = \frac{-(q_3 + q_2)}{(q_3 + q_2)^2 + (q_4 + q_1)^2} + \frac{(q_3 - q_2)}{(q_3 - q_2)^2 + (q_4 - q_1)^2}, \tag{4.82a}$$

$$\frac{\delta\psi}{\delta q_2} = \frac{(q_4 + q_1)}{(q_3 + q_2)^2 + (q_4 + q_1)^2} - \frac{(q_4 - q_1)}{(q_3 - q_2)^2 + (q_4 - q_1)^2}, \tag{4.82b}$$

$$\frac{\delta\psi}{\delta q_3} = \frac{(q_4 + q_1)}{(q_3 + q_2)^2 + (q_4 + q_1)^2} + \frac{(q_4 - q_1)}{(q_3 - q_2)^2 + (q_4 - q_1)^2}, \tag{4.82c}$$

$$\frac{\delta\psi}{\delta q_4} = \frac{-(q_3 + q_2)}{(q_3 + q_2)^2 + (q_4 + q_1)^2} - \frac{(q_3 - q_2)}{(q_3 - q_2)^2 + (q_4 - q_1)^2}, \tag{4.82d}$$

$$\frac{\delta\theta}{\delta q_1} = \frac{2q_4}{\left[1 - 4(q_2 q_3 + q_1 q_4)^2\right]^{\frac{1}{2}}}, \tag{4.83a}$$

$$\frac{\delta\theta}{\delta q_2} = \frac{2q_3}{\left[1 - 4(q_2 q_3 + q_1 q_4)^2\right]^{\frac{1}{2}}}, \tag{4.83b}$$

$$\frac{\delta\theta}{\delta q_3} = \frac{2q_2}{\left[1 - 4(q_2 q_3 + q_1 q_4)^2\right]^{\frac{1}{2}}}, \tag{4.83c}$$

$$\frac{\delta\theta}{\delta q_4} = \frac{2q_1}{\left[1 - 4(q_2 q_3 + q_1 q_4)^2\right]^{\frac{1}{2}}}, \tag{4.83d}$$

$$\frac{\delta\varphi}{\delta q_1} = \frac{-(q_3 + q_2)}{(q_3 + q_2)^2 + (q_4 + q_1)^2} - \frac{(q_3 - q_2)}{(q_3 - q_2)^2 + (q_4 - q_1)^2}, \tag{4.84a}$$

$$\frac{\delta\varphi}{\delta q_2} = \frac{(q_4 + q_1)}{(q_3 + q_2)^2 + (q_4 + q_1)^2} + \frac{(q_4 - q_1)}{(q_3 - q_2)^2 + (q_4 - q_1)^2}, \tag{4.84b}$$

$$\frac{\delta\varphi}{\delta q_3} = \frac{(q_4 + q_1)}{(q_3 + q_2)^2 + (q_4 + q_1)^2} - \frac{(q_4 - q_1)}{(q_3 - q_2)^2 + (q_4 - q_1)^2}, \tag{4.84c}$$

$$\frac{\delta\varphi}{\delta q_4} = \frac{-(q_3 + q_2)}{(q_3 + q_2)^2 + (q_4 + q_1)^2} + \frac{(q_3 - q_2)}{(q_3 - q_2)^2 + (q_4 - q_1)^2}. \tag{4.84d}$$

CHAPTER 5

GPS AMBIGUITY RESOLUTION

In order to achieve high accuracy attitude determination using GPS, it is necessary to determine the integer cycle ambiguities for the GPS double difference phase measurements. As mentioned earlier, the non-dedicated GPS receivers incorporated within the attitude system developed herein are capable of both code and carrier phase measurements. The carrier phase measurements can be made to the level of 1-10 mm, but only the fractional portion of the phase cycle can be measured. The integer number of whole cycles separating the receiver and satellite cannot be measured by the receiver and must be determined independently. When the phase observables are linearly combined as they are in the double difference, an ambiguity term still remains. The ambiguities must be estimated at system start-up and whenever phase lock is lost. An attitude system intended for kinematic applications must have an ambiguity resolution process that allows for determination of the ambiguities nearly instantaneously and with the antenna array in motion. The term 'on-the-fly' (OTF) has been coined to cover the range of techniques used to determine ambiguities within kinematic systems. Many of these techniques were originally developed for rapid static and kinematic differential phase positioning operations and include: the least squares ambiguity search technique (LSAST) (Hatch, 1989; 1991), the ambiguity function method (AFM) (Counselman and Gourevitch, 1981, Remondi 1984; 1990), the fast ambiguity resolution approach (FARA)

(Frei and Beutler, 1990), and the fast ambiguity search filter (FASF) (Chen 1993; Chen and Lachapelle, 1994).

Within this research a variation of the least squares ambiguity search technique has been used. This method is a straight forward implementation of a well known estimation technique that produces rigorous and robust results. The least squares ambiguity search technique LSAST method allows the system designer a high degree of flexibility to experiment with different search volumes with the aim of improving efficiency and reliability.

Ambiguity search methods are discussed further in section 5.1. The definition of the search volume is crucial to the success and speed of the resolution technique, and will be covered in section 5.2. Techniques for forming the ambiguity combinations will be discussed in section 5.3. The final section within this chapter will describe the ambiguity combination testing techniques.

5.1 Ambiguity Search Techniques

The goal that ambiguity resolution techniques aim for is to determine the correct set of ambiguities within the shortest measurement period possible and with a minimum of computations. An ambiguity resolution technique intended for attitude determination should have the following properties:

1. Computations should not take longer than one measurement epoch,
2. Correct ambiguities are consistently selected,
3. Incorrect ambiguities are never selected.

Several of these properties conflict and here lies the difficulty in achieving reliable, robust and fast ambiguity resolution. A desirable, but not essential, property is for the ambiguity resolution technique to resolve the ambiguities using only one epoch of data.

In general, ambiguity search techniques resolve the ambiguities using three steps (Walsh et al., 1995):

1. define a search volume,
2. form all potential ambiguity combinations,
3. arrange the ambiguities, and
4. test ambiguity combinations.

The first step is to form the search volume. It is both desirable to have a small search volume to limit the number of ambiguity computations and thus computational time, and desirable to have a large search volume to ensure that the correct combination is included in the tests. Once the search volume has been defined, the second step is to form the ambiguity sets within the search volume and arrange them in an optimal fashion. The third step is to arrange the ambiguities with the goal of limiting the computations. The fourth and final step is the testing of the combinations and the identification of the best and hopefully correct ambiguity set.

The attitude determination problem is a restricted kinematic positioning problem (Hatch, 1989). The restrictions can be used to enhance the ambiguity resolution process and allow for solutions within one epoch. These include:

1. shorter baseline lengths minimizing the effect of unmodelled ionospheric and tropospheric refraction,
2. known baseline distances and/or body frame coordinates for the antenna array provide additional information, and
3. use of measurements from auxiliary sensors such as compasses, rate gyros and inclinometers improve accuracy and reliability.

The least squares ambiguity search technique (LSAST) was introduced by Hatch (1989) for kinematic positioning and further refined in Hatch (1991). The primary steps of the technique are:

1. using the differential code solution, compute the approximate coordinates for the remote antenna,

2. form the search volume by using a three-sigma uncertainty surrounding the approximate position of the remote antenna,
3. identify the four primary satellites which have a good GDOP, with satellite ambiguities considered independent,
4. the remaining satellites form the secondary satellite group,
5. form the primary ambiguity combinations and potential solutions,
6. compute the integer ambiguities for the secondary observations,
7. update the sequential least squares solution with the secondary observations and compute the variance factor, and
8. test the variance factor and reject any combinations with a variance factor greater than a selected threshold.

Cannon (1992b) modified the LSAST for a heading system utilizing double difference phase observables. Antenna separation and auxiliary heading measurements (Cannon et al., 1992) were included to improve the efficiency and reliability of the ambiguity resolution method. Further refinements are made here to allow for the addition of another two GPS receivers and the quaternion attitude parameterization. The entire process for one epoch is shown in Figure 6.1. The following three sections discuss in more detail the ambiguity resolution process as it applies to attitude determination with a rigid multi-antenna array.

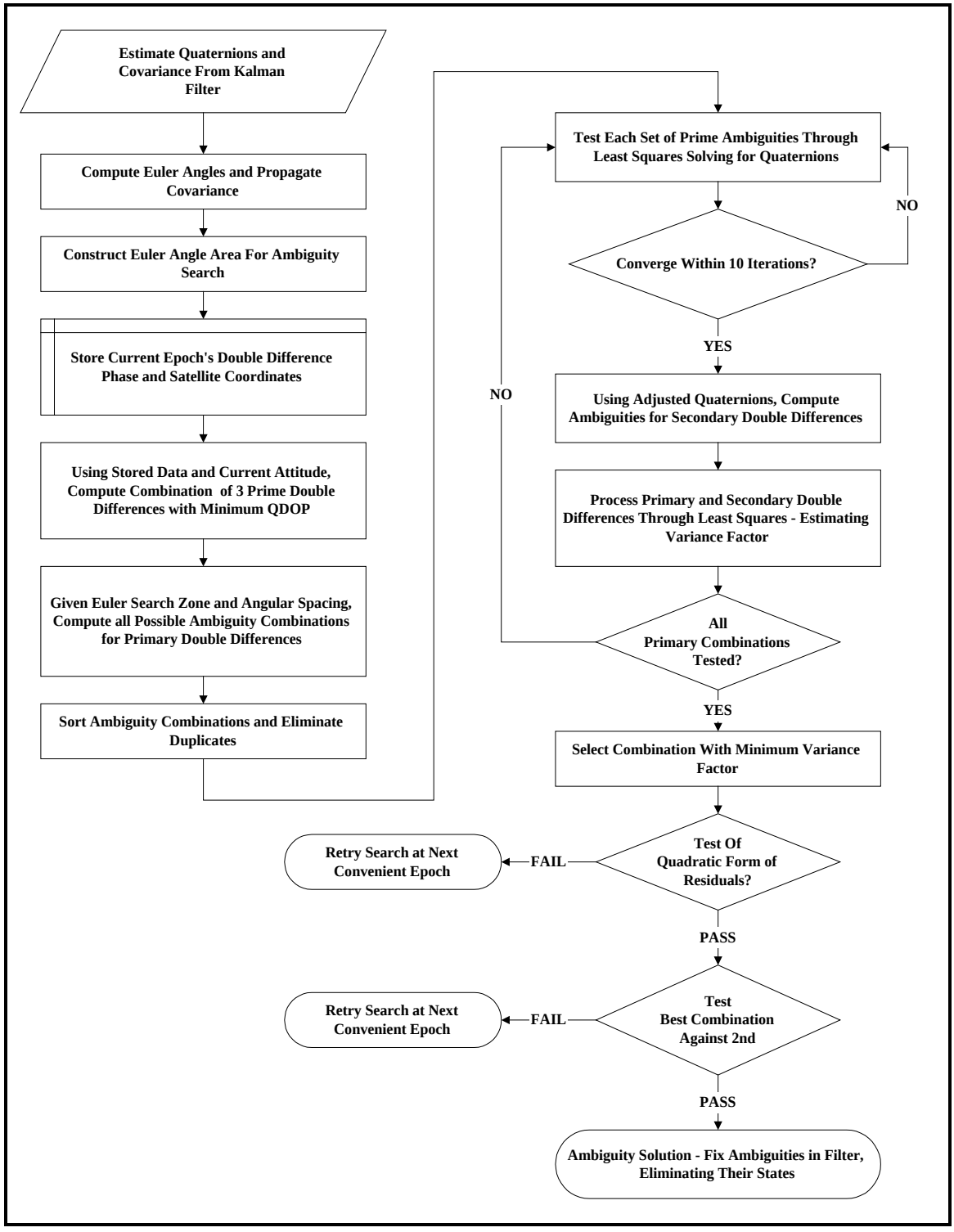

Figure 6.1 - Carrier Phase Ambiguity Resolution Flowchart

5.2 Defining Search Volumes

The search volume should define the space within which the correct ambiguity combination will fall (Walsh et al., 1995). In the case of kinematic positioning, the position of the search volume origin is set to the position of the remote antenna estimated from the pseudoranges. While this origin has been used for attitude determination (Cannon, 1992b; El-Mowafy and Schwarz, 1995), another option is to use the reference antennas position as the search volumes origin (Hatch, 1989; Brown, 1992; Quinn, 1993).

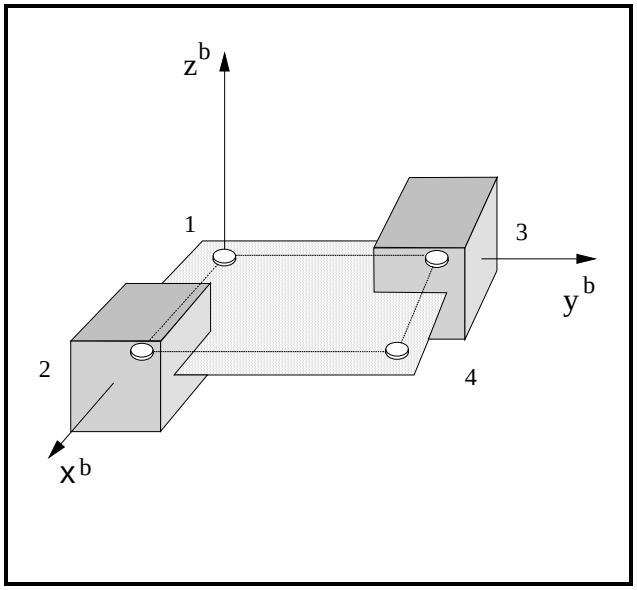

Figure 6.2 - Cubic Search Volume

The shape of the search volume also varies with the application. The cube, ellipsoid, and sphere have been used as ambiguity search volumes. The cube search volume is illustrated in Figure 6.2. For attitude determination, the sphere shape with its origin at the reference antenna has advantages when used with a multi-antenna attitude system featuring rigidly mounted antennas. Since the baseline distances between the reference and remote antennas are fixed, the potential position solution for each remote antenna corresponding to the trial of a ambiguity combinations must lie on a sphere whose radius is equal to the reference-remote antenna baseline distance. Using this technique it is only necessary to search only those combinations whose solution falls on the sphere. It is not

necessary to search inside of the sphere, thereby reducing the number of search combinations.

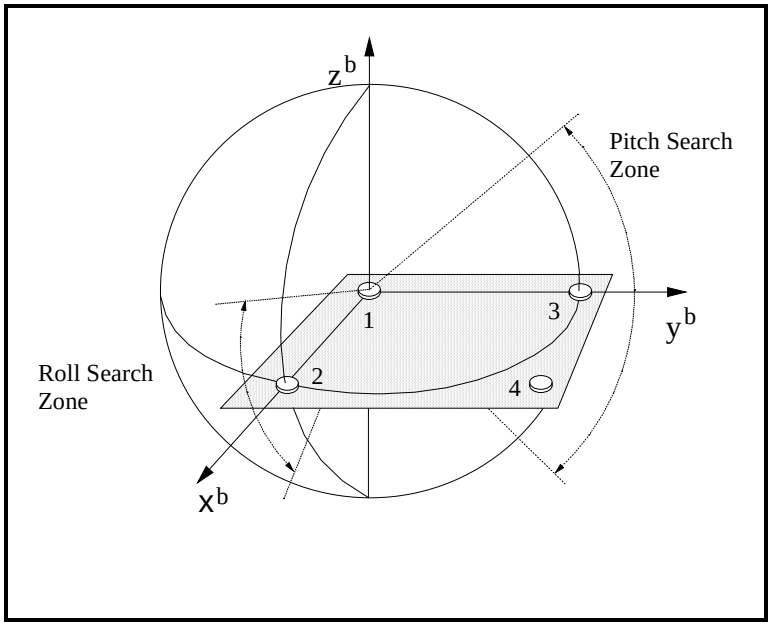

Figure 6.3 - Spherical Surface Search Volume

Within this application, the size and extent of the search zones on the sphere are based on the attitude estimates and corresponding variances from the floating ambiguity Kalman filter. The attitude estimates give the initial orientation of the search zone. The size of the search zone is determined using the standard deviations of the estimated attitude parameters and multiplying these by an expansion factor. If we could assume that the estimated attitude is only subject to random errors, the choice of an expansion factor would be governed by the confidence level we want. For example, the error estimates for the yaw, pitch or roll at a standard error level (expansion factor of unity) have a 66% probability of containing the correct ambiguity combination. Increasing the expansion factor to 2.57 will increase the confidence interval to 99%. However, systematic errors can contaminate the observations from which the approximate orientation was estimated. This makes the selection of the expansion factor a subjective one. If the factor is set to give a small search zone, the ambiguity search will be completed quickly, but there is an increased risk that systematic errors will cause the correct ambiguity combination to fall

outside of the search zone. If a large expansion factor is selected, the search zone has a very good chance of containing the correct ambiguity combination. However, the higher computational load associated with the expanded ambiguity search may make the technique unfeasible for real-time systems.

Application dependant search area constraints can also be used. For example, the pitch and roll for a land vehicle rarely exceeds 20 - 30 degrees. Hence the search area would be confined to those areas of the sphere within 30 degrees of its equator. A similar constraint for a ship could be set at 30 to 45 degrees. In cases where the forward axis of vehicle or vessel is aligned with the heading axis of the attitude system and speed is consistent, the GPS course over ground can also be used to aid the ambiguity search by providing an initial orientation. However, this will not work if the attitude system has been mounted on a turret which can rotate independent of the vehicle, or on a vehicle designed to move in directions other than the forward axis, such as a helicopter.

5.3 Forming Ambiguity Combinations

The second step in resolving the double difference ambiguities is to form all ambiguity combinations which fall within the search zone. The ambiguity combinations are formed using a set of three primary double differences observed at the same epoch. The concept of using primary observations to form the ambiguity combinations was introduced by Hatch (1989) as part of the LSAST. This concept has been adapted to attitude determination with a rigid multi-antenna array.

The LSAST uses one reference antenna and one remote antenna at a time within its ambiguity resolution process. Hence, the technique concentrates on building a search volume about the remote antenna, forming ambiguity combinations which fall within the volume and then testing them. When applying this technique to three-dimensional attitude determination, some systems (Lu, 1995; El-Mowafy and Schwarz, 1995; Ferguson et al., 1994) will compute the ambiguities separately for the primary non-collinear antenna pairs. For example, consider the case where antenna A is the reference

antenna and remote antennas B and C are situated such that the baselines from A to B and A to C are noncollinear. Some systems will perform an ambiguity resolution on baseline A-B and another on baseline A-C. However if we consider the three antennas rigidly mounted, there are only three independent ambiguities. Rather than two sets of primary double differences, we only have one set. The three primary double differences would be selected based on the combination which provides the best QDOP. Two of the primary double differences would be from one collinear antenna combination and the third would be from the other antenna combination.

The difficulty with using a search zone on a sphere when forming the primary ambiguity combinations is computing only those integer ambiguities that fall on the surface. Lu (1995) suggests a technique incorporating Cholesky decomposition to solve this problem. However, this research takes a simpler "brute force" approach. The search zone can be divided into yaw, pitch, and roll search intervals. Three nested search loops are formed, one for each of the Euler angles yaw, pitch, and roll. Each loop starts at the edge of its respective search interval and steps across the zone by small angular increments. At each node, the real value for the three primary ambiguities is computed and rounded to the nearest integer and stored in an array along with the angular coordinates of the node. The angular "step" is computed by

$$\alpha = \left(\frac{si}{d} \right), \qquad \textbf{6.1}$$

where α …is the angular step interval in radians,

si …is the step interval in metres (0.065),

and d …is the longest baseline distance in metres.

After the entire search zone has been traversed, the ambiguity combination array is sorted and duplicate combinations are discarded. Those remaining unique ambiguity combinations and their approximate angular coordinates are then tested using a sequential least squares technique.

5.4 Testing Ambiguity Combinations

The ambiguity testing is performed in three steps. The first step is to process each primary ambiguity combination within a least squares adjustment. The least squares normal matrix $\mathbf{N}_p$, and u vector $\mathbf{u}_p$ formed for each observation within the primary solution are (Vanicek and Krakiwsky, 1986)

$$\mathbf{N}_{p_i} = \left(\mathbf{A}_{p_i}^T \mathbf{C}_{l_p}^{-1} \mathbf{A}_{p_i}\right) \quad , \tag{6.2}$$

$$\mathbf{u}_{\mathrm{p_i}} = \mathbf{A}_{\mathrm{p_i}}^{\mathrm{T}} \mathbf{C}_{\mathrm{l_p}}^{-1} \boldsymbol{w}_{\mathrm{p_i}} , \tag{6.3}$$

where $\mathbf{A}_{p_i}$ …the design matrix relating the quaternion unknowns to a double difference observation,

$\mathbf{C}_{l_p}$ …is the double difference covariance matrix,

and $\boldsymbol{w}_{\mathrm{p_i}}$ …is the misclosure vector.

The vector of the unknowns, $\boldsymbol{x}$ contains the four quaternions

$$\boldsymbol{x} = \begin{bmatrix} \mathrm{q}_1 \\ \mathrm{q}_2 \\ \mathrm{q}_3 \\ \mathrm{q}_4 \end{bmatrix}. \tag{6.4}$$

The design matrix $\mathbf{A}_{p_i}$ for a single double difference observations is formed by

$$\mathbf{A}_{p_i} = \left[\frac{\partial \nabla \Delta \Phi_{\alpha\beta}^{ij}}{\partial q_1} \quad \frac{\partial \nabla \Delta \Phi_{\alpha\beta}^{ij}}{\partial q_2} \quad \frac{\partial \nabla \Delta \Phi_{\alpha\beta}^{ij}}{\partial q_3} \quad \frac{\partial \nabla \Delta \Phi_{\alpha\beta}^{ij}}{\partial q_4} \right]. \tag{6.5}$$

The misclosure vector $\boldsymbol{w}_{\mathrm{p_i}}$ for a single double difference observations is formed by

$$\boldsymbol{w}_{\mathrm{p}} = \left[\nabla \Delta \Phi_{\alpha\beta}^{\mathrm{ij}} - \left(\nabla \Delta \rho_{\alpha\beta}^{\mathrm{ij}} + \nabla \Delta \mathrm{N}_{\alpha\beta}^{\mathrm{ij}} \right) \right] \quad . \tag{6.6}$$

Since the four quaternions are dependent, the quaternion condition equation should also be added.

The design matrix $\mathbf{A}_{p_i}$ for the quaternion condition equation is formed by

$$\mathbf{A}_{p_q} = \begin{bmatrix} 2q_1 & 2q_2 & 2q_3 & 2q_4 \end{bmatrix} \quad . \tag{6.7}$$

The misclosure vector $\boldsymbol{w}_{\mathrm{p_i}}$ for the quaternion condition equation is formed by

$$\boldsymbol{w}_{\mathrm{p_i}} = \left[1 - \left(\mathrm{q}_1^2 + \mathrm{q}_2^2 + \mathrm{q}_3^2 + \mathrm{q}_4^2\right)\right] \quad . \tag{6.8}$$

The addition of normals step-by-step adjustment technique is used to combine $\mathbf{N}_{p_i}$ and $\mathbf{u}_{p_i}$ formed for each observation (Adams, 1987)

$$\mathbf{N}_p = \sum_{i=1}^{3} \mathbf{N}_{p_i} \ , \tag{6.9}$$

$$\mathbf{u}_p = \sum_{i=1}^{3} \mathbf{u}_{p_i} \ . \tag{6.10}$$

The correction vector $\hat{\boldsymbol{\delta}}_p$ for the primary solution is formed by

$$\hat{\boldsymbol{\delta}}_p = -\mathbf{N}_p^{-1}\mathbf{u}_p \, . \tag{6.11}$$

The unknown quaternions are updated by

$$\hat{\boldsymbol{x}} = \boldsymbol{x}_0 + \hat{\boldsymbol{\delta}}_{\mathrm{p}} \, . \tag{6.12}$$

Unlike the kinematic positioning LSAST technique, we must redetermine the $\mathbf{A}_p$ and $\boldsymbol{w}_{\mathrm{p}}$ with each iteration. This is one disadvantage of using the unified approach with the quaternions as our unknowns.

If the primary combination can be adjusted within a set number of iterations, the second step is to form the secondary ambiguities using the quaternion solution from the primary adjustment. The third step is to perform a second least squares adjustment including all of the primary and secondary observations and compute the variance factor. The step-by-step techniques describe above can be used to perform the second adjustment. The double difference residuals are formed by

$$\hat{\boldsymbol{r}} = \begin{bmatrix} \nabla\Delta\hat{\rho}^{ij}_{\alpha\beta} + \nabla\Delta\hat{N}^{ij}_{\alpha\beta} - \nabla\Delta\Phi^{ij}_{\alpha\beta} \\ \nabla\Delta\hat{\rho}^{ik}_{\alpha\beta} + \nabla\Delta\hat{N}^{ik}_{\alpha\beta} - \nabla\Delta\Phi^{ik}_{\alpha\beta} \\ \vdots \\ \nabla\Delta\hat{\rho}^{it}_{\alpha\delta} + \nabla\Delta\hat{N}^{it}_{\alpha\delta} - \nabla\Delta\Phi^{it}_{\alpha\delta} \end{bmatrix}. \tag{6.13}$$

The variance factor $\hat{\sigma}_0^2$ is computed using

$$\hat{\sigma}_0^2 = \frac{\hat{\boldsymbol{r}}^{\mathrm{T}}\mathbf{C}_1^{-1}\hat{\boldsymbol{r}}}{n-u}. \tag{6.14}$$

The χ^2 test of the variance factor is first performed to verify the validity of the solution and takes the form (Vanicek and Krakiwsky, 1986)

$$\frac{(n-u)\,\hat{\sigma}_0^2}{\xi_{\chi^2_{(n-u)},1-\alpha/2}} < \sigma_0^2 < \frac{(n-u)\,\hat{\sigma}_0^2}{\xi_{\chi^2_{(n-u)},\alpha/2}}. \tag{6.15}$$

The test will fail for a variety of reasons, including:

a) the residuals have a non-normal density;
b) the incorrect mathematical model was used (including the incorrect ambiguities);
c) the presence of systematic errors in the observations; and
d) the incorrect *a priori* covariance matrix of the observations was used.

This test is effective in our case since the unified approach has a higher degree of freedom than the baseline approach. For example with four receivers each tracking six satellites, the degrees of freedom for the unified approach are 16 - 4 = 12, while for the baseline approach they are only 5 - 3 = 2 since we solve for each baseline separately.

Assuming the previous test is passed by at least two ambiguity sets, a ratio test is performed on the two ambiguity sets with the smallest variance factors. The ratio test takes the form

$$\frac{\hat{\sigma}_0^2(\text{2nd Min})}{\hat{\sigma}_0^2(\text{minimum})} > \text{threshold}. \qquad 6.16$$

The threshold value is typically set at a value between 2 and 3 (Cannon, 1992b; Lachapelle et al., 1992). The selection of the threshold is dependent on the applications. A low value will reduce the chances of rejecting the correct combination, but also increase the chances of accepting the incorrect one. The type II error of accepting the incorrect ambiguity combination is undesirable and for that reason the threshold should be set at 3.

CHAPTER 6

ATTITUDE SYSTEM DESIGN AND IMPLEMENTATION

A real-time system was designed and implemented by the author to test and verify the attitude determination algorithms developed in the previous chapters. The system, named CARDINAL™, can be divided into hardware and software components, though the two are not mutually exclusive. Decisions made in one design influence the other. The hardware design was largely influenced by the materials available to the author. GPS receivers and antennas were selected from systems available at Pulsearch. In the case of the NovAtel and Motorola receivers, newer models were on the market but were not available at Pulsearch in sufficient quantities for the attitude system. The selection of the computer system influenced the software design, since a pre-emptive task method was implemented during ambiguity resolution to compensate for the performance of a laptop PC 486-66.

The first section within this chapter will provide an overview of the attitude system design. Its hardware components will be identified and described. Following the hardware description, section two will discuss the software design and implementation. Afterwards, within the last section, the test vehicle and equipment installation will be reviewed.

6.1 Hardware Overview

The hardware system for CARDINAL™ can be divided into three major components: the antenna array, the GPS receivers, and the attitude computer. Figure 6.1 illustrates the data flow between the three major components for the attitude system.

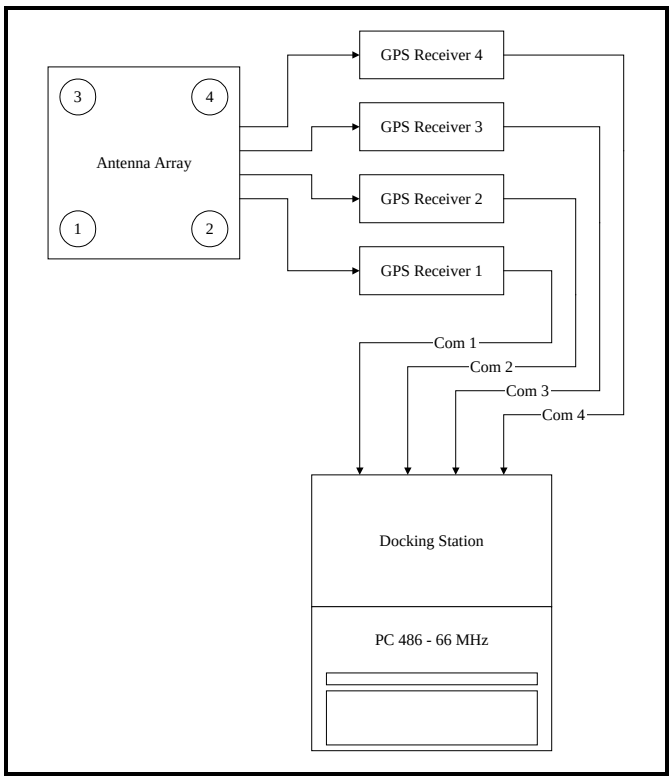

Figure 6.1 - CARDINAL™ Hardware Design

6.1.1 Antenna Array

The function of the antenna array is to intercept the L1 band signals emitted by the GPS satellites. The signals received by each of the four antennas are passed through a bandpass filter to filter out potential high-level interfering signals in adjacent frequency bands. The signal is then amplified by a signal preamplifier contained within each antenna module. Each antenna is connected to a specific GPS receiver within the system via a coaxial cable. Each of the four antennas are attached to a rigid antenna plate.

The 80 cm antenna plate was designed and constructed to attach atop the test vehicle. The plate was machined from a flat piece of 5mm aluminium plate and then drilled and tapped to accept the Sensor Systems microstrip antennas. The antennas were located at the four corners of the plate, 20 cm inside the outside edge of the plate, and form a square of 40.5 cm at each side. The antenna designated 1 is the reference antenna for the attitude system and sits at the origin of the body coordinate frame. The y axis of the body frame is parallel to the forward direction and runs through the centre antenna 3. The x axis points to the right of the vehicle and runs through the centre of antenna 2. Antenna 4 is mounted in the corner opposite antenna 1 and completes the square. In an effort to reduce carrier phase reflections, all antenna mounting hardware and cables are attached to the bottom of the plate. Straps for attaching the plate to the roof mounting brackets are run through slots in the plate and project no more than 0.5 mm above the surface of the plate. The antenna array configuration is illustrated in Figure 6.2.

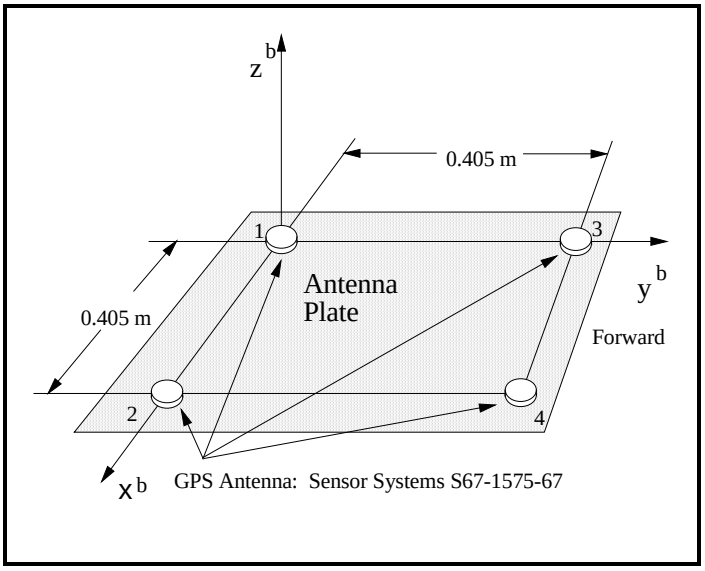

Figure 6.2 - Antenna Array Design

The Sensor Systems S67-1575-67 GPS antennas mounted on the array are an active antenna designed for land vehicle and man-pack where long cable runs are necessary. They feature a single connector with a threaded barrel and nut for installation. The antennas were selected because of their low profile, light weight, good signal reception

abilities, low cost and availability. One of the primary disadvantages of this antenna is that the connector is offset and careful alignment is required when mounting them to the antenna plate. Table 6.1 summarizes the antenna specifications.

Table 6.1 - GPS Antenna Specifications

Description	Specification
Frequency	1575.42 MHz ±2Mhz
Polarization	Right Hand Circular Polarization
Power	+4.0 to +24.0 VDC @ 25 mA max.
Gain (Preamp)	26 dB ±3 dB
Weight	85 grams
Size	55.9 mm Diameter, 16.5 mm Thick
Operating Temperature	-55°C to 85°C
Altitude	-30 m to 16,700 m
Price in US Dollars	$275

The gain pattern of the antenna as shown in Figure 6.3 is typical of a microstrip antenna and drops off from a gain of -1 dBic at 15 degrees elevation to a gain of -7.5 dBic at the horizon.

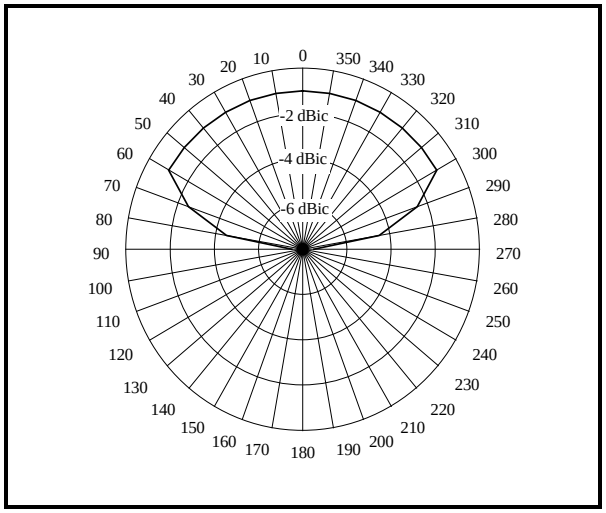

Figure 6.3 - Antenna Gain Pattern

Evans and Hermann (1989) found that microstrip antennas had the lowest signal multipath of the antenna combinations they tested. The antennas tested in addition to the microstrip antenna included: a log periodic spiral antenna, a small circularly polarized turnstile antenna, a drooping turnstile antenna, and a fixed radiation pattern antenna. The lower gain at the antenna horizon and below help discriminate against ground and vehicle induced phase multipath (Wells et al., 1986). However microstrip antennas may exhibit some degree of multipath contamination of carrier phase observations resulting in relative positioning errors of several centimetres (Georgiadou and Kleusberg, 1989). To put the multipath error effect in perspective, a 2 cm horizontal displacement of antenna 3 at right angles to the 40.5 cm antenna 1-3 baseline can result in an apparent angular displacement of the antenna array of nearly 3 degrees. The effect of multipath contamination can be decreased in the static case by long observation periods. However, this is not possible with dynamic attitude systems given the instantaneous nature of their observations and estimation methods.

Various ground planes including those constructed from RF absorbent material (Lachapelle et al., 1989) and choke rings (Lachapelle et al., 1993) have proven to be effective methods of reducing multipath. However, in the case of the cone shaped RF absorbent ground plane, Lachapelle et al. (1989) found that it was better suited to

stationary rather than dynamic applications. Choke ring ground planes, while being highly effective at reducing multipath (Evans and Hermann, 1989) are costly and relatively heavy. For example, a NovAtel choke ring ground plane constructed of cast aluminium and their Model 501 geodetic antenna cost $1270 US and have a combined weight of 3.9 kg. This is five times the cost of antenna used within the CARDINAL™ design and some 46.9 times the weight. The use of choke rings within this design while preferable was not possible, primarily because of the high cost and low probability of continued availability during system testing. However, in an effort to minimize multipath, while maintaining costs, a simple modification to the antenna plate was made. The antenna plate was designed to ensure that a minimum of 20 cm of ground plane surrounded the phase centre of each antenna. It was hoped that the ground plane along with the low profile of the microstrip antenna would produce an array with low multipath characteristics. A disadvantage of this design was discussed by Tranquilla and Colpitts (1989), who found that the edges of a flat ground plane can induce strong diffraction effects, resulting in poor single-point phase performance.

6.1.2 GPS Receivers

Coaxial cables carry the filtered and amplified GPS signals from the antenna array to the radio frequency (RF) signal processing sections of the four GPS receivers. The RF signal is demodulated to an intermediate frequency (IF) and then into the signal processing section of the GPS receivers. Within the signal processor, the IF signal is passed through an analogue to digital (A/D) converter. The A/D converter converts the IF signal to a digital sequence which is then split into separate channels for code correlation, carrier tracking, code tracking, and signal detection. The position processing module then accepts the signals from the signal processor. It will decode and process satellite data, pseudorange and carrier phase measurements to compute position and velocity. The processor will pass user requested information to the input/output (I/O) section for transfer to the users computer via a serial interface (Magnavox, 1992; Motorola, 1994; NovAtel, 1993).

The GPS receivers used within the design are OEM style receivers capable of measuring and outputting L1 C/A code pseudoranges and phase at a rate of at least 1 Hz. Receivers from three manufactures were tested within the design. The three receivers varied in terms of measurement rates and phase measurement accuracies. Table 6.2 contains the specifications for each receiver.

Table 6.2 - GPS Receiver Specifications

Specification	NovAtel 2151™	Motorola Oncore™	Leica GPS Engine™
Channels	10 discrete	6 discrete	6 discrete
Data Rate - Hz	10	1	1
Correlator	Narrow	Standard	Standard
Interface	RS232 / RS422	RS232	TTL
Power	+5 VDC @900 mA +12 VDC @80 mA -5 VDC @ 40 mA	+12 VDC@150 mA	+7 VDC@180 mA +5 VDC @ 200 mA
Size	100 mm x 167 mm	70 mm x 100 mm	65 mm x 161 mm
Operating Temperature	0°C to 70°C	-30°C to 85°C	-20°C to 70°C
Acceleration	4 g	4 g	2.5 g
Price	$3495 US (for new 12 channel version)	$1200 US (for new 8 channel version)	N/A

The NovAtel and Leica OEM cards require regulated power at various voltage levels. Each NovAtel card was installed into a NovAtel PowerPak enclosure which contains the necessary power conditioning. The Leica cards were installed into a Pulsearch NE-1 enclosure which supplied power at the necessary levels as well as converting the TTL level serial communications to RS232 levels. Both the NovAtel and Pulsearch card enclosures will use +10 to +32 VDC input power. The Motorola cards were left in their

original plastic enclosures, however an external battery was added to each to provide backup power to their real-time clock and "keep alive" RAM memory.

6.1.3 Computer

The GPS receivers were interfaced via RS232 to a PC 486 laptop with a clock speed of 66 MHz and 8 Mbytes of RAM memory. Attached to the rear of the computer via a SCSI bus was a docking station containing four serial ports. A black and white LCD screen built into the laptop was used to display program information. A 850 Mbyte hard disk stored the software and provided data storage. Power to the computer was supplied by either a 110 VAC converter or a 12 VDC converter. The operating system used was MS-DOS 6.22™. The computer system was barely capable of receiving pseudorange, phase and ephemeris data from the four GPS receivers at 1 Hz, while simultaneously running the attitude filters and if necessary the ambiguity resolution routine. In a effort to reduce the data volume, position and satellite almanac data were only requested from the reference receiver, while all of the receivers output carrier phase measurements, pseudorange mesurements and broadcast ephemeris.

6.2 Software Design and Implementation

The software package CARDINAL™ was written by the author based on the algorithms and techniques presented in the previous chapters. Its purpose was to provide a platform for testing and verifying the ability to estimate attitude in real-time using the quaternion based double difference GPS models. CARDINAL™ was written in the C language to operate on a PC machine running MS-DOS in 32bit extended mode.

Software libraries from Pulsearch Navigation Systems Inc. were relied upon to supply routines for: serial communications, GPS receiver message decoding, GPS receiver control, precise PC timing, satellite coordinate computations, GPS phase and pseudorange corrections, coordinate transformations, least squares estimation, Kalman filtering, and matrix algebra. The base of the attitude determination software was constructed using the stable, and debugged routines provided by these libraries. Added

to complete the structure of the program were routines for: operator input, task management for real-time operation, attitude parameter transformation, forming double differences, least squares estimation and Kalman filtering using quaternion based double difference observations, cycle slip detection, quality control, carrier phase ambiguity resolution on-the-fly, and information display and storage.

The software used simple pre-emptive task techniques to allow apparent simultaneous operation of user input, status display, data reception, decoding, processing, filtering and ambiguity resolution. With the software written in this way, it was not necessary to complete ambiguity resolution tasks within 1 second. In some cases, with debugging I/O and data storage tasks turned on, the ambiguity resolution routine would take 2 or 3 seconds to complete, yet data was still decoded and fed to the filters in a timely fashion. It is often a mistaken premise that ambiguity resolution must be completed within one measurement epoch. While preferable, it is more important for the decoding and filtering tasks to detect cycle slips within the phase observations so that an operating ambiguity resolution task can be interrupted and restarted.

A flowchart of the CARDINAL™ operation is shown in Figure 6.4. Pseudorange, phase, ephemeris and position data from the GPS receivers is received by the interrupt driven serial data handlers and stored in 10 Kbyte circular buffers. Independent of the serial routines, the main task manager looks for operator input, inspects the serial buffers, and displays program status. When the task manager detects a full receiver message sitting in the serial buffer it will drain the buffer, and call the decoding task to decode the message and store it within a generic internal GPS data structure (one for each of four GPS receivers).

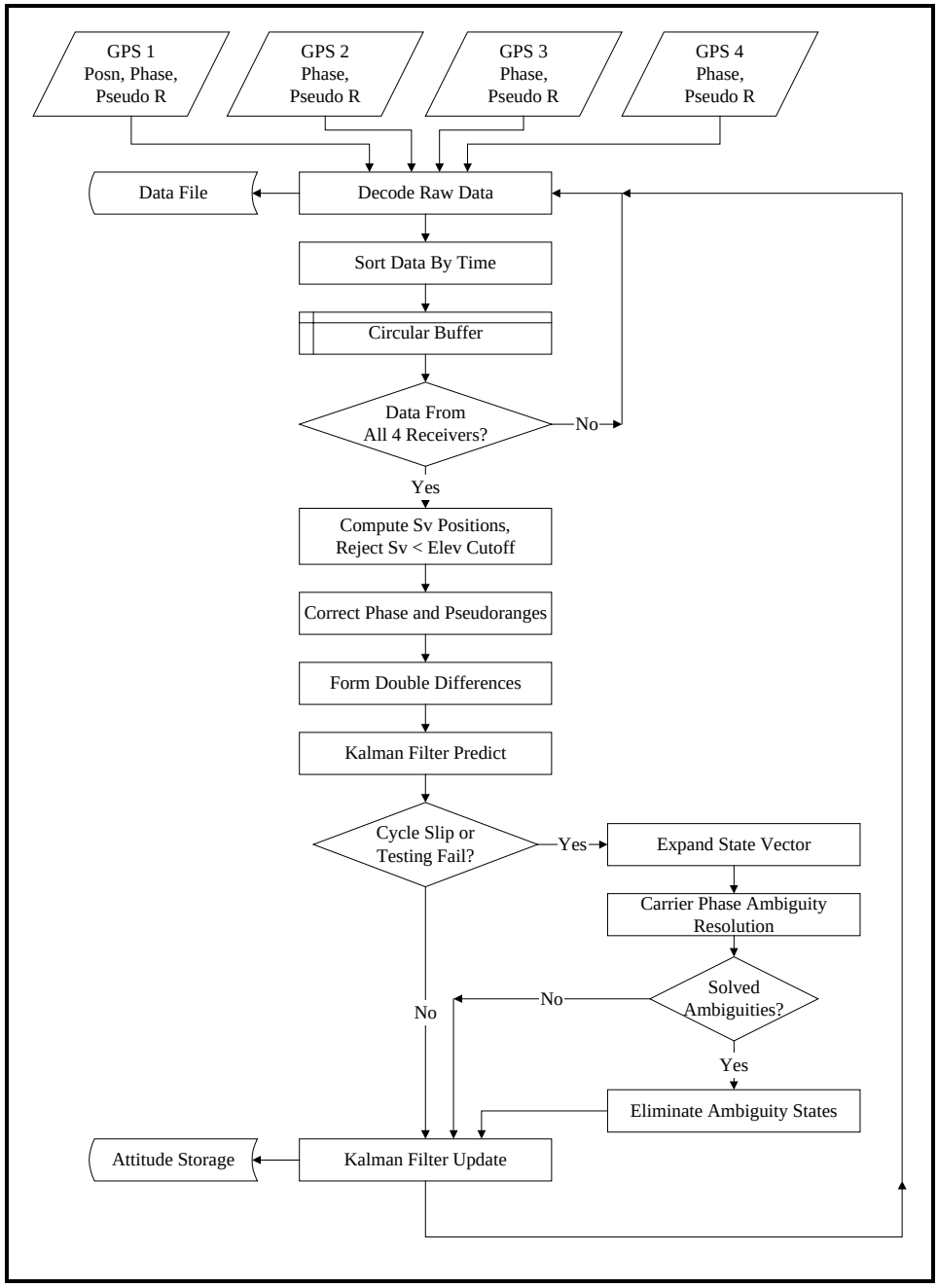

Figure 6.4 - CARDINAL™ Software Flowchart

When pseudorange and phase data are detected, the decoding task will call the double difference task which in turn will store the observations in a temporary holding buffer. The double difference task will then look for the earliest set of data within the temporary buffer from all four GPS receivers. If a full data set is detected, the pseudorange and

phase double differences are formed and the satellite coordinates are computed from the latest available ephemeris. A request is then submitted to the queue manager to execute the attitude filtering task. In addition, any partial sets of observations older than the full set are cleared from the holding buffer. The double difference task then returns control of the processor back to the task manager.

When the task manager has an opportunity, it will start-up the attitude filtering tasks. Within the task, the first operation is prediction up to the time of the new data set. Following prediction, the double difference innovations are tested. If one or more double difference observations fails the innovation testing or a cycle slip was detected within one of its phase observations, the state vector of the filter is expanded. An ambiguity state is added to the state vector (if it is not already present) for each double difference set containing a cycle slip or failing the innovations testing. In addition, a high priority request is sent to the task manager to execute the ambiguity resolution task.

The ambiguity resolution task will build a search area and form the ambiguity combinations for the three double differences giving the smallest QDOP value. The ambiguity values are tested and if a statistically significant “best” solution passes the quadratic test of the residuals, the double difference ambiguities will be fixed and the ambiguity states eliminated. While the ambiguity resolution task is executing, the filtering task is on temporary hold. Should the ambiguity resolution task finish before the next observation is detected by the double difference task, the filtering task will continue on with the phase and pseudorange double difference update of the filter with the phase ambiguities fixed. However, if the double difference task detects a new set of double differences while the ambiguity resolution task is still executing, the filtering task will be reactivated and perform the update of the filter using the first data set with the phase ambiguities floating and the ambiguity states present. Then the new data set will be fed into the filter and the prediction and testing will be performed on the new double differences. If the new double differences fail the innovations tests or cycle slips are detected, the ambiguity resolution task is restarted with the new data. Again the filter will

be suspended until either the ambiguity resolution routine is completed or a new double difference data set is detected.

6.3 Test Vehicle and System Installation

To test the attitude system under dynamic conditions, it was installed in a Ford 4x4 truck. The antenna array was securely attached to the top of the cab using a commercial roof-rack. Coaxial cables from the four antennas were run through the back window of the cab. They were connected to one of the three sets of four GPS receivers sitting in a specially constructed rack attached to the back portion of the truck cab. Serial cables from the GPS receivers were run to a laptop computer sitting on the front passenger seat. Only one set of GPS receivers could be tested at a time. Power from the 12 VDC power-point of the truck was fed to the GPS receivers and laptop computer. Safety during dynamic tests was of paramount concern and the attention of the driver must remain focused on the road. To alleviate the need for the driver to visually inspect the programs status, audible tones corresponding to the activation of certain software tasks and status were inserted into the CARDINAL™ software. Figure 6.5 illustrates the equipment configuration.

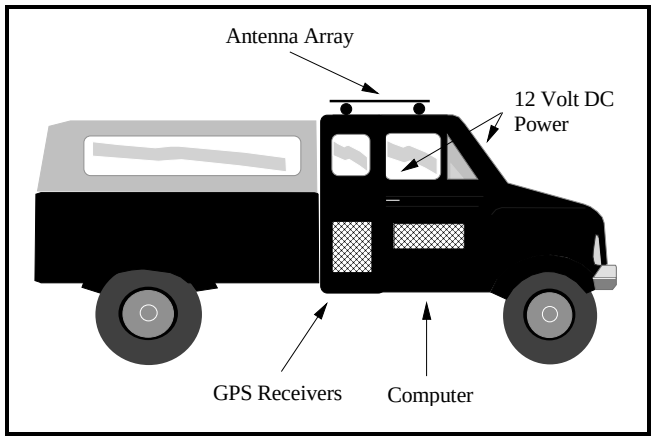

Figure 6.5 - Attitude System Installation in Test Vehicle

CHAPTER 7

TEST DESCRIPTION AND RESULTS

A series of static and dynamic tests were conducted with the prototype GPS attitude system described in the previous chapter. Three tests were performed including: a static test, a dynamic test over a level course, and a dynamic test over a hilly course. Three receiver types were used during the static test and first dynamic test. During the last dynamic test only the NovAtel 2151™ receivers were used. The real-time results from the first of the three tests are compared against those computed post-mission using the SEMIKIN™ program developed at the University of Calgary (Cannon, 1990).

The objectives of the tests were the following:

1) to verify the double difference math models,
2) to test the design of the Kalman filter,
3) to assess the performance of the ambiguity resolution routines, and
4) to gauge the achievable system accuracy using different GPS receivers.

Descriptions for the static test and two dynamic tests are given. Results for the tests are presented and comparisons are made between the results from the three GPS receivers.

7.1 Static Trials

Tests were conducted to measure the static performance of the CARDINAL™ attitude system. A test description, followed by results and analyses are given.

7.1.1 Test Description

Static tests of the attitude system were conducted on three separate days using four receivers from three manufactures, namely: NovAtel, Leica, and Motorola. The first test was performed with the NovAtel 2151™ receivers and occurred on March 30, 1996. A second test was conducted with the Leica GPS Engines™ on April 1, 1996 and on the following day the third test was done using the Motorola Oncore™ receivers. The test area selected was in the parking lot of the Calgary Soccer Centre at 7000 48th Avenue S.E. Calgary, Alberta. This area is relatively free of tall buildings, trees and traffic. With the exception of two light standards approximately 35 metres from the test spot, the horizon is clear from 5° elevation and above. Figure 7.1 illustrates the static test site.

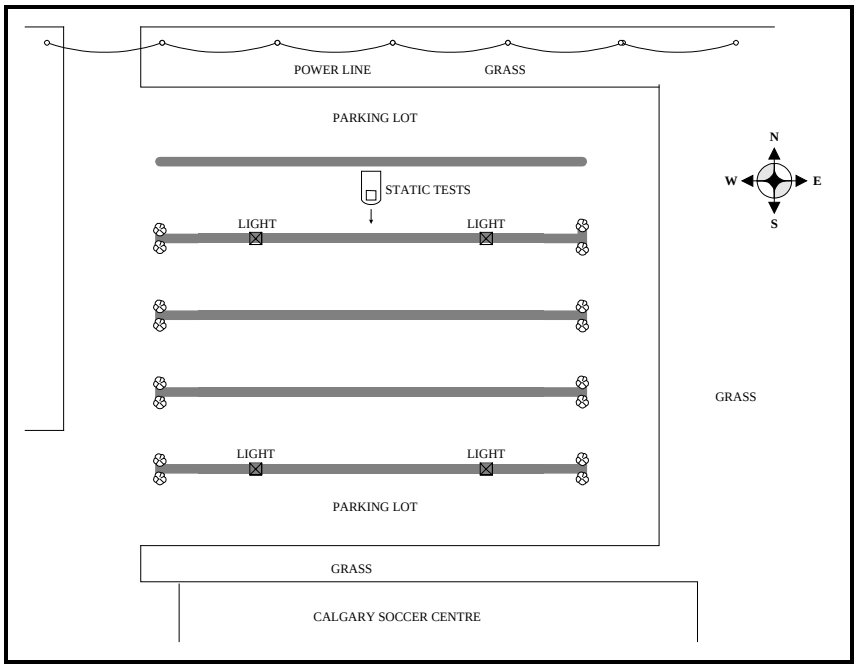

Figure 7.1 - Static Test Area - Calgary, Alberta

The test vehicle was parked at the north end of the lot and oriented approximately south. Once stationary, the attitude system was started and data logging begun. Each of the tests was conducted at approximately the same sidereal day time to ensure that the same GPS constellation was used by each set of receivers. Table 7.1 details the observation times. Satellites below 15° elevation were not used by the attitude system since signal attenuation and multipath effects are more common on the lower elevation satellites. While the NovAtel receiver is an all-in-view receiver, the Leica and Motorola receivers are not, and their tracking algorithms were set to track the highest six healthy satellites.

Table 7.1 - Static Observation Times

Receiver Type	Day of Year 1996	Start GPS time (s) h:m:s	End GPS time (s) h:m:s
NovAtel 2151™	090	587955 19:19:15	590190 19:56:30
Leica GPS Engine™	092	155475 19:11:15	157710 19:48:30
Motorola Oncore™	093	241635 19:07:15	243870 19:44:30

Following each of the three tests, the pseudorange and phase data from the four GPS receivers were processed using SEMIKIN™ in static mode. Attitude values shown in Table 7.2 were computed from the baseline results provided by SEMIKIN™.

Table 7.2 - Attitude Values Computed Using SEMIKIN™

Receiver Type	Day of Year	Heading	Pitch	Roll
NovAtel 2151™	090	181° 36.5’	1° 34.2’	-0° 28.0’
Leica GPS Engine™	092	180° 42.5’	0° 52.6’	-0° 33.1’
Motorola Oncore™	093	177° 15.2’	1° 16.8’	-0° 20.8’

The CARDINAL™ software settings used during the static test are listed in Table 7.3.

Table 7.3 - Input Parameters for CARDINAL™ Real-time System

Parameter	Setting
Standard Deviation of $\nabla\Delta\Phi$	1 cm
Standard Deviation of $\nabla\Delta P$	1 m
Spectral Density for Rotation Rate States	0.09 $rad^2\ sec^{-3}$
Spectral Density for Ambiguity States	0.0001 $m^2 sec^{-1}$
Yaw Search Zone - Ambiguity Resolution	± 360°
Pitch Search Zone - Ambiguity Resolution	± 15°
Roll Search Zone - Ambiguity Resolution	± 15°
Confidence Interval for Test of Quadratic Form of the Residuals - Ambiguity Resolution	99%
Confidence Interval for Innovations Testing	99%
Satellite Elevation Cutoff	15°

The CARDINAL™ real-time results recorded at a epoch rate of 1 second are compared against the SEMIKIN™ results in the following section.

7.1.2 Comparison of Results From NovAtel, Leica and Motorola Receivers

The results of the three static tests are presented. The results for the NovAtel test will be presented first, followed by those from the Leica test and then the Motorola test. The plots containing the heading, pitch, and roll results for each receiver feature the real-time attitude values and the two sigma standard deviations obtained from the system Kalman filter which are plotted on either side of the SEMIKIN™ derived results (plotted as a single black line spanning the graphs).

The real-time heading, pitch, and roll results obtained using the NovAtel receivers are shown in Figure 7.2, Figure 7.3, and Figure 7.4, respectively.

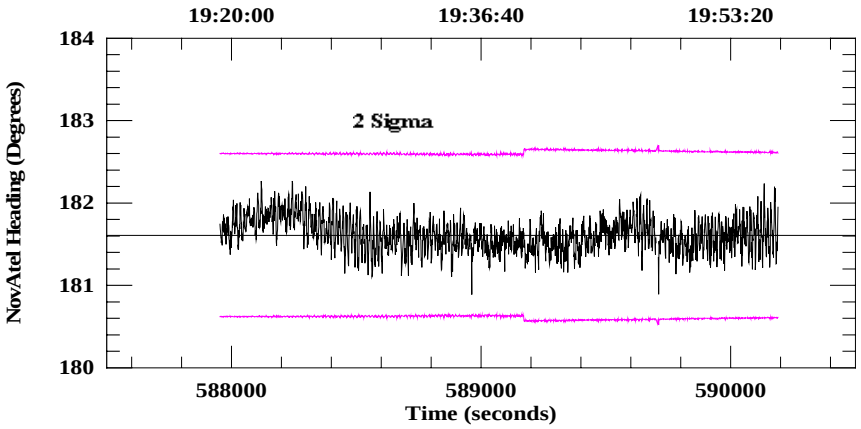

Figure 7.2 - Estimated Heading Using NovAtel 2151™

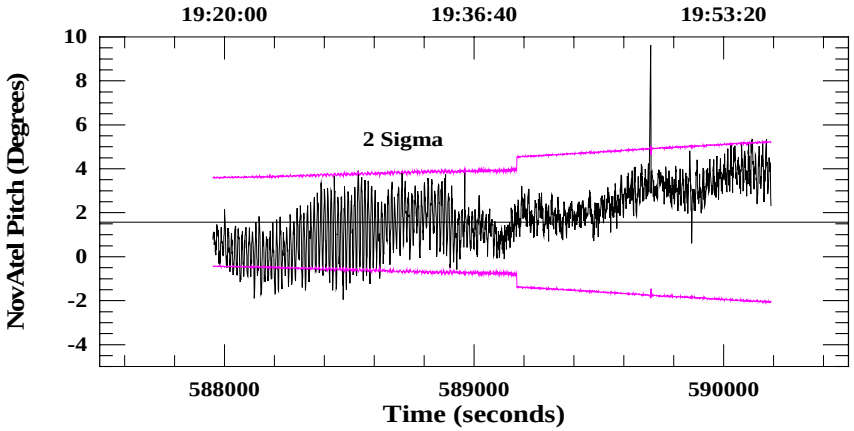

Figure 7.3 - Estimated Pitch Using NovAtel 2151™

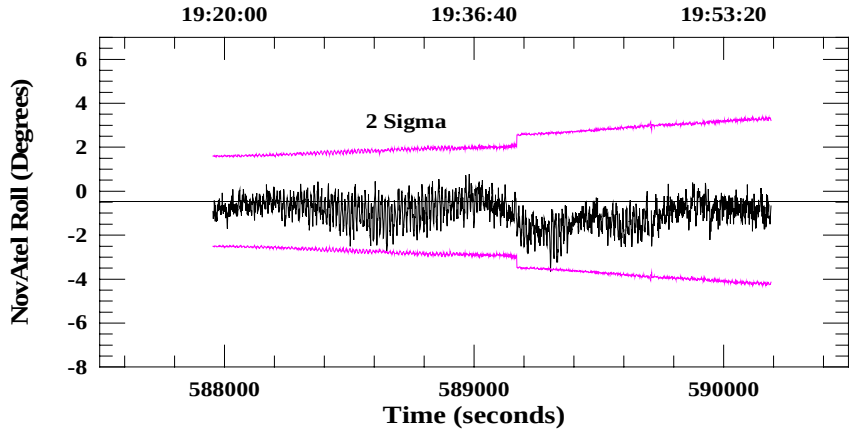

Figure 7.4 - Estimated Roll Using NovAtel 2151™

The real-time heading, pitch and roll results obtained using the Leica receivers are shown in Figure 7.5, Figure 7.6, and Figure 7.7, respectively.

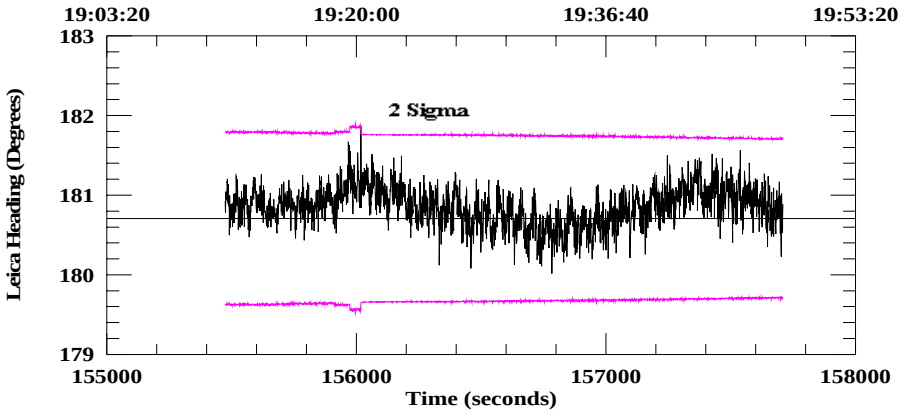

Figure 7.5 - Estimated Heading Using Leica GPS Engine™

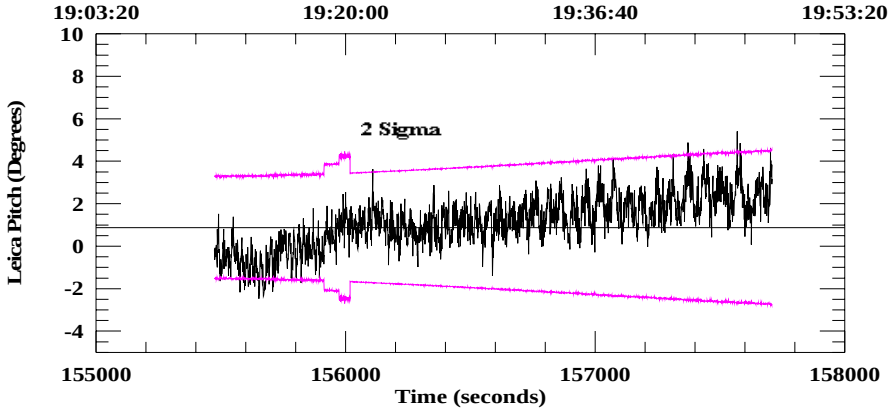

Figure 7.6 - Estimated Pitch Using Leica GPS Engine™

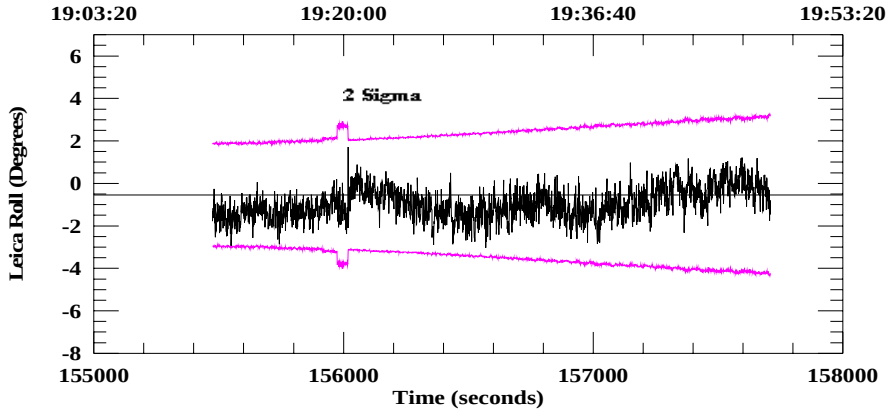

Figure 7.7 - Estimated Roll Using Leica GPS Engine™

The real-time heading, pitch and roll results obtained using the Motorola receivers are shown in Figure 7.8, Figure 7.9, and Figure 7.10, respectively.

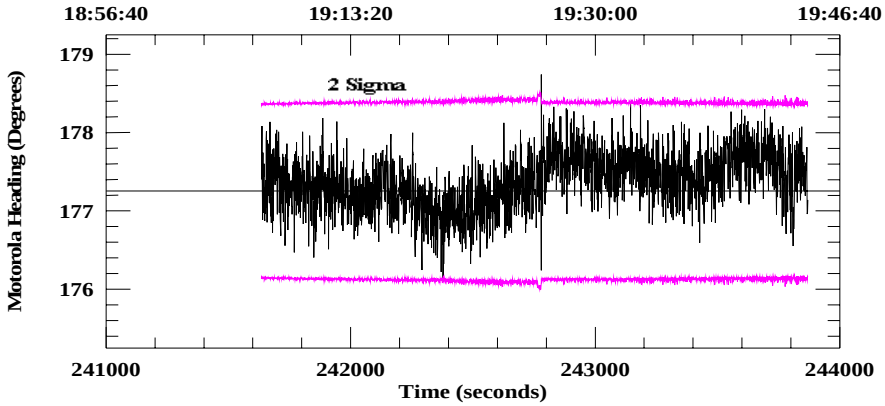

Figure 7.8 - Estimated Heading Using Motorola Oncore™

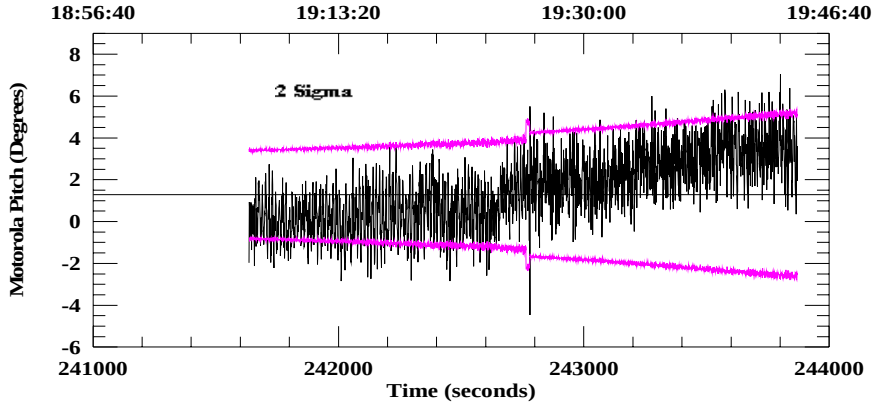

Figure 7.9 - Estimated Pitch Using Motorola Oncore™

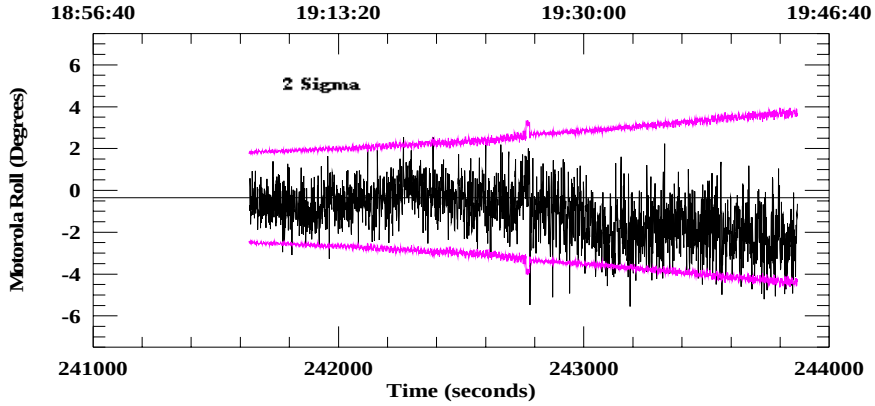

Figure 7.10 - Estimated Roll Using Motorola Oncore™

Two trends are evident from the figures: a high frequency noise component probably due to receiver noise, and a lower frequency noise component possibly due to edge diffraction effects from the ground plane, antenna phase centre instability, or phase multipath. Inspection of the attitude plots from the three receiver tests indicates good agreement between the CARDINAL™ and SEMIKIN™ values. The real-time results are distributed about the SEMIKIN™ values, with an occasional bias. Especially evident is the trend in the pitch component for all three receiver types. For all three receivers, the pitch begins to increase midway through the data and continues to increase until the end of the data. The total increase in pitch is approximately 2 degrees. This significant change in pitch over 1000 seconds could be due to either edge diffraction effects from the large antenna plate or a phase centre instability in the Sensor Systems antennas used. Examination of the satellite tracks for the sessions indicate that GPS satellite PRN 24 rises above the system 15 degree elevation cutoff from the south (forward direction of vehicle) midway through the data collection. GPS satellite PRN 24 continues to rise as the data collection continues. This low satellite rising from the forward direction, coupled with antenna phase centre instability or edge diffraction could account for the pitch bias. Further tests with different GPS satellite constellations and antenna alignments are required to determine the exact cause of the bias.

A spike in the pitch from the NovAtel receiver is evident in Figure 7.3 at the GPS time of 589708 seconds. This spike corresponds to a cycle slip and the unsuccessful ambiguity resolution attempt at the same time. The ambiguities were successfully resolved during the next epoch.

The attitude results from the Motorola Oncore™ system appear more noisy than those from the NovAtel or Leica receivers. In most cases, the attitude values are bounded by the two sigma covariance values, indicating that the *a priori* estimate of the double difference phase observation noise used within the system Kalman filter was reasonable.

Cohen and Parkinson (1991) demonstrated that a multipath environment is highly repeatable from day to day. Comparing the attitude results between the receivers indicates no repeatable pattern to the lower frequency heading or roll noise from one data set to another. In examining the static data sets, we see that each data set was gathered at approximately the same sidereal time each day with the same antenna array. However the vehicle orientation varied by 1° to 2° each day and more importantly, different receivers with different tracking loops were used.

A comparison of the static results obtained using the three receiver types are presented in Table 7.4. The root mean square (RMS) values were determined relative to the SEMIKIN™ derived results.

Table 7.4 - Comparison of Static Attitude Results

Receiver	SEMIKIN	Mean	Max.	RMS	RMS
NovAtel Heading	181° 36.5’	181° 36.6’	178° 03.9’	0.225°	3.9 mrads
NovAtel Pitch	1° 34.2’	1° 49.7’	9° 36.7’	1.430°	25.0 mrads
NovAtel Roll	-0° 28.0’	-0° 57.4’	11° 25.1’	0.860°	15.0 mrads
Leica Heading	180° 42.5’	180° 50.9’	181° 51.9’	0.282°	4.9 mrads
Leica Pitch	0° 52.6’	1° 08.4’	5° 23.7’	1.234°	21.5 mrads
Leica Roll	-0° 33.1’	-0° 57.8’	-3° 03.7’	0.851°	14.9 mrads
Motorola Heading	177° 15.2’	177° 22.6’	173° 18.8’	0.392°	6.8 mrads
Motorola Pitch	1° 16.8’	1° 30.1’	7° 02.3’	1.744°	30.4 mrads
Motorola Roll	-0° 20.8’	-1° 07.6’	-5° 33.8’	1.488°	26.0 mrads

The RMS values for the Euler angles agree with our observations from the graphs, indicating that while the NovAtel and Leica receivers give similar results, those from the Motorola are more noisy. The heading from the NovAtel system has an RMS of 3.9 mrads, while that for the Leica system is 4.9 mrads and for the Motorola system is 6.8 mrads.

Further inspection of the static data reveals several reasons the results from Motorola exhibiting higher noise levels relative to the NovAtel and Leica receivers. The first reason follows from inspection of Figure 7.11, which shows that the Motorola receivers were only tracking 5 satellites during the day 093 tests, while the NovAtel receivers were tracking 6 and 7 satellites on day 090 and the Leica receivers were tracking 6 satellites on day 092. Closer inspection of the data reveals that the ephemeris for PRN 2 was not successfully transferred from the Motorola receivers to the software, resulting in CARDINAL™ rejecting the PRN 2 observations. The second reason for Motorola attitude estimates exhibiting higher noise levels are revealed in graphs made of the root mean square (RMS) of all the double difference phase residuals for a single epoch output by CARDINAL™. The RMS values are presented Figure 7.12, Figure 7.13, and Figure 7.14 for the NovAtel, Leica and Motorola receivers respectively.

Inspection of the three graphs reveals that the RMS residual values for the Motorola based attitude system exhibit higher noise levels and generally exceed those for the NovAtel or Leica based systems. This indicates that the phase measurements from the Motorola may have higher noise levels than those from the other two receivers.

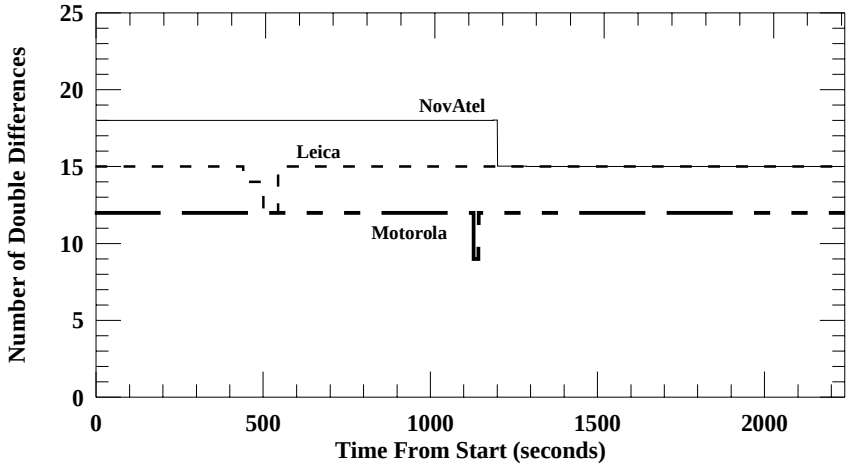

Figure 7.11 - Number of Observations - Static

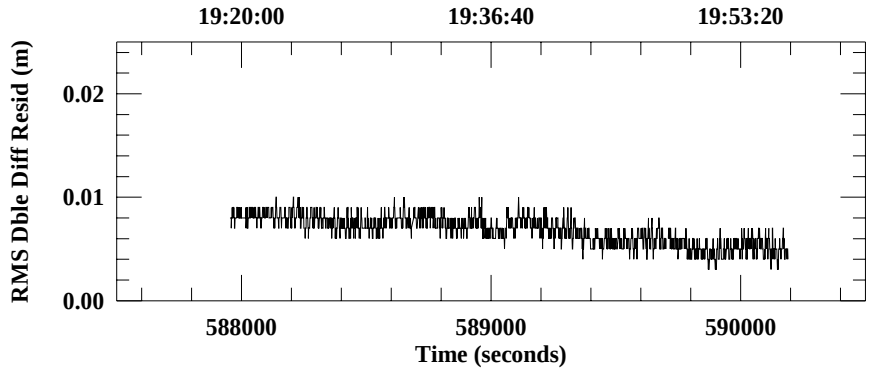

Figure 7.12 - NovAtel RMS Double Difference Residuals

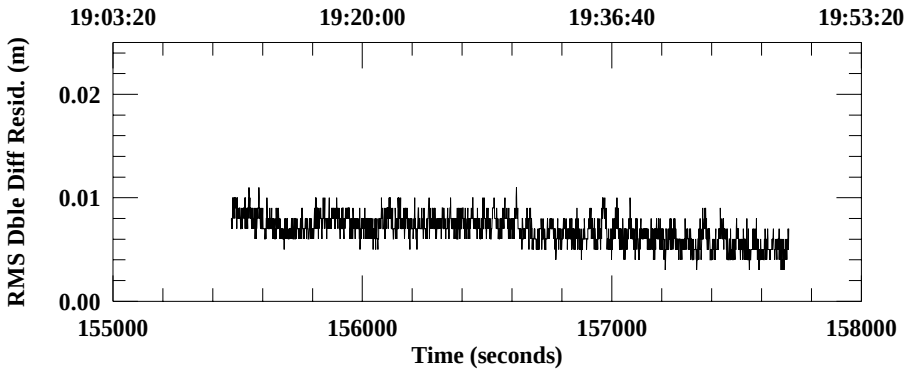

Figure 7.13 - Leica RMS Double Difference Residuals

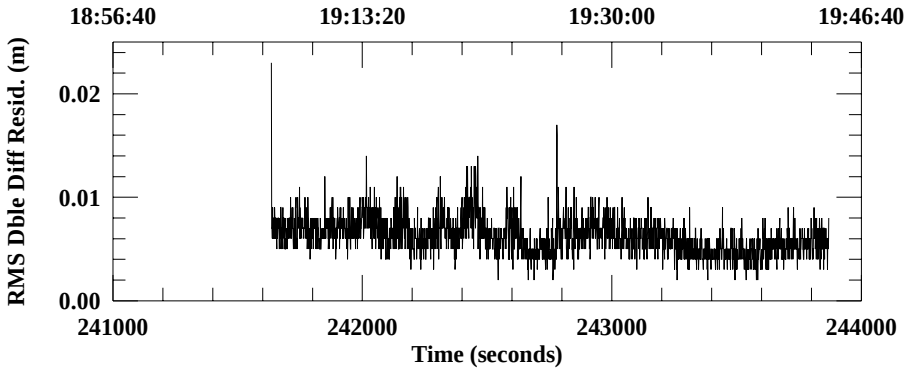

Figure 7.14 - Motorola RMS Double Difference Residuals

The static assessment of the attitude system would not be complete without visiting the ambiguity resolution performance. Table 7.5,

Table 7.6, and Table 7.7 summarize the ambiguity resolution statistics for the NovAtel, Leica and Motorola receiver tests, respectively.

The tables contain the following data:

	Solution	…whether the solution was successful (fixed) or not (float),
	Test	…if the correct ambiguity combination was chosen or if the resolution was not successful, the reason for the failure,
	Total	…total number of primary ambiguity combinations formed on search area,
	Sorted	…number of unique primary ambiguity combinations follow sort,
	Adjust	…number of ambiguity combinations that were successfully adjusted,
	Min	…the minimum sum squared residuals,
	2nd	…the second lowest sum squared residuals,
	Vf	…aposteriori variance factor,
and	Df	…degrees of freedom.

Table 7.5 - NovAtel Static Ambiguity Resolution

Solution	Test	Total	Sorted	Adjust	Min	2nd	Vf	Df
Fixed	Correct	745	65	34	0.0012	0.027	1.07	15
Fixed	Correct	787	58	30	0.0011	0.021	0.71	15
Float 1sec	Fail Vf Test	566	31	14	0.010	0.015	8.75	15
Fixed	Correct	568	32	14	0.00066	26.22	0.55	15

Table 7.6 - Leica Static Ambiguity Resolution

Solution	Test	Total	Sorted	Adjust	Min	2nd	Vf	Df
Fixed	Correct	622	34	14	0.00058	0.0021	0.48	12
Fixed	Correct	738	51	15	0.00063	0.024	0.52	12
Fixed	Correct	745	51	15	0.00069	0.027	0.57	12

Table 7.7 - Motorola Static Ambiguity Resolution

Solution	Test	Total	Sorted	Adjust	Min	2nd	Vf	Df
Fixed	Correct	654	54	34	0.00087	0.0035	0.96	9
Fixed	Correct	743	40	11	0.00076	0.018	0.85	9
Fixed	Correct	743	38	8	0.00058	0.017	0.64	9

The NovAtel ambiguity resolution results indicate that four resolutions were attempted during the test period. Of the four attempts, three were successful within one epoch and the correct ambiguities were resolved. Analysis of the one unsuccessful attempt shows that the incorrect combination was chosen, but was rejected during the quadratic test of combinations *a posteriori* variance factor.

The ambiguity resolution results for the Leica test indicate that three resolutions were attempted and all were successful. The Motorola data set also contained three resolution attempts and all three were also successful.

It is interesting to note in all of the resolution attempts the large disparity between the initial number of primary combinations formed on the search surface and the actual number of unique combinations. In addition, in most cases only one half of the unique combinations converge during their least squares adjustment.

7.2 Vehicle Trials Over a Level Course

Tests were conducted with a land vehicle travelling over a level course to measure the dynamic performance of the CARDINAL™ attitude system. A test description, followed by results and analyses are given.

7.2.1 Test Description

Dynamic tests of the attitude system were conducted on three separate days using four receivers from three manufactures, namely: NovAtel, Leica and Motorola. The first test was performed with the NovAtel 2151™ receivers and occurred on March 31, 1996. A second test was conducted with the Leica GPS Engines™ on April 2, 1996 and on the following day the third test was done using the Motorola Oncore™ receivers. The test area selected was in the parking lot of the Calgary Soccer Centre at 7000 48th Avenue S.E. Calgary, Alberta. This area is relatively free of tall buildings, trees and traffic. With the exception of four light standards, the area horizon is clear from 5° elevation and above. Figure 7.15 illustrates the test site.

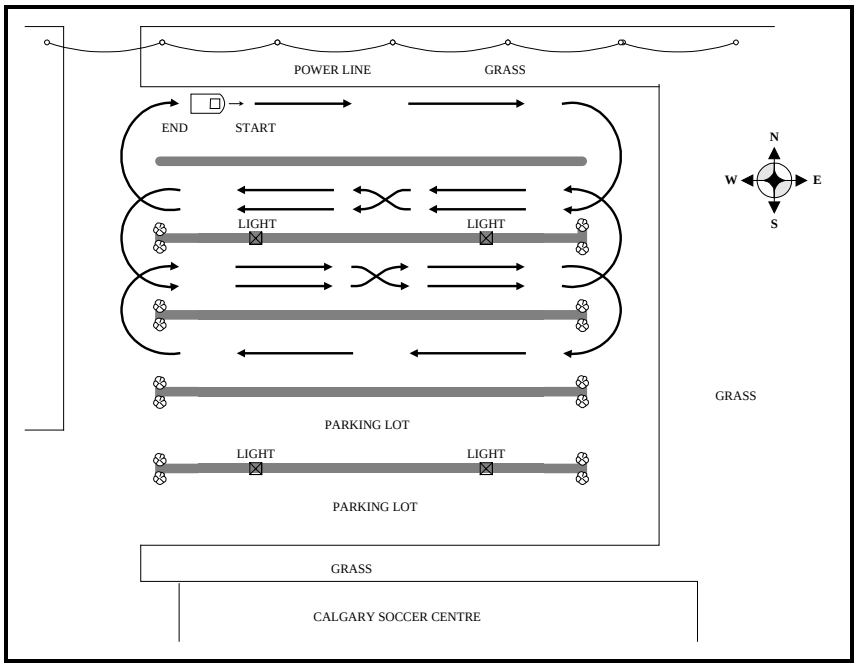

Figure 7.15 - Dynamic Test Area - Calgary, Alberta

The dynamic test started with the vehicle pointing east. The vehicle remained stationary for 1 minute and then moved off at a speed of 10 to 15 km/h. A series of 180° right and left turns were performed as the vehicle negotiated the test area. The test ended at the same location as it started and static data were logged for 1 minute before the system was shut down. Data were also recorded at a control station located atop the Pulsearch office. The control station was located 1.5 km west of the test area. The base receiver used was a NovAtel 3151R™ GPS receiver with a NovAtel 501 geodetic antenna and chokering groundplane. Following each of the three tests, the pseudorange and phase data from the system reference receiver (antenna 1) were processed relative to control station data using SEMIKIN™. The results from SEMIKIN™ were used to derive the trajectory of the vehicle. The trajectories of the vehicle for the NovAtel, Leica and Motorola receiver tests are shown in Figure 7.16, Figure 7.17, and Figure 7.18.

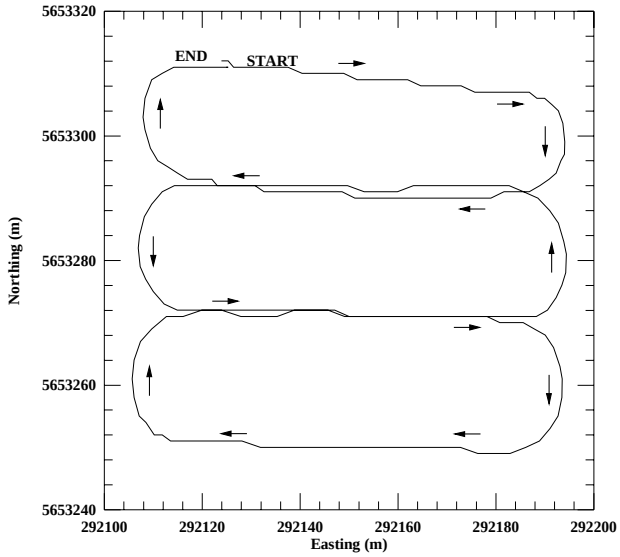

Figure 7.16 - Vehicle Trajectory For NovAtel 2151™ Trial

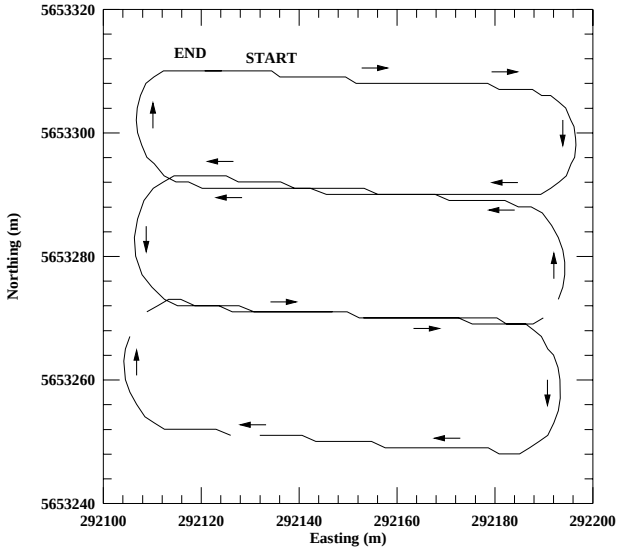

Figure 7.17 - Vehicle Trajectory For Leica GPS Engine™ Trial

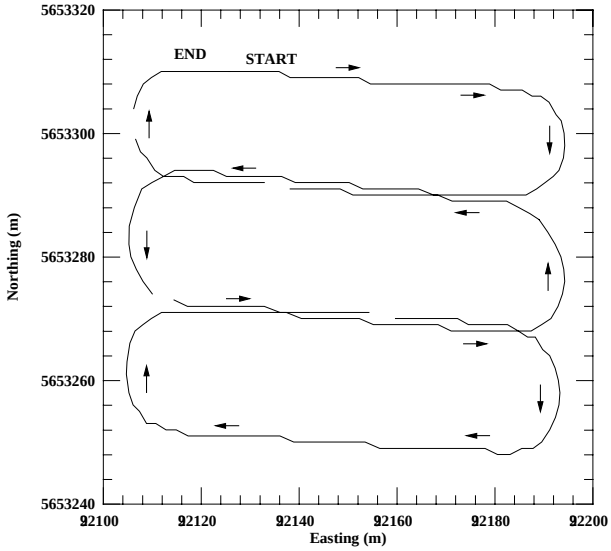

Figure 7.18 - Vehicle Trajectory For Motorola Oncore™ Trial

Each of the tests were conducted at approximately the same time each day to ensure that the GPS constellation was similar for the dynamic tests of each set of receivers. At least six GPS satellites were visible above 15° elevation during each of the tests and satellites below 15° were not used by the attitude system. Table 7.8 details the observation times and the number of satellites used for attitude determination during each of the tests.

Table 7.8 - Dynamic Test Observation Times

Receiver Type	Day of Year 1996	# of Svs Used	Start GPS time (s) h:m:s	End GPS time (s) h:m:s
NovAtel 2151™	091	8	58501 16:15:01	58863 16:21:03
Leica GPS Engine™	093	6	232799 16:39:59	233175 16:46:15
Motorola Oncore™	094	6	318959 16:35:59	319329 16:42:09

Software parameters were set to the same values as used during the static tests (see Table 7.3). The CARDINAL™ real-time results recorded at a epoch rate of 1 second are presented and discussed in the following section.

7.2.2 Comparison of Results From NovAtel, Leica and Motorola Receivers

The attitude system dynamic test was first performed using four NovAtel 2151™ GPS receivers. The test was performed in the morning of day 091 following a heavy snow fall the night before. The entire test area was covered in 30 cm of snow with the exception of the east end of the lot, which had been packed down by traffic. The real-time heading and two sigma heading standard deviations derived from the system Kalman filter are shown in Figure 7.19 and Figure 7.20 respectively. The heading appears smooth throughout the static and dynamic portions of the test run. Examination of the two sigma covariance plot indicates that the heading precision was fairly consistent at ± 1° with 0.2° improvements in accuracy as the vehicle was pointing southerly or northerly.

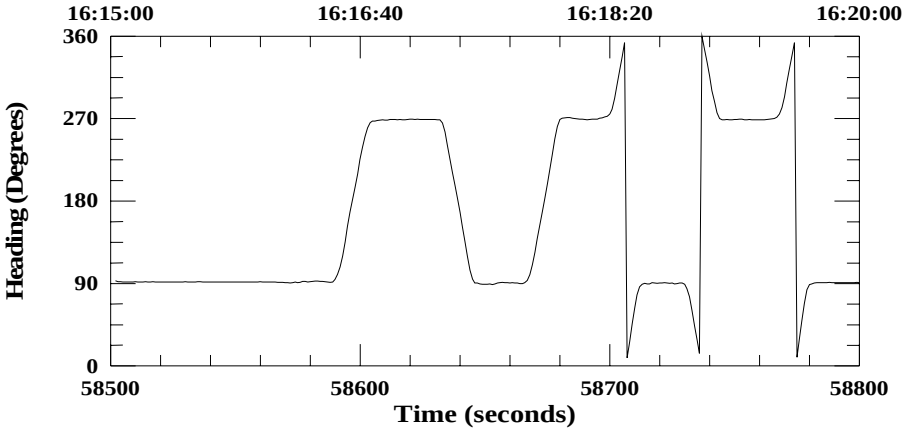

Figure 7.19 - Estimated Dynamic Heading Using NovAtel 2151™

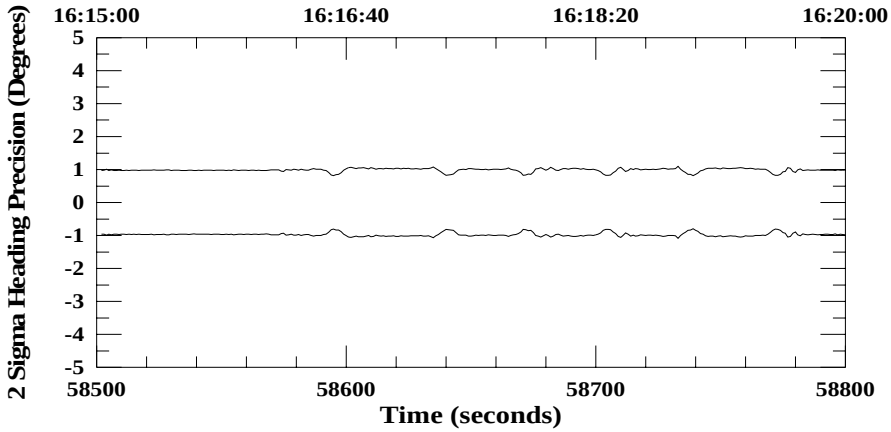

Figure 7.20 - Heading Covariance Using NovAtel 2151™

The real-time pitch and roll results are shown in Figure 7.21 and Figure 7.22. The pitch and roll appear random throughout the dynamic run, but are consistent during the static portions. The test area had a slight east-west slope for drainage. It was expected that the NovAtel pitch results from the attitude system would reflect this as it does for the Leica and Motorola tests. However, the heavy snow cover present over the test area probably affected the attitude of the test vehicle to some degree.

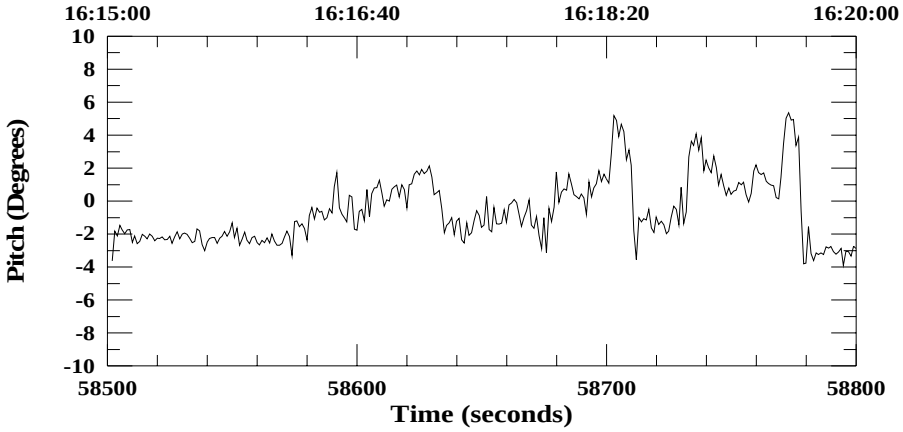

Figure 7.21 - Estimated Dynamic Pitch Using NovAtel 2151™

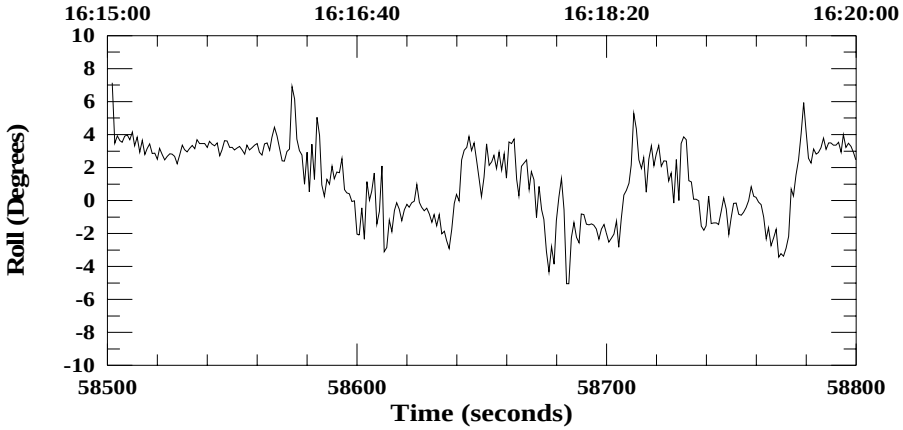

Figure 7.22 - Estimated Dynamic Roll Using NovAtel 2151™

The root mean square (RMS) was determined for all of the double difference phase residuals for each epoch. A comparison of the real-time RMS double difference phase residuals against system heading is given in Figure 7.23. The vehicle speed during the test is plotted against time in Figure 7.24.

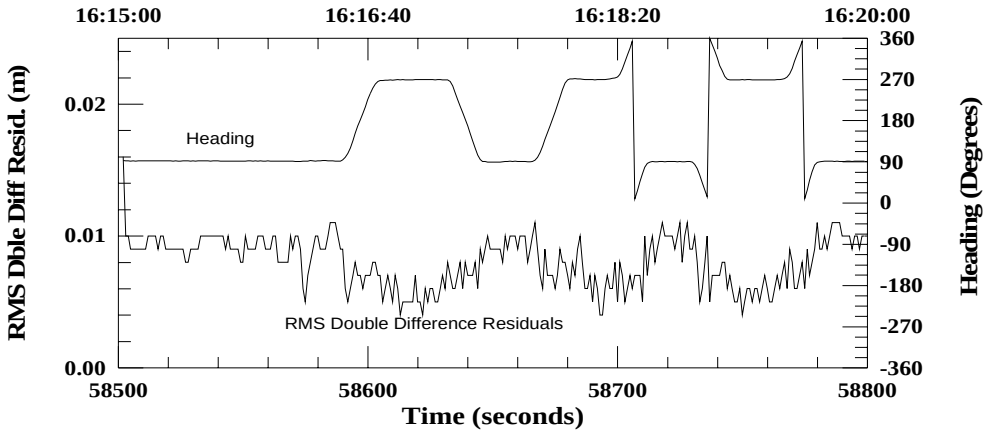

Figure 7.23 -NovAtel RMS Double Difference Phase Residuals Compared to Heading

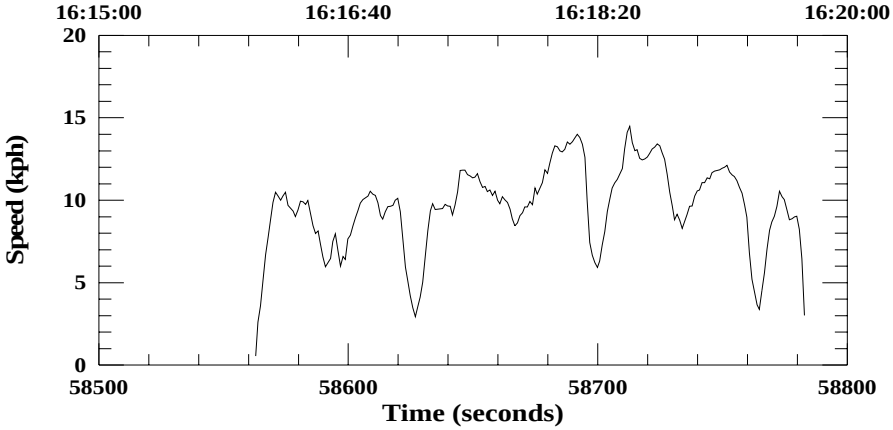

Figure 7.24 - Vehicle Speed During NovAtel 2151™ Test

The second dynamic test of the attitude system was performed using four Leica GPS Engines™. The area was partially covered with 10 cm of snow. The heavily travelled section on the west end of the lot was bare. The real-time heading and two sigma heading standard deviations derived from the Kalman filter are shown in Figure 7.25 and Figure 7.26, respectively. The heading appears smooth throughout the static and dynamic portions of the test run. Examination of the two sigma covariance plot indicates that the heading precision was fairly consistent at ± 1° with 0.25° improvements in accuracy as the vehicle was pointing southerly or northerly.

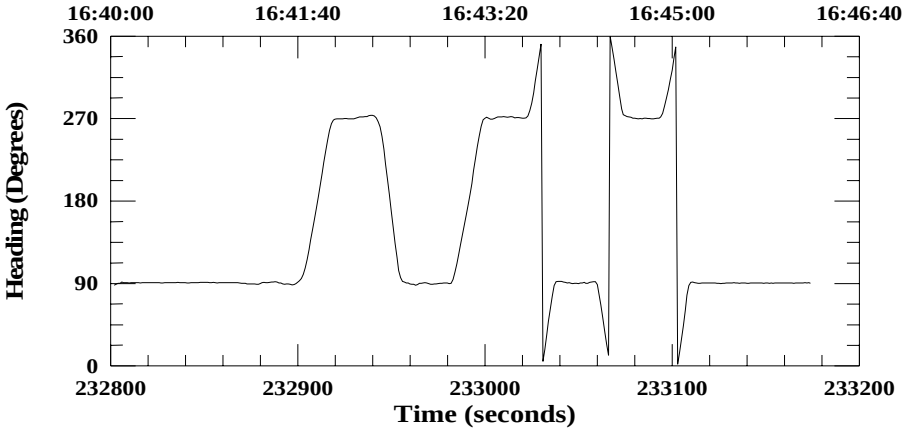

Figure 7.25 - Estimated Dynamic Heading Using Leica GPS Engine™

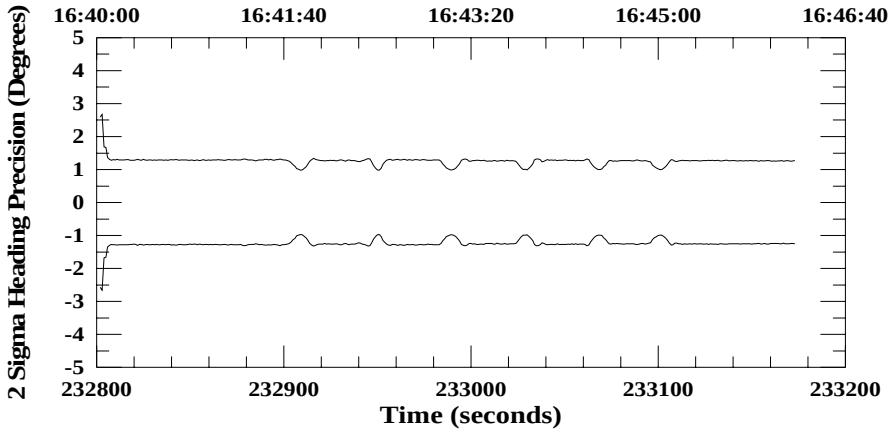

Figure 7.26 - Heading Covariance Using Leica GPS Engine™

The real-time pitch and roll results are shown in Figure 7.27 and Figure 7.28. The pitch appears consistent during the static and dynamic portions of the test. The roll appears random throughout the dynamic run, but are consistent during the static portions. The test area had a slight east-west slope for drainage which accounts for the high-low pattern in the pitch data. As the vehicle headed west the pitch was -1.5°, while it was approximately +3° as the vehicle was facing east. In should be noted that the antenna array on the test vehicle has a slight nose up pitch of approximately 1°.

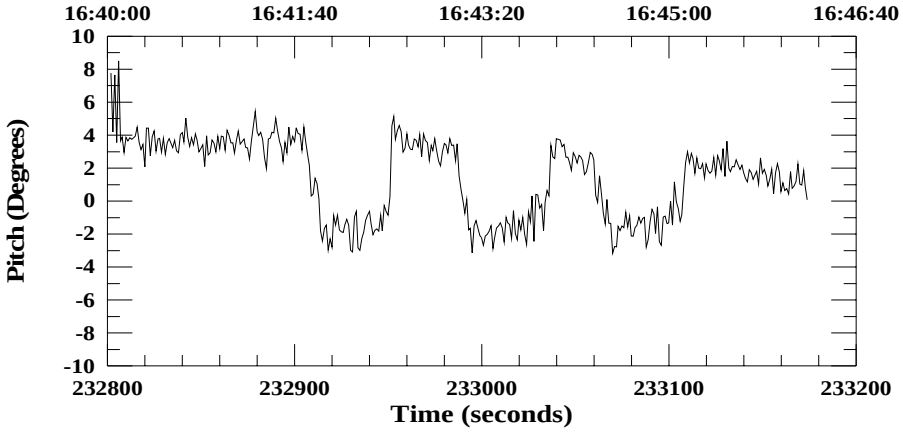

Figure 7.27 - Estimated Dynamic Pitch Using Leica GPS Engine™

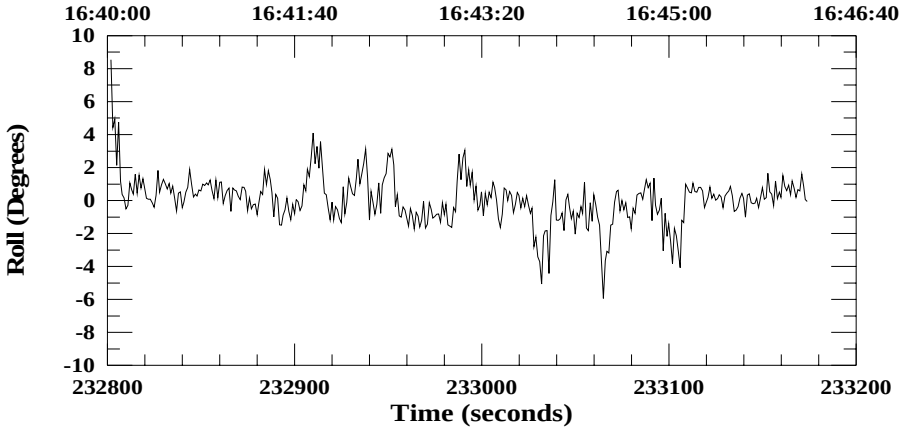

Figure 7.28 - Estimated Dynamic Roll Using Leica GPS Engine™

The root mean square (RMS) was determined for all of the double difference phase residuals for each epoch. A comparison of the real-time RMS double difference phase residuals against system heading is given in Figure 7.29. The vehicle speed during the test is plotted against time in Figure 7.30.

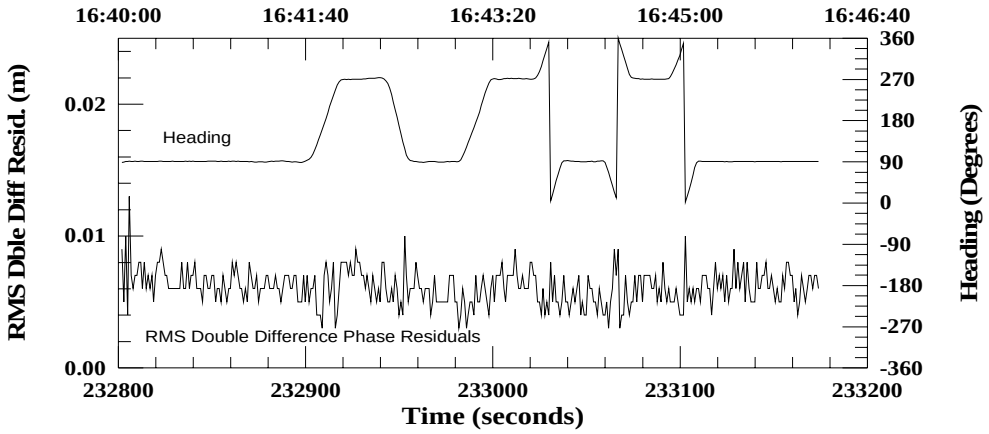

Figure 7.29 - Leica RMS Double Difference Phase Residuals Compared to Heading

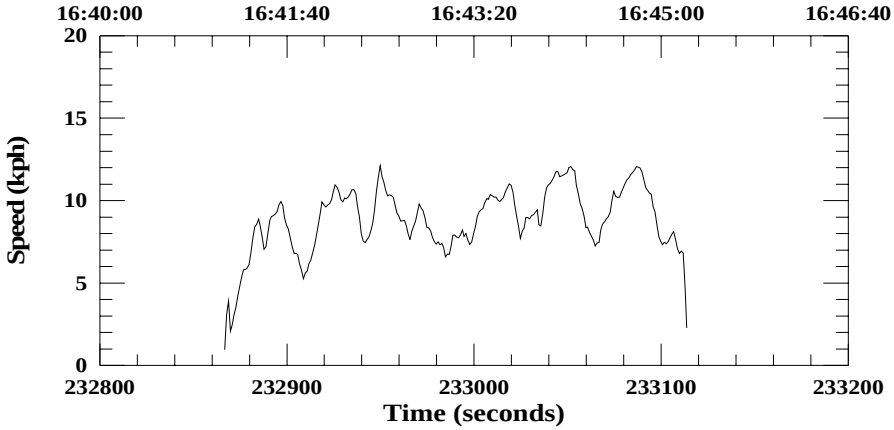

Figure 7.30 - Vehicle Speed During Leica GPS Engine™ Test

The third dynamic test of the attitude system was performed using four Motorola Oncore™ GPS receivers. The real-time heading and two sigma heading standard deviations derived from the Kalman filter are shown in Figure 7.31 and Figure 7.32, respectively. The heading appears smooth throughout the static and dynamic portions of the test run. Examination of the two sigma covariance plot indicates that the heading precision was consistent at ± 1.5° with 0.25° improvements in accuracy as the vehicle was pointing southerly or northerly.

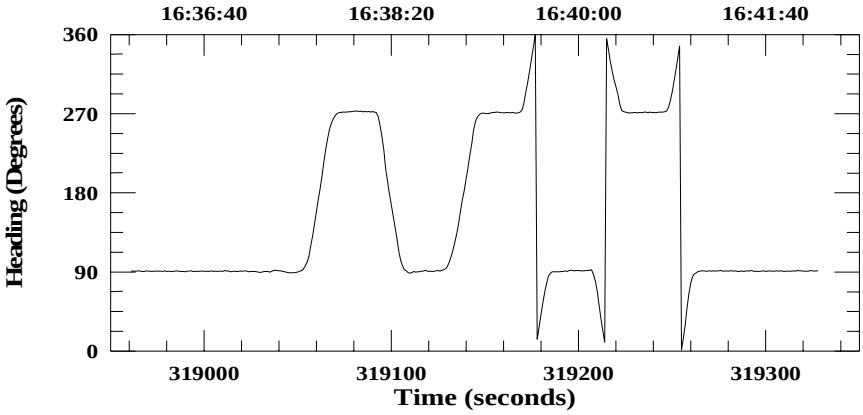

Figure 7.31 - Estimated Dynamic Heading Using Motorola Oncore™

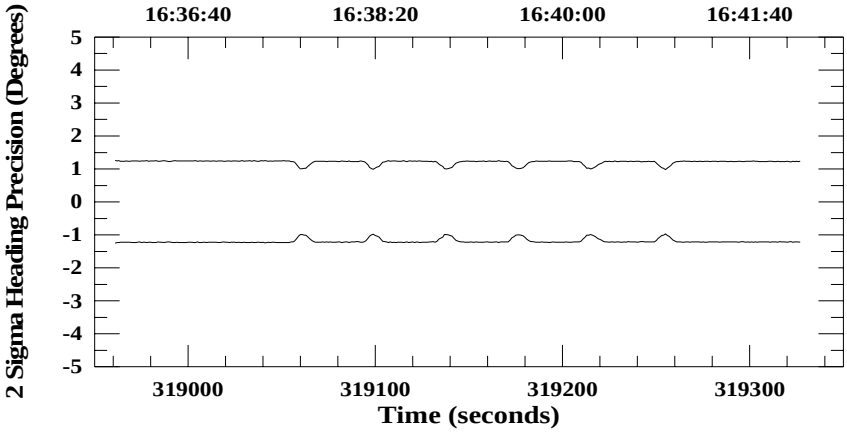

Figure 7.32 - Heading Covariance Using Motorola Oncore™

The real-time pitch and roll results are shown in Figure 7.33 and Figure 7.34. A high-low pattern similar to that seen in the Leica results is present in the pitch data. The periods of maximum pitch correspond with the vehicle heading east and the periods of minimum pitch correspond with the vehicle heading west. The roll results show more of a pattern than seen in either one of the other tests. A positive roll is discernible while the vehicle is heading west and a negative roll is present while the vehicle is heading east.

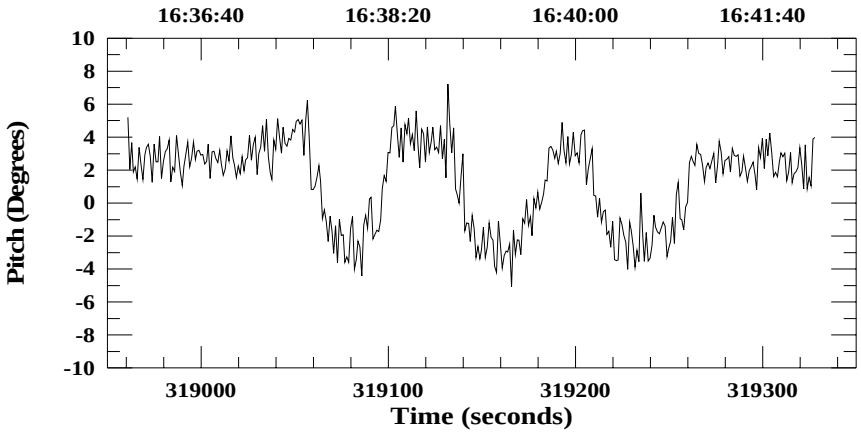

Figure 7.33 - Estimated Dynamic Pitch Using Motorola Oncore™

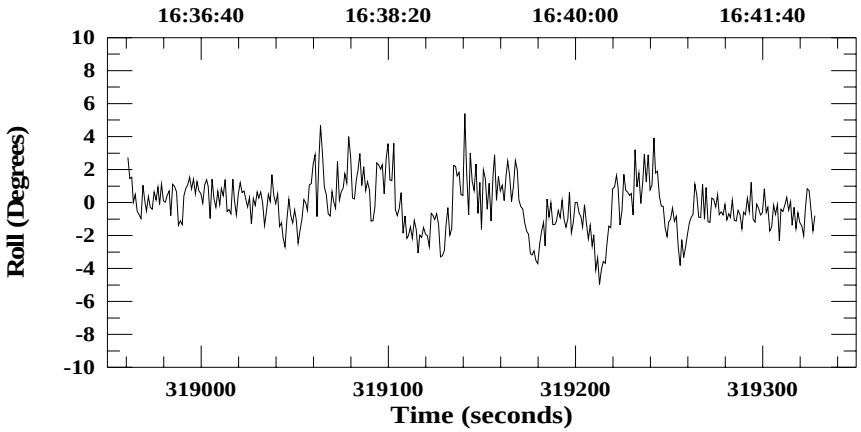

Figure 7.34 - Estimated Dynamic Roll Using Motorola Oncore™

The root mean square (RMS) was determined for all of the double difference phase residuals for each epoch. A comparison of the real-time RMS double difference phase residuals against system heading is given in Figure 7.35.

It is interesting to note that in the RMS residual plots for all three receivers there is a slight increase in the RMS of the double difference phase residuals when the vehicle is travelling west. An unaccounted for bias in the system could account for the increase in the RMS of the residuals. The source of the bias is unknown at this time, but antenna phase centre instability or diffraction in the near zone due to the rough edges of the antenna plate could account for the pattern observed. In both cases, as the vehicle

changes orientation within the GPS constellation, the effect of the antenna phase centre instabilities or edge diffraction will also change.

Further examination of the plot reveals no appreciable observed increase in the RMS of the residuals during vehicle turns, indicating that the Kalman filter tuning is loose and not causing overshoots. The vehicle speed during the test is plotted against time in Figure 7.36. An increase in vehicle speed does not appear to affect the magnitude of the RMS of the double difference phase residuals.

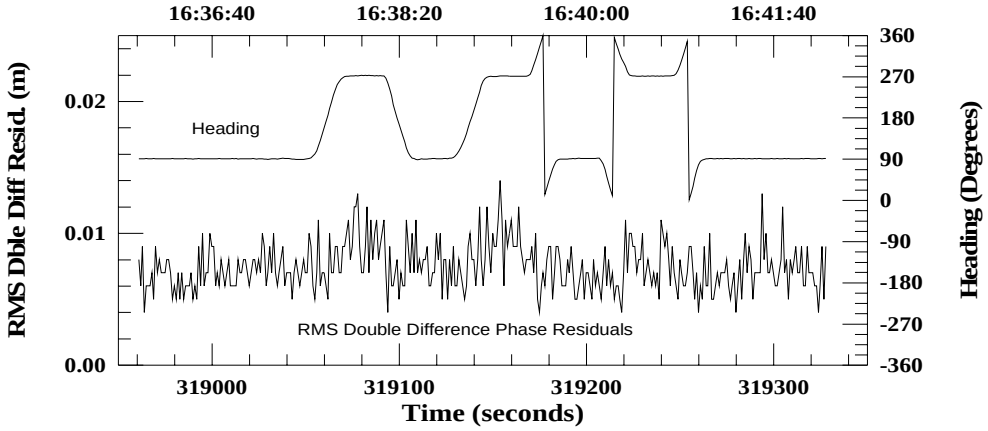

Figure 7.35 -Motorola RMS Double Difference Phase Residuals Compared to Heading

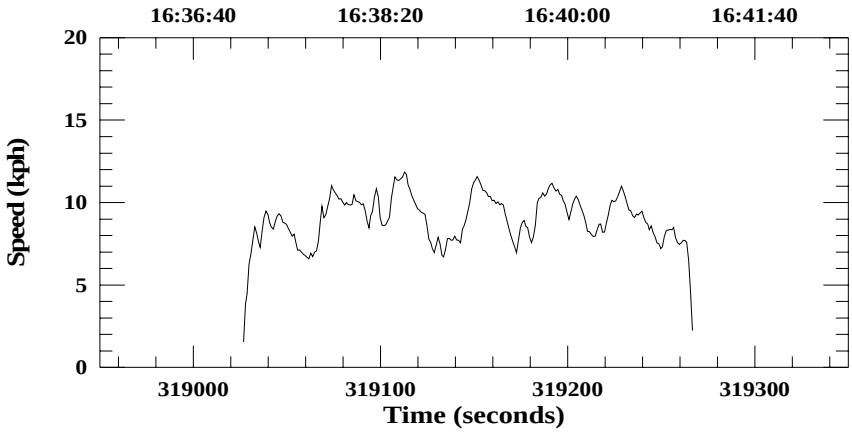

Figure 7.36 - Vehicle Speed During Motorola Oncore™ Test

The ambiguity resolution results are summarized in Table 7.9, Table 7.10, and Table 7.11 for the NovAtel, Leica and Motorola receiver tests, respectively. The NovAtel based system only performed one ambiguity resolution at the start of the session. The resolution was successful and the ambiguities were fixed. Three ambiguity resolutions were attempted during the Leica receiver test. All three resolutions were performed at start-up, while the vehicle was stationary. Each resolution was successful and the ambiguities were fixed. Only one resolution was attempted during the Motorola receiver tests. This resolution was performed during start-up and was successful.

Table 7.9 - NovAtel Dynamic Ambiguity Resolution

Solution	Test	Total	Sorted	Adjust	Min	2nd	Vf	Df
Fixed	Correct	790	55	37	0.0017	0.019	0.95	18

Table 7.10 - Leica Dynamic Ambiguity Resolution

Solution	Test	Total	Sorted	Adjust	Min	2nd	Vf	Df
Fixed	Correct	586	44	17	0.00021	0.0018	0.36	6
Fixed	Correct	572	42	15	0.00038	0.0063	0.42	9
Fixed	Correct	589	44	15	0.00073	0.014	0.61	12

Table 7.11 - Motorola Dynamic Ambiguity Resolution

Solution	Test	Total	Sorted	Adjust	Min	2nd	Vf	Df
Fixed	Correct	700	60	29	0.00055	0.013	0.46	12

7.3 Land Vehicle Trials over Hilly Terrain

A test was conducted with a land vehicle travelling over a hilly course to measure the dynamic performance of the CARDINAL™ attitude system. A test description, followed by results and analyses are given.

7.3.1 Test Description

A dynamic test of the attitude system was conducted on April 4, 1996 using four NovAtel 2151™ GPS receivers. The test area selected was on 17th Avenue, at the west edge of Calgary. This area features a 3.8 km straight length of road running over several hills and through an agricultural area with 3 to 4 m bare poplar trees along 30% of it. In some areas taller trees are present. Figure 7.37 illustrates the test site.

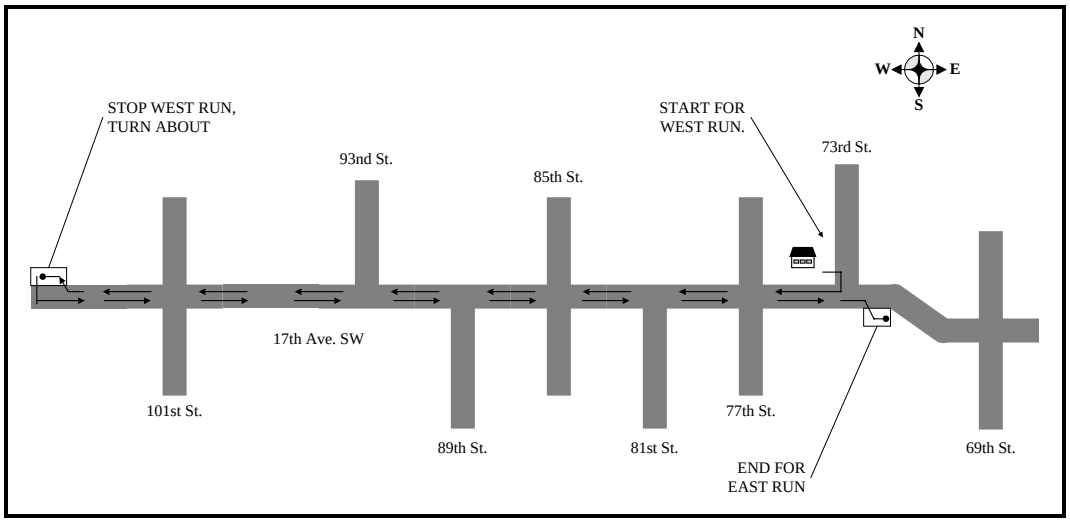

Figure 7.37 - Hill Testing Course - Calgary, Alberta

The test started with the vehicle parked near 73rd Street, facing east. The vehicle remained stationary for 6 minutes and then pulled on 73rd Street heading south. A right turn onto 17th Avenue was made and the vehicle was driven west for 4 minutes, 40 seconds until the pull-in area 400 m west of 101st Street was reached. The test vehicle pulled over at the pull-in area and remained stationary for 3 minutes, 20 seconds. The vehicle was then turned around and it proceeded east bound on 17th Avenue for 5 minutes, 24 seconds. The vehicle pulled over to the side of 17th Avenue on the east edge of the test area and data were recorded for an additional 1 minute. In total the test lasted 20 minutes, 30 seconds, of which 10 minutes, 4 seconds were with the vehicle in motion.

7.3.2 Data Analysis

The vehicle heading and two sigma standard deviation are plotted as a function of time in Figure 7.38, and Figure 7.39. The heading plot reveals some interesting features. The short positive heading jump at middle of the run (404670 seconds) corresponds to the test vehicle pulling off 17th Avenue, into the pull-in area and then straightening out. Following the static session at 404884 seconds, an aborted turn and short heading plateau are evident. This occurred when the test vehicle started to move out of the pull-in area in preparation for a U-turn. A vehicle was observed coming from the opposite direction and so the U-turn was aborted until the vehicle passed.

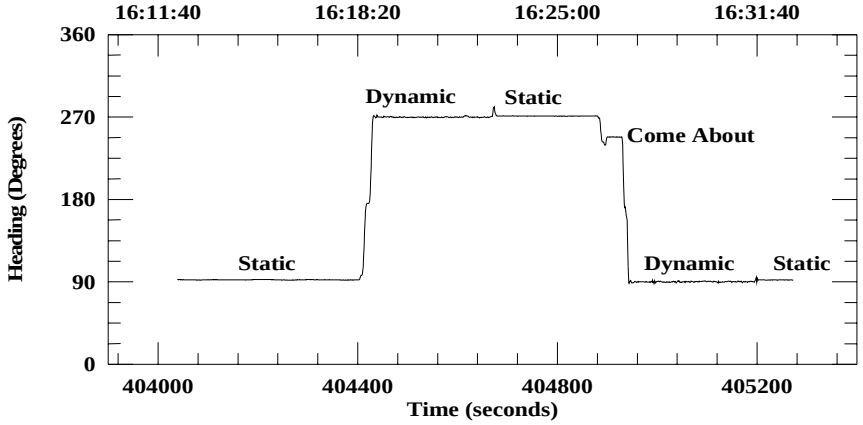

Figure 7.38 - Vehicle Heading During Hill Trials

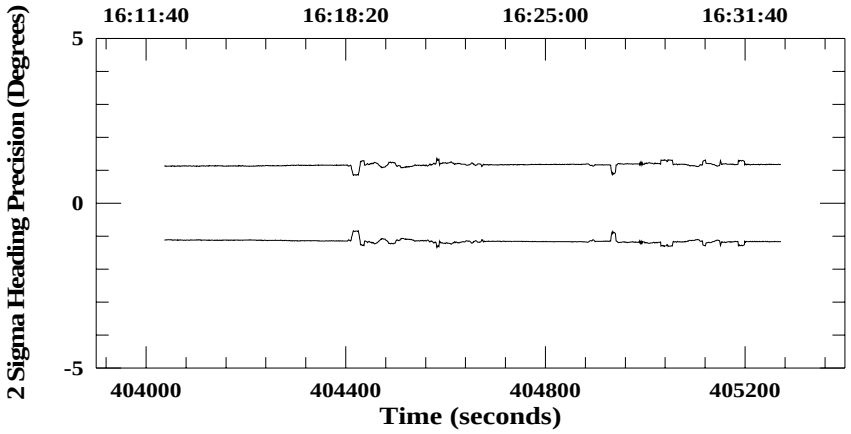

Figure 7.39 - Heading Covariance During Hill Trials

The system two sigma heading precision is consistent at 1.2°, with occasional 0.2° improvements when the vehicle is heading north.

The systems pitch and two sigma standard deviation are shown in Figure 7.40, and Figure 7.41, respectively. The graph of pitch as a function of time shows a definite pattern. The static portions feature a consistent pitch, while the dynamic portions appear more random.

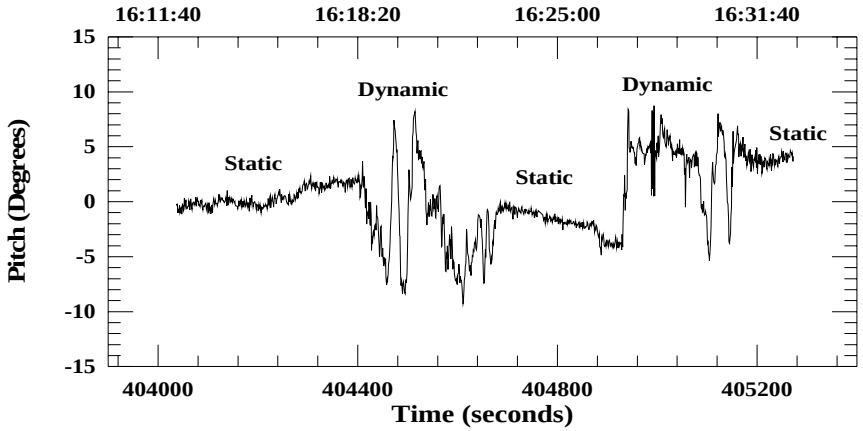

Figure 7.40 - Vehicle Pitch During Hill Trials

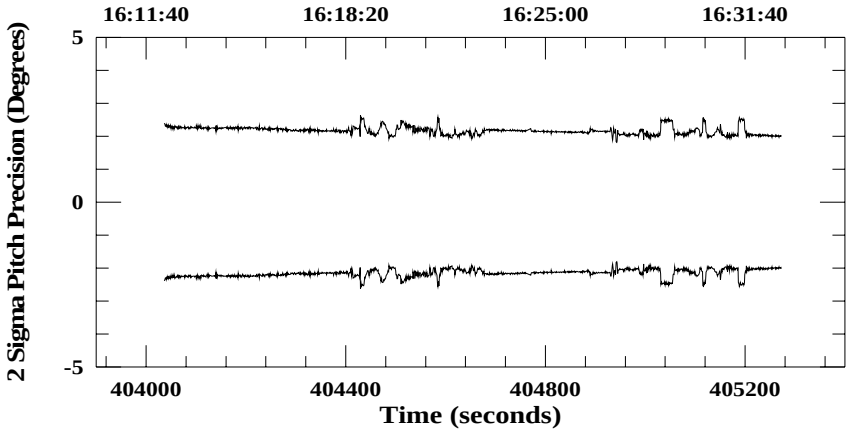

Figure 7.41 - Pitch Covariance During Hill Trials

In an effort to reveal correlations between pitch and the vehicle path, the pitch was plotted as a function of vehicle easting in Figure 7.42, along with a vertical profile of the trajectory. Examination of Figure 7.42 reveals a definite correlation between the system pitch and the terrain. Positive pitches are evident as the vehicle moved up hills and

corresponding negative pitches were present as the vehicle moved down hills. Two sigma pitch precision was estimated at ± 2.2° with 0.4° variations corresponding to changes in vehicle attitude.

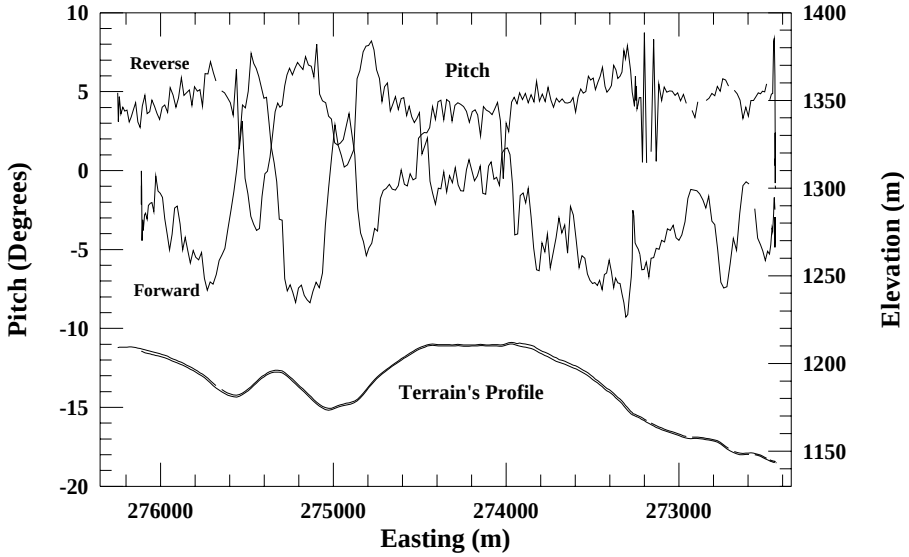

Figure 7.42 - Vehicle Pitch Compared to Terrain Profile

The systems roll and two sigma standard deviation are shown in Figure 7.43, and Figure 7.44, respectively.

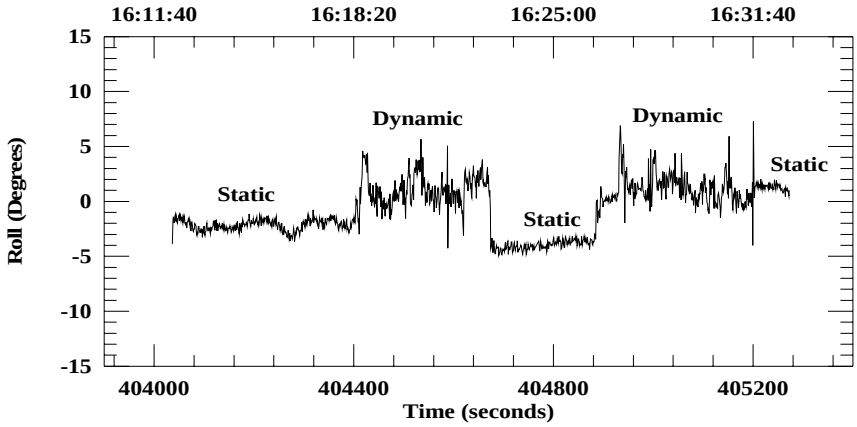

Figure 7.43 - Vehicle Roll During Hill Trials

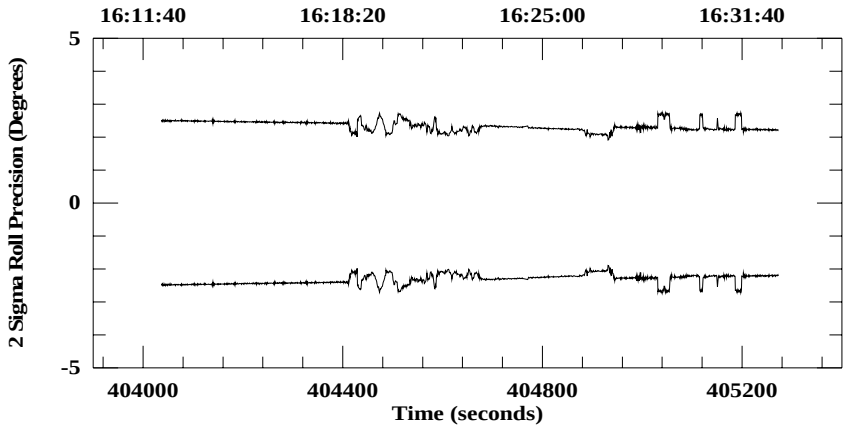

Figure 7.44 - Roll Covariance During Hill Trials

As with the pitch, the roll also shows a noticeable pattern. The positive roll during the dynamic portions of the test corresponds to road crown. Good roll consistency is especially evident during the second static session at the west end of the test area. The two sigma roll precision was estimated at ± 2.5° with 0.5° variations corresponding to changes in vehicle attitude.

Figure 7.45 shows the vehicle speed as a function of time. The two peaks correspond with the west and east test runs and reveal that vehicle speed varied from 50 to 60 kph during the dynamic portions of the test.

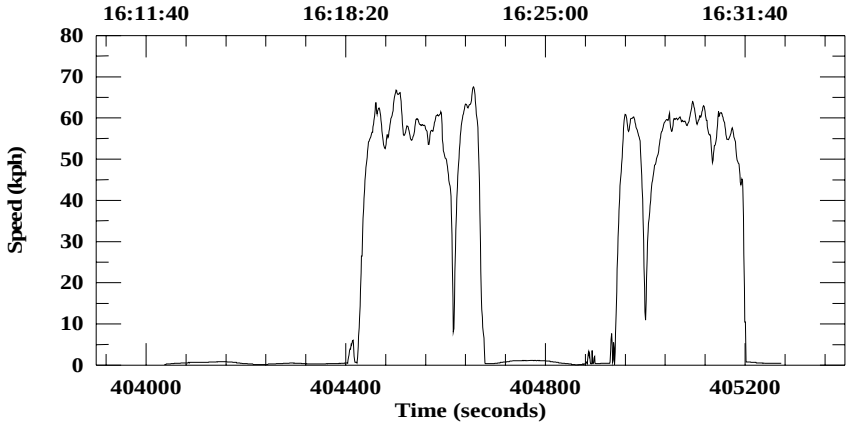

Figure 7.45 - Vehicle Speed During Hill Trials

Ambiguity resolution statistics were compiled for the test run. In total 75 resolutions were attempted with 22 successfully fixing the ambiguities. Of the other 53 resolution attempts all failed during the quadratic test of the variance factor. Further examination revealed that the resolution attempts were executed when the lowest satellite PRN 29 (elevation 18-19°) was blocked by terrain and trees. The 53 failed resolution attempts can be grouped into 7 time periods. The longest period of floating ambiguities was 13 seconds and only the 3 double differences containing PRN 29 were affected. All other double differences already had their ambiguities fixed. Following each of the 7 floating ambiguity periods an ambiguity resolution did successfully fix the ambiguities of those double differences containing PRN 29.

CHAPTER 8

CONCLUSIONS AND RECOMMENDATIONS

A real-time attitude determination system was developed using a quaternion attitude parameterization and three types of non-dedicated GPS receivers. Direction cosine, Euler angle and quaternion attitude parameterizations were developed for the 3-1-2 rotation series and transformations between the attitude representations were derived. Double difference phase and pseudorange models were developed with respect to the quaternions and a *direct* approach for attitude determination was presented to allow for the direct computation of quaternions from double difference phase and pseudorange observations. This approach coupled with the use of non-dedicated GPS receivers had not been previously investigated. A Kalman filter was designed for a state vector which includes the quaternions, body frame axis rotation rates and double difference phase ambiguities. To permit accurate, and robust on-the-fly ambiguity resolution, a technique was developed based on the least squares ambiguity search (LSAST) technique and using the double difference models developed herein.

A system was designed and built using off-the-shelf hardware and using PC based software written by the author. The hardware designed featured a relatively short 2λ antenna array and four non-dedicated OEM GPS receivers. A system based on the Motorola Oncore™ would cost approximately $5,800 US to build not including the laptop

computer. The real-time software package was developed to control and process input from NovAtel, Leica and Motorola GPS receivers. Through simple message based task manager, the software allowed for the operator-apparent simultaneous execution of input, output and computation tasks. Extensive status reporting features were incorporated into the software for the engineering tests.

A series of static and dynamic tests were conducted to gauge the performance of the quaternion based algorithms and math models. Static tests with NovAtel, Leica and Motorola receivers were performed and compared against static SEMIKIN™ baseline solutions. RMS heading results of 3.9 mrads were achieved with the attitude system while using four NovAtel 2151™ GPS receivers. Heading results from the system when using Leica GPS Engine™ and Motorola Oncore™ GPS receivers had rms values of 4.9 mrads and 6.8 mrads, respectively. Pitch and roll rms values of 21.5 mrads and 15 mrads respectively, were also attained. Dynamic tests verified the operation of the algorithms, models and Kalman filter. Consistent results were obtained during the dynamic tests verifying the feasibility of the system, however tests against an inertial reference system or against a proven commercial GPS attitude system are needed to verify the dynamic accuracy of the system.

The ambiguity resolution routines proved to be robust and allowed for rapid real-time resolution on-the-fly. The *direct* approach to attitude determination allowed for higher degrees of freedom during ambiguity estimation, resulting in higher reliability in solution testing. Ambiguities were typically resolved within one epoch. In the worst case, where the ambiguities were not resolved immediately, the software was able to fix the ambiguities within 13 seconds. In no case were the incorrect ambiguities resolved. However, the non-linearity of the double difference interferometeric model did present some challenges. Trial solutions within the ambiguity resolution least squares would often take from 6 to 10 iterations to converge and approximately one half of the solutions tested diverged. It is interesting to note that in most cases the correct ambiguity set would converge and divergence was adopted as the primary method to reject trial solutions.

The following are recommendations for further work and improvements to the attitude systems hardware and software.

1) The system should be tested against an inertial reference system or a proven commercial GPS attitude system under a variety of conditions.

2) The ambiguity resolution routine speed should be improved. The Cholesky decomposition technique presented by Lu (1995) should be tested as a method to form the primary ambiguity trial solutions.

3) The correlation amongst double difference observations for an epoch should be investigated and a comparison made with the results obtained herein.

4) An antenna body frame coordinate self-survey option should be added.

5) An antenna array with longer baselines should be built and tests performed to verify the system operation and accuracy.

6) Tests using the 8 Channel Motorola Oncore™ and the NovAtel 3151™ GPS receivers should be conducted.

7) A 20 Hz system using four NovAtel OEM or PC Cards could be built.

8) The addition of low cost rate gyros to the antenna array should be explored. The Kalman filter designed herein is suited to input from gyros aligned with the arrays body frame axes. The gyros would provide useful rate information for periods of GPS signal blockage.

9) The software could be migrated in two directions: a Windows based package sold for real-time and post-mission applications with customer supplied equipment, or an embedded program sold with an attitude hardware system.

10) Field trials should be conducted onboard the various target market platforms including land, marine and airborne vehicles.

11) Trials with different antenna geometery should be conducted.

12) Algorithms suitable for use in high latitudes should be investigated.

Attitude determination using GPS is capable of enhancing and in some cases replacing existing attitude systems. The keys to its success will be the availability of quality low-cost OEM GPS receivers, robust ambiguity resolution techniques and our own hard work and imagination.

REFERENCES

Abousalem, M.A. (1993): **Development of Robust GPS Kinematic Positioning Module For Automatic Vehicle Location and Navigation Systems**, M.Sc. Thesis, Department of Geomatics Engineering, University of Calgary, Alberta, Canada.

Adams, J.R. (1987): 'Step by Step' Least Squares Estimation, **Papers for the CISM Adjustment and Analysis Seminars**, The Canadian Institute of Surveying and Mapping, 1987.

Axelrad, P., and L.M. Ward (1994): On-Orbit GPS Based Attitude & Antenna Baseline Estimation, **Proceedings of the 1994 National Technical Meeting**, The Institute of Navigation, San Diego, California, January 24-26, 1994.

Brown, A.K, W.M. Bowles, T.P. Thorvaldsen (1982): Interferometric Attitude Determination Using the Global Positioning System: A New Gyrotheodolite, **Proceedings of the Third Geodetic Symposium on Satellite Doppler Positioning, Las Cruces**, New Mexico, February, 1982.

Brown, R.A., and A.G. Evans (1990): GPS Pointing System Performance, **Proceedings of the Third International Technical Meeting of The Satellite Division of The Institute of Navigation**, GPS-90, Colorado Springs, Colorado, September 19-21, 1990.

Brown, R. (1992): Instantaneous GPS Attitude Determination, **Proceedings of IEEE Position Location and Navigation Symposium**, PLANS '92, Monterey, California, March, 1992.

Brown, R.G., and P.Y.C. Hwang (1992): **Introduction of Random Signals and Applied Kalman Filtering**, Second Edition, John Wiley & Sons, Inc., New York.

Cannon, M.E. (1990): High-Accuracy GPS Semikinematic Positioning: Modeling and Results, **Navigation**, Journal of The Institute of Navigation, Vol. 37, No. 1, Spring 1990.

Cannon, M.E. (1992a): **Airborne GPS/INS with an Application to Aerotriangulation**, USCE Report #20040, Department of Geomatics Engineering, The University of Calgary, Canada.

Cannon, M.E. (1992b): **Report on the Design of a Real-time Heading Determination System**, Internal Pulsearch Navigation Systems Report, January 1992.

Cannon, M.E., J.B. Schleppe, J.F. McLellan and T.E. Ollevier (1992): Real-time Heading Determination Using an Integrated GPS-Dead Reckoning System, **Proceedings of the Fifth International Technical Meeting of The Satellite Division of The Institute of Navigation**, GPS-92, Albuquerque, New Mexico, September 16-18, 1992.

Chen, D. (1993): Fast Ambiguity Search Filter (FASF): A Novel Concept for GPS Ambiguity Resolution. **Proceedings of the Sixth International Technical Meeting of The Satellite Division of The Institute of Navigation**, GPS-93, Salt Lake City, Utah, September 22-24, 1993.

Chen, D. and G. Lachapelle (1994): A Comparison of the FASF and Least-Squares Search Algorithms for Ambiguity Resolution On The Fly, **Proceedings of the International Symposium on Kinematic Systems in Geodesy, Geomatics and Navigation**, KIS94, Banff, Alberta, August 30 - September 2, 1994, Department of Geomatics Engineering, The University of Calgary.

Crenshaw, J.W. (1994): Secrets of the Spin Doctors, **Embedded Systems Programming**, A Miller Freeman Publication, Vol. 7, No. 4, April 1994.

Crenshaw, J.W. (1994a): The Hard Way, **Embedded Systems Programming**, A Miller Freeman Publication, Vol. 7, No. 5, May 1994.

Crenshaw, J.W. (1994b): The End in Sight, **Embedded Systems Programming**, A Miller Freeman Publication, Vol. 7, No. 7, July 1994.

Cohen, C.E., B.W. Parkinson (1991): Expanding the Performance Envelope of GPS-Based Attitude Determination, **Proceedings of the Fourth International Technical Meeting of the Satellite Division of The Institute of Navigation**, GPS-91, Albuquerque, New Mexico, September 11-13, 1991.

Counselman, C.C. and S.A. Gourevitch (1981): Miniature Interferometer Terminals for Earth Surveying: Ambiguity and Multipath with Global Positioning System, **IEEE Transactions on Geoscience and Remote Sensing**, Vol. GE-19, No. 4, pp.244-252, October, 1981.

Defense Mapping Agency (1987): **Supplement to Department of Defense World Geodetic System 1984 Technical Report**, DMA Technical Report 8350.2-B, December 1, 1987.

El-Mowafy, A., and K.P. Schwarz (1995): Epoch-by-Epoch Ambiguity Resolution for Real-Time Attitude Determination Using a GPS Multiantenna System**, Navigation,** Journal of The Institute of Navigation, Vol. 42, No. 2, Summer 1995.

Erickson, C. (1992): **Investigations of C/A Code and Carrier Measurements and Techniques for Rapid Static GPS Surveys**, UCGE Report #20044, Department of Geomatics Engineering, The University of Calgary, Canada.

Euler, H. and C. Hill (1995): Attitude Determination: Exploiting all Information for Optimal Ambiguity Resolution, **Proceedings of The Eighth International Technical Meeting of the Satellite Division of The Institute of Navigation**, GPS-95, Palm Springs, California, September 12-15, 1995.

Evans, A.G., and B.R. Hermann (1989): A Comparison of Several Techniques to Reduce Signal Multipath From the Global Positioning System, **Global Positioning System: An Overview, Symposium No. 102**, Edinburgh, Scotland, August 7-8, 1989, Springer-Verlag, New York.

Fenton, P.C., B. Falkenberg, T. Ford, K. Ng and A.J. VanDierendonck (1991): NovAtel's GPS Receiver - The High Performance OEM Sensor of the Future, **Proceedings of the Fourth International Technical Meeting of the Satellite Division of The Institute of Navigation**, GPS-91, Albuquerque, New Mexico, September 11-13, 1991.

Frei, B. and G. Beutler (1990): Rapid Static Positioning Based on the Fast Ambiguity Resolution Approach "FARA": Theory and First Results, **Manuscripta Geodaetica**, Volume 15, Number 6, pp. 325-356.

Ferguson, K., J. Kosmalska, M. Kuhl, J. Eichner, K. Kepski, and R. Abtahi (1991): Three-Dimensional Attitude Determination with the Ashtech 3DF 24-Channel GPS Measurement System, **Proceedings of the National Technical Meeting of The Institute of Navigation**, Phoenix, Arizona, January 22-24, 1991.

Gao, Y. (1992): **A Robust Quality Control System For GPS Navigation and Kinematic Positioning**, Ph.D. Thesis, Department of Geomatics Engineering, The University of Calgary, Alberta, Canada.

Gelb, A., ed. (1974): **Applied Optimal Estimation**, M.I.T Press, Cambridge, Massachusetts.

Georgiadou, Y., and A. Kleusberg (1989): Multipath Effects in Static and Kinematic GPS Surveying, **Global Positioning System: An Overview, Symposium No. 102**, Edinburgh, Scotland, August 7-8, 1989, Springer-Verlag, New York.

Giardina, C.R., J. Heckathorn, D. Krasnjanski (1981): A Comparitive Study of Strapdown Algorithms, **Navigation:** Journal of The Institute of Navigation, Vol. 28, No. 2, Summer 1981.

Hatch, R. (1989): Ambiguity Resolution in the Fast Lane, **Proceedings of the Second International Technical Meeting of the Satellite Division of The Institute of Navigation**, GPS-89, Colorado Springs, Colorado, September 26-29, 1989.

Hatch, R. (1991): Instantaneous Ambiguity Resolution, **Proceedings of the IAG International Symposium 107 on Kinematic Systems in Geodesy, Surveying and Remote Sensing**, Banff, Canada, September 10-13, 1990, Springer-Verlag, New York, pp.299-308.

Hofmann-Wellenhof, B., H. Lichtenegger, and J. Collins (1994): **GPS Theory and Practice**, Third Edition, Springer-Verlag, Wien, New York.

Jurgens, R.D., C.E. Rodgers, L.C. Fan (1991): Advances in GPS Attitude Determining Technology as Developed for the Strategic Defense Command, **Proceedings of The Fourth International Technical Meeting of the Satellite Division of The Institute of Navigation**, GPS-91, Albuquerque, New Mexico, September 11-13, 1991.

Kruczynski, L.R., P.C. Li , A.G. Evans, and B.R. Hermann (1989): Using GPS To Determine Vehicle Attitude: USS Yorktown Test Results, **Proceedings of The Second International Technical Meeting of the Satellite Division of The Institute of Navigation**, GPS-89, Colorado Springs, Colorado, September 27-29, 1989.

Kruczynski, L.R., J. Delucchi, and T. Iacobacci (1995): Results of DC-10 Tests Using GPS Attitude Determination, **Proceedings of The Eighth International Technical Meeting of the Satellite Division of The Institute of Navigation**, GPS-95, Palm Springs, California, September 12-15, 1995.

Kuhl, M., X. Qin, and W. Cottrell (1994): Design Considerations and Operational Results of a GPS Attitude Determination Unit, **Proceedings of The Seventh International Technical Meeting of the Satellite Division of The Institute of Navigation**, GPS-94, Salt Lake City, Utah, September 20-23, 1994.

Lachapelle, G., W. Falkenberg, D. Neufeldt, and P. Kielland (1989): Marine DGPS Using Code and Carrier in a Multipath Environment, **Proceedings of The Second International Technical Meeting of the Satellite Division of The Institute of Navigation**, GPS-89, Colorado Springs, Colorado, September 27-29, 1989.

Lachapelle, G., M.E. Cannon, G. Lu (1992): High-Precision GPS Navigation with Emphasis on Carrier-Phase Ambiguity Resolution, **Marine Geodesy**, Vol. 15, pp. 253-269.

Lachapelle, G., C. Liu, G. Lu, B. Townsend, M.E. Cannon, and R. Hare (1993): Precise Marine DGPS Positioning Using P Code and High Performance C/A Code Technologies, **Geomatica**, Canadian Institute of Geomatics, Ottawa, Vol. 47, No. 2, pp.117-128.

Lu, G. (1995): **Development of a GPS Multi-Antenna System for Attitude Determination**, UCGE Report #20073, Department of Geomatics Engineering, The University of Calgary, Canada.

Lu, G., M.E. Cannon, G. Lachapelle (1993): Attitude Determination in a Survey Launch Using Mult-Antenna GPS Technologies, **Proceedings of the National Technical Meeting of The Institude of Navigation**, San Francisco, January 20-22, 1993.

Magnavox Electonic Systems Company (1992**): Magnavox GPS Engine™ Integration Guide and Applications Manual**, Publication Number R-7187D, June 1992.

McMillan, J.C. (1987): An Integrated System for Land Navigation, **Navigation:** Journal of The Institute of Navigation, Vol. 34, No. 1, Spring 1987, pp.43 - 63.

McMillan, J.C. (1994): A GPS Attitude Error Model for Kalman Filtering, **Proceedings of the IEEE Position Location and Navigation Symposium**, PLANS 1994, Las Vegas, Nevada, April 11-15, 1994.

Motorola (1994): **Oncore™ User's Guide**, Report 68P41117U01, Revision 6.1, Motorola Inc.

Nesbo, I. (1988): Applications of GPS Determined Attitude for Navigation, **Proceedings of The First International Technical Meeting of the Satellite Division of The Institute of Navigation**, GPS-88, Colorado Springs, Colorado, September 19-23, 1988.

NovAtel (1993): **GPSCard™ OEM Performance Series - 2100 Series User Manual**, Document OM-20000003, Revision D, NovAtel Communications Ltd.

NRC (1995): **The Global Positioning System, A Shared National Asset, Recommendations for Technical Improvements and Enhancements**, Committee on the Future of the Global Positioning System, Commission on Engineering and Technical Systems, National Research Council, Washington, D.C., 1995.

Quinn, P.G. (1993): Instantaneous GPS Attitude Determination, **Proceedings of the Sixth International Technical Meeting of The Satellite Division of The Institute of Navigation**, GPS-93, Salt Lake City, Utah, September 22-24, 1993.

Remondi, B.W. (1984): **Using the Global Positioning System (GPS) Phase Observable for Relative Geodesy: Modeling, Processing and Results**, Ph.D Dissertation, Centre for Space Research, University of Texas at Austin, Texas.

Remondi, B.W. (1990): Kinematic GPS Results Without Static Initialization**, Proceedings of the 47th Annual Meeting of The Institute of Navigation**, Washington, D.C.

Schwarz, K.P., M.E. Cannon, R.V.C Wong (1989): A Comparison of GPS Kinematic Models for the Determination of Position and Velocity Along a Trajectory, **Manuscripta Geodaetica**, No. 14, pp. 345 - 353.

Tranquilla, J.M. and B.G. Colpitts (1989): GPS Antenna Design Characteristics For High Precision Applications, **Journal of Surveying Engineering**, ASCE, Vol. 115, No. 1, February 1989.

Teunissen, P.J.G. and M.A. Salzmann (1989): A Recursive Slippage Test For Use In State-Space Filtering**, Manuscripta Geodaetica**, Vol. 14, No. 6, pp.383-390.

Vanicek, P. and E.J. Krakiwsky (1986): **Geodesy: The Concepts,** North-Holland, Amsterdam.

VanBronkhorst, A. (1978): Strapdown System Algorithms, **Strap-Down Inertial Systems**, AGARD Lecture Series No. 95.

Van Dierendonck, A.J. (1994): Understanding GPS Receiver Terminology: A Tutorial on What Those Words Mean, **Proceedings of the International Symposium on Kinematic Systems in Geodesy, Geomatics and Navigation**, Banff, Alberta, August 30 - September 2, 1994, Department of Geomatics Engineering, The University of Calgary.

Van Graas, F. and M. Braasch (1991): GPS Interferometric Attitude and Heading Determination: Initial Flight Test Results, **Navigation**: Journal of The Institute of Navigation, Vol. 38, No. 4, Winter 1991.

Walsh, D., V. Ashkenazi, G. Ffoulkes-Jones (1995): Performance of OTF Ambiguity Resolution Search Algorithms for Real Time Positioning Under Varying Conditions, **Proceedings of the National Technical Meeting of The Institute of Navigation**, Anaheim, California, January 18-20, 1995.

Wells, D., N. Beck, D. Delikaraoglou, A. Kleusberg, E.J. Krakiwsky, G. Lachapelle, R.B. Langley, M. Nakiboglou, K.P. Schwarz, J.M. Tranquilla, and P. Vanicek (1986): **Guide to GPS Positioning**, Canadian GPS Associates, Fredericton, N.B.

Wertz, J.R. (Ed.) (1978): **Spacecraft Attitude Determination and Control**, Kluwer Academic Publishers, The Netherlands.

Wilson, G.J. and J.D. Tonnemacher (1992): Trimble Navigation GPS Attitude Determination System, **Proceedings of the Fifth International Technical Meeting of The Satellite Division of The Institute of Navigation**, GPS-92, Albuquerque, New Mexico, September 16-18, 1992.

Wong, R.V.C (1988): **Development of a RLG Strapdown Inertial Survey System**, UCSE Report #20027, Department of Geomatics Engineering, The University of Calgary, Canada.